# Structural Exploration of Secondary Metabolites from *Rhaphidophora decursiva* by HPLC-DAD-ESI-MS and GC-MS Techniques



A dissertation submitted to the department of Chemistry, Quaid-i-Azam University, Islamabad, Pakistan, in the partial fulfillment of the requirement for the degree of

**Master of Philosophy**

in

**Organic Chemistry**

by

**Rabia Bibi**

Department of Chemistry

Quaid-i-Azam University, Islamabad, Pakistan

**2023**

بسم الله الرحمن الرحيم

**In the name of ALLAH, the Most Gracious, the Most Merciful.**

**Almighty Allah says in the Quran.**

"We will show them Our signs in the horizons and within themselves until it becomes clear to them that it is the truth. But is it not sufficient concerning your Lord that He is, over all things, a Witness?"

Surah Fussilat [41:53]

# Dedication

I dedicate this thesis to my mother **Asmat Firdous** whose love and strength has taken me to this point, my father **Muhammad Anwar** who lives through me and taught me that success has no bounds, and last but not the least my siblings who instilled in me the virtues of perseverance and commitment and relentlessly encouraged me to strive for excellence.

# Acknowledgements

# LIST OF FIGURES

# LIST OF SCHEMES

# LIST OF TABLES

# LIST OF ABBREVIATIONS/ACRONYMS

| | |
|---|---|
| **2D** | Two-dimension |
| **2D PC** | Two-dimension paper chromatography |
| ***a.m.u.*** | Atomic mass unit |
| **Ara** | Arabinose |
| **DAD** | Diode Array Detector |
| **DPPH** | 2,2-diphenyl picryl hydrazyl |
| **EC$_{50}$** | Half maximal effective concentration |
| **ESI** | Electrospray Ionization |
| **Fruc** | Fructose |
| **Gal** | Galactose |
| **Glc** | Glucose |
| **HPLC** | High Performance liquid Chromatography |
| **HPLC-DAD-ESI-MS** | High Performance Liquid Chromatography-Diode Array Detector-Electrospray Ionization-Mass Spectrometry |
| **IC$_{50}$** | Half-maximal Inhibitory Concentration |
| ***m/z*** | Mass to charge ratio |
| **MIC** | Minimum Inhibitory Concentration |
| **MTT** | 3-(4,5-Dimethylthiazol-2-yl)-2,5-diphenyl-2*H*-tetrazolium bromide |
| **NMR** | Nuclear Magnetic Resonance |
| **RDH** | *Rhaphidophora decursiva* extract in *n*- Hexane |
| **RDH-1** | Compound 1 identified from *n*- Hexane extract of *Rhaphidophora decursiva* |
| **RDH-2** | Compound 2 identified from *n*-Hexane extract of *Rhaphidophora decursiva* |
| **RDH-3** | Compound 3 identified from *n*- Hexane extract of *Rhaphidophora decursiva* |
| **RDH-4** | Compound 4 identified from *n*- Hexane extract of *Rhaphidophora decursiva* |
| **RDH-5** | Compound 5 identified from *n*- Hexane extract of *Rhaphidophora decursiva* |
| **RDH-6** | Compound 6 identified from *n*- Hexane extract of *Rhaphidophora decursiva* |
| **RDH-7** | Compound 7 identified from *n*- Hexane extract of *Rhaphidophora decursiva* |
| **RDH-8** | Compound 8 identified from *n*- Hexane extract of *Rhaphidophora decursiva* |
| **RDH-9** | Compound 9 identified from *n*- Hexane extract of *Rhaphidophora decursiva* |
| **RDH-10** | Compound 10 identified from *n*- Hexane extract of *Rhaphidophora decursiva* |

| | |
|---|---|
| **RDHM** | *Rhaphidophora decursiva* extract in 20% Hydromethanol |
| **RDHM-1** | Compound 1 identified from 20% Hydromethanolic extract of *Rhaphidophora decursiva* |
| **RDHM-2** | Compound 2 identified from 20% Hydromethanolic extract of *Rhaphidophora decursiva* |
| **RDHM-3** | Compound 3 identified from 20% Hydromethanolic extract of *Rhaphidophora decursiva* |
| **RDHM-4** | Compound 4 identified from 20% Hydromethanolic extract of *Rhaphidophora decursiva* |
| **RDHM-5** | Compound 5 identified from 20% Hydromethanolic extract of *Rhaphidophora decursiva* |
| **RDHM-6** | Compound 6 identified from 20% Hydromethanolic extract of *Rhaphidophora decursiva* |
| **RDHM-7** | Compound 7 identified from 20% Hydromethanolic extract of *Rhaphidophora decursiva* |
| **RDL** | *Rhaphidophora decursiva* leaves |
| **RDM-1** | Compound 1 identified from Methanolic extract of *Rhaphidophora decursiva* |
| **RDM-2** | Compound 2 identified from Methanolic extract of *Rhaphidophora decursiva* |
| **RDM-3** | Compound 3 identified from Methanolic extract of *Rhaphidophora decursiva* |
| **RDM-4** | Compound 4 identified from Methanolic extract of *Rhaphidophora decursiva* |
| **RDM-5** | Compound 5 identified from Methanolic extract of *Rhaphidophora decursiva* |
| **RDM-6** | Compound 6 identified from Methanolic extract of *Rhaphidophora decursiva* |
| **RDM-7** | Compound 7 identified from Methanolic extract of *Rhaphidophora decursiva* |
| $\mathbf{R}_f$ | Retardation Factor |
| **Rha** | Rhamnose |
| **TIC** | Total Ion Current |
| **TLC** | Thin Layer Chromatography |
| **UV** | Ultra Violet |
| **Xyl** | Xylose |

# ABSTRACT

*Rhaphidophora decursiva,* an ornamental plant of the Araceae family, exhibits immense biological properties. For example, it can be used for the treatment of colon cancer, skin diseases, and malaria, as well as an activating agent to enhance blood circulation. A detailed literature survey revealed that only a limited number of alkaloids and lignins have been identified from this genus. Therefore, the current study aimed to conduct detailed phytochemical analyses of *Rhaphidophora decursiva* using hyphenated mass spectrometric techniques. The leaf extracts were prepared by refluxing the leaves of *Rhaphidophora decursiva* in various solvents (*n*-hexane, methanol, and 20% hydromethanol). Prior to mass spectrometric analyses, preliminary assessments of these extracts were performed to ascertain the classes of compounds and the types of sugars present. Mass spectrometric analyses led to the tentative identification of twenty four phytochemicals from this plant. Fourteen of these phytochemicals were identified by using the negative ionization mode of HPLC-DAD-ESI-MS whereas the GC-MS analysis assisted in the characterization of the remaining ten phytochemicals. The identified compounds seemed to have connections with significant biological outcomes. The exploration of biologically significant phenolics and hydrocarbons illustrated that the plant is enriched in phytochemicals. It can be used as a potential candidate for further research to use in various life-saving drugs.

# CHAPTER 1: INTRODUCTION

## 1.1 Introduction to Genus *Rhaphidophora*

Nature has been a source of herbal medicines since ancient times. These herbs were used as a folk medicine because of their potential remedial properties. Herbal treatments are demonstrating growing effectiveness in addressing diverse health conditions with reduced toxicity to the human body. The urge to discover more medicinal drugs is rising with the time because of constantly emerging more resistant strains of pathogens. Different species of family Araceae reported to exhibit antibacterial, antifungal, antimalarial and antioxidant properties.

*Rhaphidophora* is one of the genera which belong to Araceae family with 100 species and it is distributed in Japan, Australia and tropical regions of Asia and Africa as reported by **Boyce *et al.,* (1999)**. The family Araceae commonly known as aroids comprises of 105 genera and 3300 species. The members of the Araceae family have been commonly used as curative herbs for the treatment of certain ailments such as stings, dermatitis, wound **(Hertian *et al.,* 2021)** and insect bites documented by **Chen *et al.,* (2007)**. The pharmacological and therapeutic properties of genus *Rhaphidophora* aid in prevention and cure of certain diseases. *Rhaphidophora pinnata* exhibits pharmacological properties, such as serving as anthelmintics. Certain species in this genus are efficacious in treating sunburn as reported by **Rahman and Kamri (2019)**. The scientific studies on this genus revealed the presence of secondary metabolites such as alkaloids, flavonoids, glycosides, saponins, tannins, steroids anthraquinones, phenols and triterpenoids **(Firdaus *et al.,* 2023)**. Limited literature has been reported on *Rhaphidophora* genus because it is less distributed on earth crust.

### 1.1.1 Common Species of Genus *Rhaphidophora*

> ➢ *Rhaphidophora korthalsii*
> ➢ *Rhaphidophora glauca*
> ➢ *Rhaphidophora elliptica*
> ➢ *Rhaphidophora cryptantha*
> ➢ *Rhaphidophora pertusa*
> ➢ *Rhaphidophora decursiva*

- *Rhaphidophora hookeri*
- *Rhaphidophora pinnata*
- *Rhaphidophora hongkongensis*
- *Rhaphidophora aurea*

*Rhaphidophora decursiva* is an everlasting, semi-succulent and evergreen epiphyte having vernacular name "Climbing Dragon" distributed worldwide as documented by **Arsad *et al.,* (2013)**.

Leaves, stems, flower and aerial roots of the *Rhaphidophora decursiva* are given below in the **figure 1.1**.



(a) **Leaves**                    (b) **Stem**

(c) **Flower**                    (d) **Aerial roots**

**Figure 1.1** Morphology of *Rhaphidophora decursiva*

## 1.2   Ethnobotanical Uses of Genus *Rhaphidophora*

The *Rhaphidophora* genus comprises of several plant species, with known ethnobotanical and pharmacological uses. **Wong and Tan (1996)** elaborated the useful curative properties of *Rhaphidophora korthalsii.* It had been used for the treatment of cancer and for diseases related to skin. *Rhaphidophora decursiva* was

commonly used as a medicinal bath by Yao communities in China for the cure of rheumatoid pain in the waist and legs, for the treatment of common injuries, skin ulcer and to activate the blood circulation as evaluated by **Li *et al.,* (2006)**. He also reported the medicinal use of *Rhaphidophora lancifolia* in the cure and treatment of fractures, injuries and rheumatoid numbness.

## 1.3 Phytoconstituents Identified from Genus *Rhaphidophora*

**Wong *et al.,* (1996)** isolated the 5,6-Dihydroxyindole **(1)** through the process of bio-guided fractionation using freshly harvested leaves of *Rhaphidophora korthalsii.*. The compound is unstable in vitro and undergoes spontaneous oxidation to form melanin. The compound demonstrates cytotoxicity showing an $ED_{50}$ of 3.5 µg/mL against P388 cells.

**Zhang *et al.,* (2001)** isolated fourteen compounds from bioassay-directed fractionation of leaves and stem of *Rhaphidophora decursiva* out of which 8 known compounds were isolated by gravity and reversed phase column chromatography, (+)-Medioresinol **(2)** (-)-pinoresinol **(3)**, (-)-syringaresinol **(4)**, (+)-glaberide I **(5)**, (+)-dehydrovomifoliol **(6)**, (-)-liliolide **(7)**, (-)-hydroxydihydrobovolide **(8)** and *N*-butylbenzamide **(9)**. The six compounds were isolated by using preparative HPLC technique. The names of the isolated compounds are polysyphorin **(10)**, rhaphidecursinol A **(11)**, rhaphidecursinol B **(12)**, Rhaphidecurperoxin **(13)**, grandisin **(14)** and epigrandisin **(15)**. Structural identification and interpretation were done by using spectroscopic analysis. Two new indole alkaloids, decursivine **(16)** and serotobenine **(17)** were isolated as shown below, from the bioassay directed fractionation from the leaves and stem extract of *Rhaphidophora decursiva* by using revers phase HPLC. Structural elucidation was done by 2D NMR spectroscopy documented by **Zhang *et al.,* (2002 a)** isolation of trichothecene sesquiterpenoid, Roridin E **(18)** reported by **Zhang *et al.,* (2002 b)** using chromatographic techniques such as reverse phase HPLC and reverse phase flash chromatography. Structural identification was carried out by using spectroscopic techniques.

The RP-HPLC analysis of *Rhaphidophora hongkongensis* was performed. Three compounds in the ethanol extract were identified by **Phukan *et al.,* (2016)**, including two phenolic acids, namely gallic acid **(19)** and protocatechuic acid **(20)**, and one flavonoid, quercetin **(20)**.

Fatty acid esters compounds identified and isolated through Thin-layer chromatography and column chromatography from aerial root extract of *Rhaphidophora aurea*. Characterization involved UV, IR, GC-MS/MS, 1D and 2D NMR techniques. Six fatty acids isolated and characterized, including 4-oxo-tricosanoic acid icosyl ester **(21)**, butyl octadecanoate **(22)**, dodecanoic acid dodec-3-enyl ester **(23)**, octacosa-23, 26-dien-12-one **(24)**, ethyl cis-6-octadecenoate **(25)** and 15,18-dotriacontadienoic acid methyl ester **(26)** as reported by **Ponnusamy *et al.*, (2021)**.

Structures of the phytoconstituents identified from the genus *Rhaphidophora* are given below:
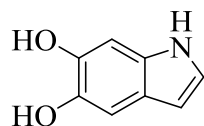
5,6-Dihydroxyindole **(1)**
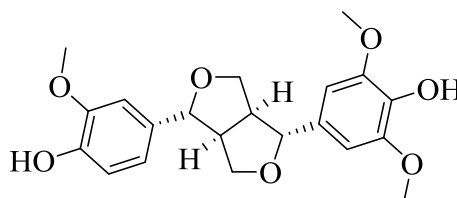
(+)-Medioresinol **(2)**
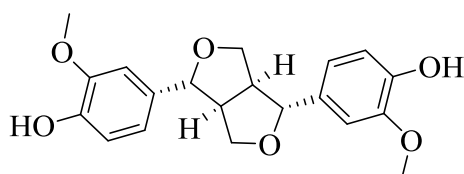
(-)-Pinoresinol **(3)**
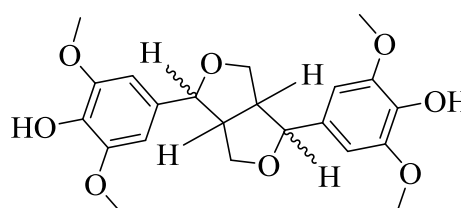
(-)-Syringaresinol **(4)**
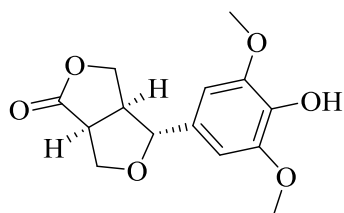
(+)-Glaberide I **(5)**
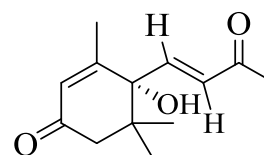
(+)-Dehydrovomifoliol **(6)**
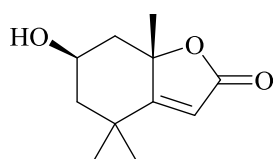
(-)-Loliolide **(7)**
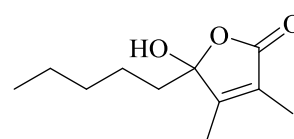
(-)-Hydroxydihydrobovolide **(8)**
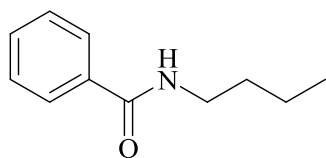
*N*-butylbenzamide **(9)**
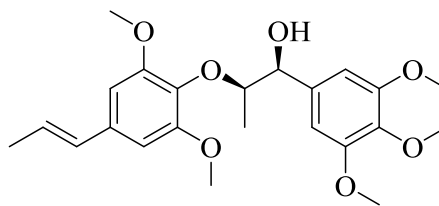
Polysyphorin **(10)**
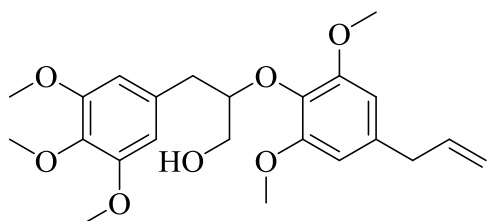
Rhaphidecursinol A **(11)**
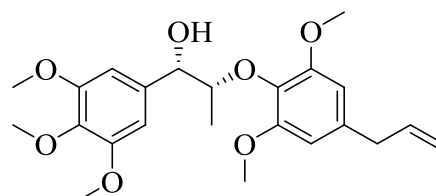
Rhaphidecursinol B **(12)**
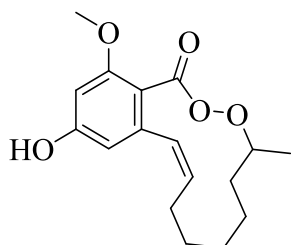
Rhaphidecurperoxin **(13)**
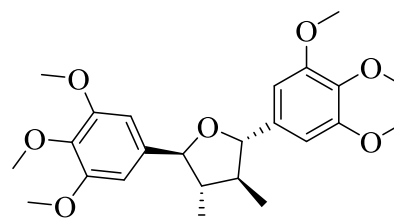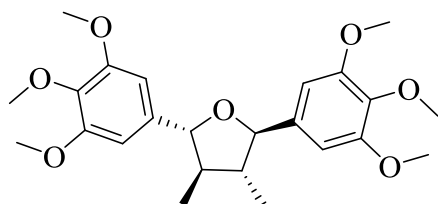
Grandisin **(14)**

Epigrandisin **(15)**
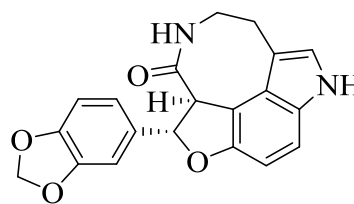
Decursivine **(16)**
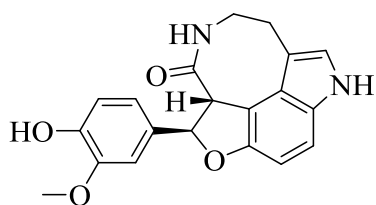
Serotobenine **(17)**
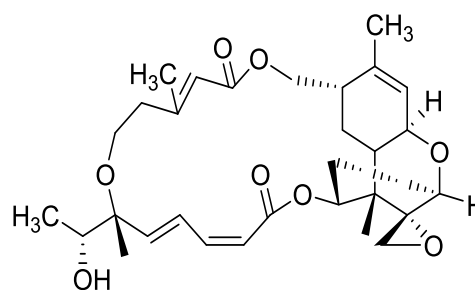
Roridin E **(18)**
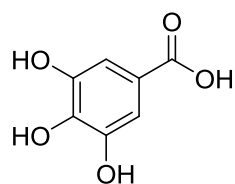
Gallic acid **(19)**
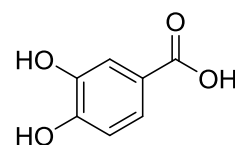
Protocatechuic acid **(20)**
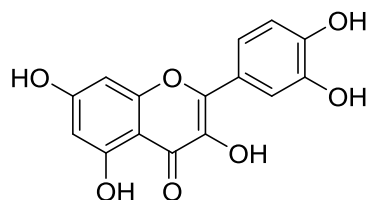
Quercetin **(21)**
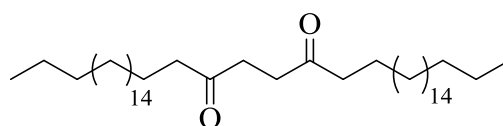
4-Oxo-tricosanoic acid icosyl ester **(22)**
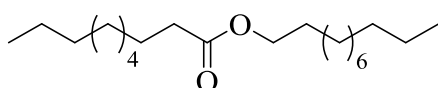
Butyl octadecanoate **(23)**
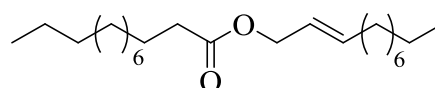
Dodecanoic acid dodec-3-enyl ester **(24)**
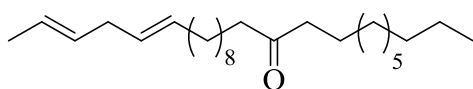
Octacosa-23, 26-dien-12-one **(25)**
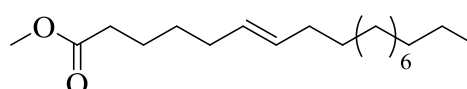
Ethyl cis-6-octadecenoate **(26)**
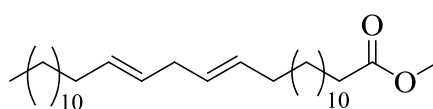
15,18-dotriacontadienoic acid methyl ester **(27)**

## 1.4 Biological Activities of Genus *Rhaphidophora*

### 1.4.1 Analgesic activity

**Linnet *et al.,* (2010)** reported the analgesic potential of ethanol extracts obtained from *Rhaphidophora pertusa* and *Rhaphidophora pinnata* was evaluated in Swiss albino mice. *Rhaphidophora pertusa* exhibited an analgesic effect similar to aspirin, a standard drug. The ethanol extract derived from the leaves of *Rhaphidophora pinnata* has demonstrated analgesic properties in mice subjected to acetic acid-induced pain. The research findings suggest that this extract possesses the potential to alleviate pain in mice. The analgesic mechanism of *Rhaphidophora pinnata* appears to involve

peripheral processes. The ethanol extract of *Rhaphidophora pinnata* is efficacious in alleviating pain in affected mice at a dosage of 50 mg per kilogram of body weight as documented by **Masfria and Dalimunthe (2018).**

**Summaiyah *et al.,* (2018)** investigated *Rhaphidophora pinnata's* pain-relief potential in mice using acetic acid-induced writhing. Five groups of animals received various treatments like ethanol extract of *Rhaphidophora pinnata* leaves at doses of 50, 100, and 200 mg/kg BW with sodium Carboxy Methyl Cellulose (CMC) 0.5% as the negative control and acetosal 200 mg/kg BW as the positive control. Treatments were given orally 30 minutes prior to acetic acid-induced pain. The remedial action was evaluated by measuring writhing movements. The results demonstrated significant pain relief with all doses of the ethanol extract compared to the control group having the most effective dose at 50 mg/kg of body weight.

### 1.4.2   Anti-inflammatory Activity

Ethanol extracts from *Rhaphidophora pertusa* and *Rhaphidophora pinnata* were assessed for anti-inflammatory effects in Wistar albino rats. Both species exhibited significant inhibition of carrageenan-induced rat paw swelling compared to the standard drug Indomethacin which showed maximum inhibition at 5mg/kg. They also displayed notable suppression of acetic acid-induced writhing in mice at all doses (125 and 250mg/kg) examined as reported by **Linnet *et al.,* (2010)**.

**Walidah *et al.,* (2020)** documented the anti-inflammatory activity of *n*-hexane fraction cream extracted from *Rhaphidophora Pinnata* on carrageenan-induced back edema in mice. The study included five sets of animal groups, consisting of a positive control group which was Hydrocortisone Cream (1%), placebo a negative control group and three groups being treated with *Rhaphidophora pinnata* leaf *n*-hexane fraction cream at different concentrations (2.5%, 5%, and 10%). The results indicated a significant anti-inflammatory effect with the highest concentration (10%) demonstrating the most pronounced impact. The study concluded that *Rhaphidophora pinnata* leaf *n*-hexane fraction cream showed potential as an anti-inflammatory agent.

Anti-inflammatory activity was assessed using the paw edema method in 30 male albino mice. **Sumaiyah *et al.,* (2020)** used 96% ethanol in the percolation method to extract *Rhaphidophora pinnata* leaves at room temperature. The substances

administered included a negative control group as sodium carboxyl cellulose suspension, *Rhaphidophora pinnata* leaf extract doses (35, 70, 140, and 280 mg/kg) and a positive control group diclofenac. These substances were given orally 60 minutes before injecting 0.2 mL of inflammation inducer that is 1% carrageenan. The optimal anti-inflammatory dosage for *Rhaphidophora pinnata* leaf extract was 140 mg per kilogram of body weight. It can be concluded that ethanol extract of *Rhaphidophora. Pinnata* leaves showed strong anti-inflammatory activity on male albino mice.

### 1.4.3    Antimalarial Activity

**Zhang *et al.,* (2001)** reported the antimalarial activity of dried leaves and stems of *Rhaphidophora decursiva* by using *in vitro* radioisotope method against *Plasmodium falciparum*. A total of fourteen compounds were isolated out of which 6 compounds showed antimalarial activity. Studies showed that Polysyphorin (**10**) and Epigrandisin (**15**) possess strong antimalarial activity with $IC_{50}$ value of 400 and 500 ng/mL respectively. While Rhaphidecursinol A (**11**), Rhaphidecursinol B (**12**), Rhaphidecurperoxin (**13**) and Grandisin (**14**) were less potent against *Plasmodium* clones.

Decusivine (**16**) an antimalarial agent found to be potent against D6 (chloroquine-sensitive) and W2 (chloroquine-resistant) clones of *plasmodium falciparum* with $IC_{50}$ values 3.93 and 4.41 $\mu$g/mL, respectively as reported by **Zhang *et al.,* (2002a)**. Roridin E (**18**) a new macrocyclic sesquiterpenoid was considered to be more effective against *Plasmodium falciparum* by inhibiting the growth with $IC_{50}$ less than 1ng/mL. **(Zhang *et al.,* 2002 b)**

### 1.4.4    Antimicrobial Activity

Methanolic extract of *Rhaphidophora pertusa* proved to be effective against gram-positive and gram-negative bacteria. **Sasikumar and Doss (2006)** carried out the antibacterial activity of methanolic extract while Ampicillin was taken as a reference standard with MIC value of 0.015-0.031 mg/mL. The MIC value recorded for methanolic extract against pathogens was 1.0-4.0 mg/mL range. Antifungal and antibacterial activity in aerial roots of *Raphidophora aurea* was analyzed by

**Arulpriya and Lalitha (2011)** against *Escherichia coli, Staphylococcus aureus, Candida albicans* and *Aspergillus flavus*.

The antibacterial properties of *Rhaphidophora pinnata* leaves were evaluated by **Masfria (2015)** through the agar diffusion method. The ethyl acetate and ethanol extracts exhibited antibacterial efficacy against four distinct bacterial strains *Streptococcus mutans*, *Pseudomonas aeruginosa*, *Salmonella typhi*, and *Shigella dysenteriae*. The ethyl acetate extract demonstrated effective antibacterial activity against all four bacterial strains tested while the ethanol extract displayed satisfactory activity primarily against *Pseudomonas aeruginosa*.

The antimicrobial efficacy of *Rhaphidophora hongkongensis* was evaluated by **Phukan *et al.,* (2016)** against five bacterial strains: *Bacillus subtilis*, *Pseudomonas aeruginosa*, *Staphylococcus aureus*, *Proteus vulgaris* and *Escherichia coli*. The findings indicated that the ethanol extract of *Rhaphidophora hongkongensis* produced zone of inhibition values measuring 12 mm, 10 mm, 11 mm, 9 mm, and 8 mm, respectively against these bacteria.

**Uddin *et al.,* (2016)** reported the antibacterial activity of two different fractions one from ethyl acetate extract and the other from chloroform extract of *Rhaphidophora glauca* through disc diffusion and minimal inhibitory concentration method. The inhibition zone of these fractions was 8-26 mm in 2000 $\mu$g/disc. Kanamycin and Ciprofloxacin were taken as the reference standard with zone of inhibition 11-28 mm and 20-25 mm at 30 $\mu$g/discs respectively.

The antimicrobial activity of the synthesized silver nanoparticles (AgNPs) of *Rhaphidophora pertusa* was tested using the disc diffusion technique on Mueller-Hinton agar. The experiment was run in duplicate and the zone of inhibition was measured in mm after incubating the plates for 24 hours at 37 °C. **Deivanathan and Prakash (2023)** found that the bio-synthesized AgNPs had high antimicrobial activity when compared to 10 $\mu$L of amoxicillin which was taken as a positive drug controls.

### 1.4.5  Antimutagenic activity

*Rhaphidophora pinnata* showed potential in the prevention and treatment of cancers associated with genetic mutations. The ethanol extract from its leaves were administered orally at various doses over a seven-day interval it exhibited noteworthy

antimutagenic properties in a mouse bone marrow micronucleus assay. These findings by **Masfria *et al.,* (2017)** suggested its potential to alleviate drug-induced gene mutations, particularly after exposure to cyclophosphamide-induced gene mutation.

The bone marrow micronucleus assay method was used by **Sumaiyah *et al.,* (2018)** to assess the antimutagenic properties of the ethanol extract from *Rhaphidophora pinnata* leaves. Administering ethanol extract nanoparticles of *Rhaphidophora pinnata* at doses of 200, 400, and 800 mg/kgBW resulted in a reduction in micronucleus formation in the spinal cord of rats. The ethanol extract nanoparticles of *Rhaphidophora pinnata* exhibited antimutagenic activity and provided dose-dependent protection against cyclophosphamide.

*In vivo* tests on mice were performed to check the antimutagenic activity by using *Rhaphidophora pinnta* nanoparticles through micronucleus method. The cyclophosphamide was delivered to the mice followed by induction of nanoparticles at doses of 50, 100 and 200 mg/kg for 7 days. It resulted in the decrease of micronucleus in 200 polychromatic erythrocytes cells of mice as reported by **Masfria *et al.,* (2021)**.

### 1.4.6 Antioxidant Activity

**Sasikumar and Doss (2006)** reported the effective antioxidant activity of *Rhaphidophora pertusa* by three test models that were DPPH, $Fe^{3+}$ metal chelation method and reducing power. The methanolic extracts of *Rhaphidophora pertusa* stem strongly scavenged the DPPH radicals with $IC_{50}$ of 54.56 ± 0.205 $\mu$g/mL while butylated hydroxy anisole was taken as reference standard with $IC_{50}$ of 53.27 ± 0.727 mg/mL. The extract effectively formed stable complexes with $Fe^{3+}$ ions at a concentration of 1000 μg/ml, it led to a notable increase in reducing power. The higher absorbance value at higher concentration showed the maximum increase in the reduction potential value. The extract showed efficacy in all three antioxidant test models.

The antioxidant activity was evaluated by using *β*-carotene bleaching, DPPH and ferric reducing antioxidant power. **Esa and Phuah (2009)** used ascorbic acid as a standard with $EC_{50}$ value of 0.10 ± 0.00 mg/mL to compare the antioxidant property of the aqueous and methanolic extract of *Rhaphidophora decursiva* leaves. Multiple

assays were conducted to evaluate the antioxidant activity. It was concluded that methanolic extract showed $EC_{50}$ value $1.18 \pm 0.05$ mL while the aqueous extract appeared to be at the $EC_{50}$ of $3.60 \pm 0.10$.mL Lowest the $EC_{50}$ value maximum will be the antioxidant activity. It was concluded that methanolic extract showed the highest scavenging activity compared to aqueous extract.

**Phukan *et al.,* (2016)** reported the antioxidant potential of *Rhaphidophora hongkongensis* through the DPPH radical scavenging assay. The $IC_{50}$ value of the ethanol extract from *Rhaphidophora hongkongensis* was determined to be 49.05 $\mu$g/mL, slightly exceeding the $IC_{50}$ values of *Olax acuminata* (41.34 $\mu$g/mL) and *Gnetum gnemon* (45.72 $\mu$g/mL).

Bio-synthesized *Rhaphidophora pertusa* silver nanoparticles (RP-AgNPs) demonstrated significant antioxidant potential. In the DPPH assay, RP-AgNPs exhibited escalating inhibition percentages of 64.38%, 69.57%, 71.34%, 75.49%, and 77.53% at concentrations ranging from 100 to 500 $\mu$g/mL. Significantly, at elevated doses, RP-AgNPs surpassed ascorbic acid in terms of antioxidant efficacy. This improvement is associated with the presence of molecules that enhance the surface area of the nanoparticles and increase their ability to scavenge free radicals as documented by **Deivanathan and Prakash (2023)**.

### 1.4.7 Cytotoxic Activity

The cytotoxic activity of ether extract of *Rhaphidophora korthalsii* was performed by **Wong and Tan (1996)** through MTT assay. Four different tumor cells were used to investigate the cytotoxic activity of *Rhaphidophora korthalsii* leaves extract including human epidermoid carcinoma of nasophyranx (Kb), human colon adenocarcinoma of nasophyranx (SW 620), human leukemic cells (Molt 40) and murine lymphocytic leukemia P388. $ED_{50}$ values against Kb, SW 60, Molt 40 and P388 were 8, 13, 14 and 12 $\mu$g/mL respectively at concentration of 50 $\mu$g/ml and 100 $\mu$g/ml while 6-Mercaptopurine was taken as a reference standard.

**Wong *et al.,* (1996)** discovered the melanin precursor with cytotoxic properties in *Rhaphidophora Korthalsii*. Experimental investigations have demonstrated that this compound identified as 5,6-Dihydroxyindole exhibits cytotoxic effects with an $ED_{50}$ of 3.5 $\mu$g/ml against a mouse lymphocytic leukemia cell line (P388 cells).

*Rhaphidophora korthalsii* methanol extract displayed significant cytotoxicity against hepatocellular carcinoma (HepG2). Pre-treated Peripheral Blood Mononuclear Cells (PBMCs) exhibited the highest cytotoxicity resulting in 8.59% apoptosis and 0.91% necrosis upon treatment with the extract. In contrast, untreated PBMCs caused 43.36% apoptosis and 1.92% necrosis in HepG2 cells. Notably, extract-activated PBMCs induced even more substantial cytotoxicity with 51.51% apoptosis and 3.92% necrosis in HepG2 cells as reported by **Yeap *et al.,* (2007)**.

The cytotoxic effects of different fractions of *Rhaphidophora pinnata* leaves on MCF-7 cells using MTT method was assessed by **Masfria *et al.,* (2013).** The results of the cytotoxicity assay indicated that the chloroform fraction exhibited the most substantial cytotoxic effect against MCF-7 cells with an $IC_{50}$ value of 59.082 $\mu$g/ml. Additionally the ethanol extract, ethyl acetate fraction, *n*-hexane fraction and water fraction also demonstrated notable cytotoxic activity against MCF-7 cells.

This study extracted plant with ethanol and separated the chloroform fraction. The fraction was tested on MCF-7 cancer cells using MTT assay. The fraction induced apoptosis in MCF-7 cells that was observed by flow cytometry and fluorescence microscopy. The cells showed signs of apoptosis such as nuclear contraction, blebbing and fragmentation **(Masfria *et al.,* 2014).**

**Uddin *et al.,* (2016)** executed the brine shrimp lethality test to check the cytotoxic activity of hydromethanolic fractions from chloroform and ethyl acetate extracts of *Rhaphidophora glauca*. The $LC_{50}$ values for chloroform and ethyl acetate extracts were observed to be 428.54 and 287.37 $\mu$g/mL respectively. The colchicine was used as a standard with $LC_{50}$ 11.16 $\mu$/mL.

**Firdhouse and Lalitha (2017)** investigated the cytotoxic effects of synthesized gold nanoparticles on MCF-7 breast cancer cells. Results showed that as the concentration of gold nanoparticles increased, cytotoxicity also increased and led to a 57% reduction in cell proliferation at 200 $\mu$g/mL. In comparison, the standard anticancer drug cisplatin induced 98% apoptosis at 30 $\mu$g/mL.

Cytotoxicity of bio-synthesized *Rhaphidophora pertusa* silver nanoparticles (RP-AgNPs) was tested on MCF-7 cells using the MTT assay. An increased dosage of RP-AgNPs from 10 to 100 $\mu$g/mL decreased cancer cell viability with an $IC_{50}$ of 102.4

$\mu$g/mL **(Deivanathan and Prakash 2023)**. The anticancer potential of RP-AgNPs was highlighted by DNA damage, leading to cell death, marked morphological changes such as cell shrinkage, membrane damage and altered cell volume, highlighting their anticancer potential.

### 1.4.8 Hepatoprotactive activity

**Sasikumar *et al.,* (2010)** investigated the hepatoprotective potential of methanolic extract from *Rhaphidophora pertusa* stems against acetaminophen-induced liver damage in albino rats. The levels of liver enzyme, bilirubin, urea, and total protein were examined. A significant rise in bilirubin, liver enzymes, and total protein was observed after 7 days of oral acetaminophen administration (500 mg/kg). Treatment with methanolic *Rhaphidophora pertusa* extract (100 and 200 mg/kg) significantly reversed the acetaminophen-induced liver changes by reducing enzyme activity and bilirubin levels. These results validate the traditional medicinal use of *Rhaphidophora pertusa*.

### 1.4.9 Hypoglycemic activity

**Kabir *et al.,* (2016)** assessed the hypoglycemic effects of ethanol extract and its chloroform and ethyl acetate fractions from *Rhaphidophora glauca* leaves in both normal and glucose-induced hyperglycemic mice. The study also involved calculating the Area Under the Curve (AUC) during an Oral Glucose Tolerance Test (OGTT). The ethanol extract and fractions of. *Rhaphidophora glauca* leaves were administered at 400 and 800 mg/kg doses, which significantly reduced fasting glucose levels in normal mice compared to the standard drug glibenclamide (5 mg/kg). Among the extracts and fractions, the 800 mg/kg dose of the ethanol extract exhibited the most pronounced hypoglycemic effect. It lowered blood glucose levels by 25.13% after 2 hours whereas glibenclamide showed a 49.30% reduction of blood glucose level.

### 1.4.10 Antihyperuricemia

**Pascila *et al.,* (2020)** documented the effectiveness of ethanol extracts from *Rhaphidophora pinnata* leaves in lowering uric acid levels and determining the best dosage of its extract. Hyperuricemia was induced with chicken liver juice and potassium oxonate. In this activity, Allopurinol served as a positive control. The research followed a randomized design with five interventions, each involving a

group of five mice. Results revealed that dose II (250 mg/kgBB) was the most effective in reducing uric acid levels by 45.22%. Dose III (375 mg/kgBB) produced a 44.66% reduction and dose I (125 mg/kgBB) led to a 39.60% decrease in uric acid level. In summary, all doses of ethanol extracts from *Rhaphidophora pinnata* leaves displayed anti-hyperuricemic properties with dose II demonstrating the highest efficacy in lowering uric acid levels.

### 1.4.11 Anti-hyperglycemic activity

The Oral Glucose Tolerance Test (OGTT) was used to assess the anti-hyperglycemic effects of *Rhaphidophora pinnata.* Samples included ethanol extract of dragon tail leaves with acarbose as a positive control in a completely randomized design (CRD) study involving five treatments with seven mice each. Results revealed the extract's *Rhaphidophora pinnata* effects with the most effective dose being dose III (375 mg/kgBB) leading to a 38.79% reduction in blood glucose levels as reported by **Lestari *et al.,* (2021)**. Dose II at a concentration of 250 mg/kg body weight led to a 17.01% decrease while dose I at 125 mg/kg body weight resulted in a 5.325% reduction. In summary, the ethanol extract of dragon tail leaves showed notable anti-hyperglycemic properties with the highest efficacy observed at 375 mg/kgBB dose.

### 1.4.12 Immunomodulatory Activity

The assessment of *Rhaphidophora korthalsii* methanolic extract's immunomodulatory activity performed by **Yeap *et al.,* (2011)** included *in vitro* and *in vivo* experiments. The plant extract was tested on human PBMC, mice splenocyte proliferation, cytokine expression, and NK cell cytotoxicity against mouse lymphoma cells (Yac-1) *in vitro*. The *in vivo* immunomodulatory activity of extract was evaluated by post-injection activity, mice weight gain, bone marrow proliferation and splenocyte. It resulted in increased mice weight gain post-injection activity, stimulates splenocyte and bone marrow proliferation. The results indicated that the extract enhances immune cell proliferation, natural killer (NK) cell levels, interleukin-2 (IL-2), interferon-gamma (IFN-γ) cytokines, and cytotoxicity against mouse Yac-1 cells. Furthermore, it also supports independent bone marrow cell growth.

### 1.4.13  α-amylase Inhibition Activity

**Kabir *et al.,* (2015)** explored the *α*-amylase inhibitory effect of *Rhaphidophora glauca* leaf extracts and their fractions. The chloroform, petroleum ether, *n*-hexane and ethyl acetate along with the fractions were evaluated for *α*-amylase inhibition using a modified starch iodine test. Levamisole (1 mg/ml) was used as a standard reference. The ethanol extract and all fractions showed substantial *α*-amylase inhibitory effects. Notably, petroleum ether fraction demonstrated the highest activity [$IC_{50}$=1.757±0.025mg/ml] compared to standard Acarbose (0.912±0.015) mg/mL. It portrayed significant *α*-amylase inhibitory effect of this plant.

### 1.4.14  Anthelmintic Activity

**Kabir *et al.,* (2015)** assessed the anthelmintic potential of ethanol extract and fractions from *Rhaphidophora glauca* leaves. After processing the leaves with pure ethanol and fractionation of ethanolic extract into chloroform, petroleum ether, *n*-hexane and ethyl acetate was obtained. These fractions were tested on *Tubifex tubifex* at concentrations of 5, 10, and 20 mg/ml. Notably, petroleum ether fraction demonstrated significant anthelmintic effects inducing paralysis (4.54±0.39 min.) and mortality (8.37±0.86 min.) of the *Tubifex tubifex* at the 20 mg/ml dose. The inhibition of α-amylase suggested the plant's capability to serve as a source for novel anthelmintic agents.

### 1.4.15  Miscellaneous Activity

The aqueous extract of *Rhaphidophora pinnata* demonstrated diverse pharmacological properties, encompassing antioxidant, anti-inflammatory, and anticancer effects. Additionally, **Masfria *et al.,* (2019)** detected the elevated levels of potassium within the extract, implying its potential as a diuretic agent and its capability to aid in the dissolution of calcium stones typically found in the kidneys.

## 1.5   Aims and Objectives

The literature review revealed that the genus *Rhaphidophora* is rich in various phytoconstituents such as alkaloids, flavonoids, glycosides, saponins, tannins, steroids, anthraquinones, phenols and triterpenoids. The preliminary analyses like 2D PC and Acid hydrolysis of the leaves extracts prepared by refluxing the leaves in various solvents also asserted the presence of biologically useful phytoconstituents along with different sugar moieties. These bioactive compounds have therapeutic effects against certain diseases, but the phytochemical profile of *Rhaphidophora decursiva* has not been reported yet. The objective of this research is to identify the polar and nonpolar constituents in the leaves extracts of this plant by using different analytical techniques like HPLC-DAD-ESI-MS and GC-MS.

## 1.6  Plan of Work

```
                    ┌──────────────┐
                    │ Collection of│
                    │    plant     │
                    └──────┬───────┘
                           │
                           ▼
                    ┌──────────────┐
                    │Extraction    │
                    │through reflux│
                    └──────┬───────┘
                           │
                           ▼
                    ┌──────────────┐
                    │Concentrated  │
                    │on rotary     │
                    │evaporator    │
                    └──────┬───────┘
                           │
                           ▼
                    ┌──────────────┐
                    │Defatted with │
                    │  n-Hexane    │
                    └──────┬───────┘
                           │
                           ▼
   ┌──────────────┐  ┌──────────────┐
   │Spectrometric │◄─│ Qualitative  │
   │  analyses    │  │   analyses   │
   └──────────────┘  └──────┬───────┘
                            │
                            ▼
 ┌────────┐ ┌──────────┐ ┌──────────┐
 │ GC-MS  │ │HPLC-DAD- │ │Preliminary│
 │analysis│ │ ESI-MS   │ │ analyses │
 └────────┘ └──────────┘ └────┬─────┘
                              │
                     ┌────────┴────────┐
                     ▼                 ▼
                ┌────────┐       ┌────────┐
                │  Acid  │       │ 2D PC  │
                │hydrolysis│     │        │
                └────────┘       └────────┘
```
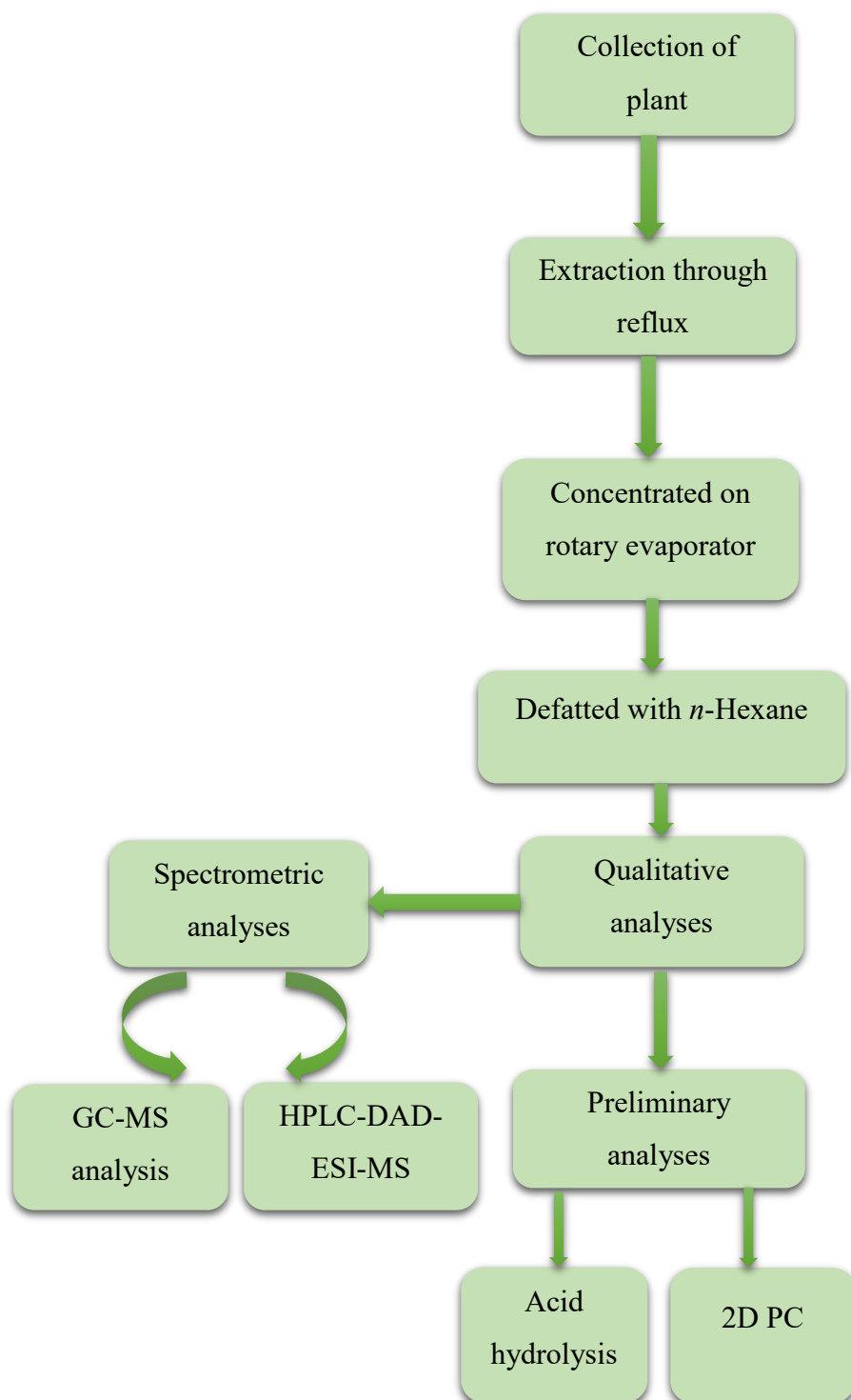
# 2 CHAPTER 2: MATERIALS AND METHODOLOGY

## 2.1 Selection of Plant

The selection of plant is the first priority before moving to the detailed analysis of phytoconstituents. In this regard, *Rhaphidophora decursiva* that belongs to family Araceae was selected due to its pharmacological and therapeutic properties. **Zhang *et al.*, (2001)** reported the antimalarial activity of the aerial part of *Rhaphidophora decursiva*. **Esa and Phuah (2015)** documented that the plant is the first line of defense against colon cancer. This plant also possesses strong antioxidant properties. So, it was further processed through different extraction steps in order to determine the chemical constituents in it.

## 2.2 Plant Collection and Authentication

*Rhaphidophora decursiva* was collected from Quaid-i-Azam University, Islamabad. Plant specimen was authenticated by Dr Mushtaq Ahmad, Professor at Plant Sciences Department, Quaid-i-Azam University, Islamabad.

## 2.3 Extraction Procedure

Fresh leaves (10 g) of *Rhaphidophora decursiva* were refluxed for 3 hours in 100 mL of methanol and 20% hydromethanol respectively. The solutions were filtered by using Whatman filter paper No. 1 and defatted with *n*-hexane by using separatory funnel. After defatting, the solvents (*n*-hexane, methanol and 20% hydromethanol) were concentrated on rotary evaporator in *vacuo*. The amount in grams of concentrated leaves extracts obtained is given below in the **table 1.1**.

**Table 1.1** Mass in grams of *Rhaphidophora decursiva* leaves crude extract

| Sample codes | Codes deciphering | Crude extract obtained in grams |
|:---:|:---:|:---:|
| RDH | *R. decursiva* leaves extract in *n*-hexane | 1.2 |
| RDM | *R. decursiva* leaves extract in methanol | 2.0 |
| RDHM | *R. decursiva* leaves extract in 20% hydromethanol | 3.5 |

## 2.4 Percentage Extraction Yield

Extraction yield is the quantitative assessment of amount of phytoconstituents extracted from different solvents like *n*-hexane, methanol and 20% hydromethanol. Percentage extraction yield of phytoconstituents from the fresh leaves of the *Rhaphidophora decursiva* was evaluated by using formula.

$$\text{Percentage extraction yield} = \frac{\text{mass of dried extract}}{\text{mass of plant material}} \times 100$$

## 2.5 Preliminary Analyses of Phytoconstituents

Chromatographic techniques including two-dimension paper chromatography and acid hydrolysis of methanolic and 20% hydromethanolic extract was performed for the identification of secondary metabolites in the plant.

### 2.5.1 Two-Dimensional Paper Chromatography

Paper chromatography is considered to be a powerful analytical tool it is readily accessible and inexpensive. It is used for the separation of low molecular-mass compounds depending upon the differences in their affinity towards stationary and mobile phase. Two-dimensional paper chromatography was employed with two different solvent systems (BAW and 15% acetic acid) to get information regarding various types of secondary metabolites in the plant extract.

#### 2.5.1.1 Materials and Chemicals Required for 2D PC

➢ Whatman filter paper No. 1(11 $\mu$m pore size)
➢ Chromatographic tank
➢ UV lamp
➢ BAW (*n*-Butanol: Acetic acid: Water) (4: 1: 5; upper layer)
➢ 15% Acetic acid
➢ NH$_3$ solution

#### 2.5.1.2 Protocol of Two-Dimensional Paper Chromatography

2D PC was performed for each of *n*-hexane, methanolic and 20% hydromethanolic extracts of *Rhaphidophora decursiva* leaves. The spots of each extract were applied three times on 2D PC (20×20 cm) leaving distance of 2 cm from bottom and left side of the sheet with the help of capillary tube and dried completely. The sample loaded sheets were suspended in the pre-saturated chromatographic tank containing mobile

phase BAW and allowed to develop in the first dimension. When the solvent front reached to its maximum point the chromatogram was removed, dried, visualized under UV light (365 *nm*) and respective bands were marked. The chromatogram was rotated 90 degrees and developed in 15 % acetic acid. After development, two-dimension paper chromatogram was monitored under UV light. The colored spots were marked and $R_f$ values were calculated. The obtained chromatogram was exposed to ammonia vapours and the change in color of the spots was monitored under UV lamp.

### 2.5.2   Acid Hydrolysis

The main objective of acid hydrolysis was to identify the sugar moieties present in the polar extracts of leaves. This method aided in identification of glycosidic linkages between glycan and aglycone moieties as acid hydrolysis is more effective for the cleavage of *O*-linked glycosides while partially and ineffective for the cleavage of *C*-linked glycosides. The time required to break the linkage depends upon the type of sugars, site of sugar moiety upon the aglycone nucleus and strength of the acid used. Further confirmation about type of sugars and nature of linkage is confirmed by mass spectral analysis.

#### 2.5.2.1   Materials and Chemicals Required for Acid Hydrolysis
  ➢ 0.2M $NaH_2PO_4$
  ➢ 2M HCl
  ➢ Precoated silica gel 60 $F_{254}$ TLC plate
  ➢ Aniline hydrogen phthalate (spraying reagent)
  ➢ 0.05% standard sugar solutions
  ➢ 10% isopropyl alcohol
  ➢ Acetone: water (9:1)

Following solutions were prepared in order to execute acid hydrolysis.

#### 2.5.2.2   Preparation of 2M HCl Solution
16.7 mL of commercially available HCl was taken in the 100 mL volumetric flask and distilled water was added up to the mark.

### 2.5.2.3 Preparation of 0.2M NaH₂PO₄ Solution

2.4 g of commercially available sodium dihydrogen phosphate was taken in a 100 mL of volumetric flask and distilled water was added to dissolve the solute. Distilled water was added up to the mark to obtain the desired concentration.

### 2.5.2.4 Preparation of 0.05% Standard Sugar Solutions

To make 0.05% standard sugar solutions, 0.05 grams of each sugar *i.e.*, glucose, galactose, fructose, arabinose and rhamnose was dissolved in 10 mL of distilled water. The 10% of aqueous solution of isopropyl alcohol was added as a preservative.

### 2.5.2.5 Preparation of Spraying Reagent

Aniline hydrogen phthalate was used as a spraying reagent to visualize the sugar spots as they do not have any chromophoric part. It was prepared by dissolving 1.6 g of phthalic acid in 0.92 mL of aniline and 100 mL of saturated butanol was also added into the solution.

### 2.5.2.6 Protocol of Acid Hydrolysis

The 2 g of concentrated methanolic extract was taken in a round bottom flask. Then 2M HCl and methanol were added to it in equal proportion (1:1). The whole mixture was refluxed for about 8 hours and concentrated on rotary evaporator after adding water and methanol in (1:1) ratio. The concentrated solution was taken in the separatory flask and defatted with ethyl acetate. The two layers were separated and concentrated. The TLC plate was kept in the oven at 110 ℃ for 20 minutes for activation of silica gel. Impregnation of TLC was done by using 0.2M NaH₂PO₄ to neutralize the acidic nature of silica gel so that the resolution of spots can be enhanced. Impregnated TLC plate was dried in oven at 100℃ for 10 minutes. Standard sugar solutions were prepared, 0.025 g of each sugar (glucose, galactose, fructose, xylose, rhamnose and arabinose) was taken in the 5mL volumetric flask and distilled water was added up to the mark. Then 2 to 3 drops of 10% isopropyl alcohol were added to each sugar solution as a preservative. The spots of each standard sugars and hydrolysate were applied three times on TLC plate. The TLC plate was developed in acetone: water (9:1) mobile phase in ascending order. The developed plate was placed in open air to evaporate the solvent and sprayed with aniline hydrogen phthalate to make the sugars spots visible. After spraying, the plate was placed in the oven at 100℃ for 30 minutes.

## 2.6 Liquid Chromatography-Mass Spectrometry (LC-MS)

High Performance Liquid Chromatography equipped with Diode Array Detection (DAD) is an analytical technique that is developed to examine the purity of analyte which is further assembled with Electro Spray Ionization-Mass Spectrometry (ESI-MS). It is well established technique for the structural identification of complex molecule through fragmentation. This method is developed for the identification of chemical constituents.
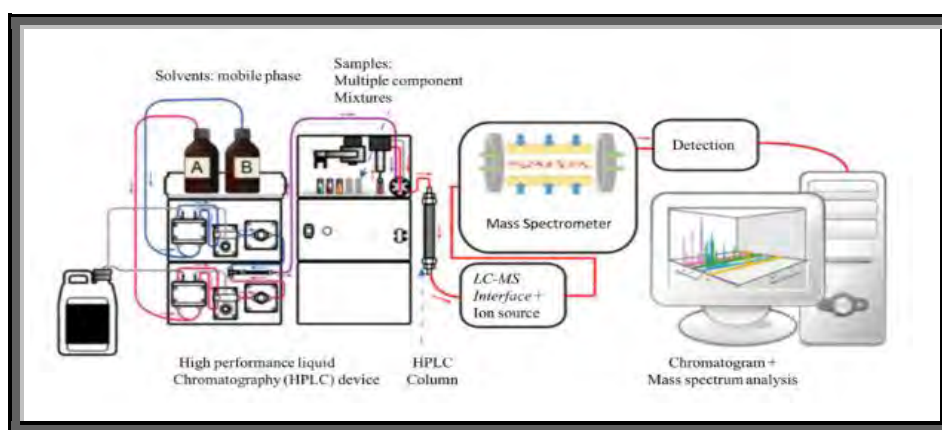


**Figure 1.2** Schematic diagram of HPLC-MS system

### 2.6.1 Instrumental Specifications

HPLC was performed on an Agilent Model No.1200 instrument. The separation was carried out on XDB C-18 stationary phase with stainless steel column (4.6 ×150 mm). Deionized water and acetonitrile of HPLC grade were used as mobile phase represented as solvent A and solvent B respectively in a gradient manner. 0.1% formic acid was used as modifier along with the mobile phase. The flow rate was 0.5 mL/min and injection volume was 5 $\mu$L in split mode. The composition of mobile phase with time is described below in the **table 1.2**.

**Table 1.2** Mobile composition with time in LC-MS column

| Time (minutes) | % of Deionized water (Solvent A) | % of Acetonitrile (Solvent B) | Composition of eluate |
|---|---|---|---|
| **0-15** | 90 | 10 | Polyglycosides |
| **15-40** | 60 | 40 | Tetraglycosides |

| 40-50 | 20 | 80 | Triglycosides, diglycosides and monoglycosides |
|---|---|---|---|
| 50-60 | 90 | 10 | Re-equilibration of mobile phase |

Detection was carried out using DAD. The ion trap mass analyzer was fitted in MS with ESI probe operated in a negative mode with mass scan range 50-1000 atomic mass units. The gradient elution of mobile phase during HPLC-MS is shown below the **figure 1.3**.
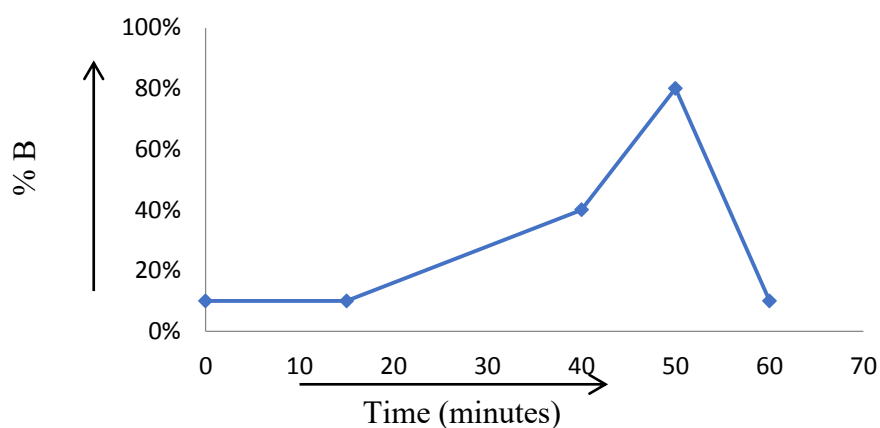


**Figure 1.3** Graph of mobile phase gradient elution

## 2.6.2   Sample Preparation for LC-MS Analysis

1 g of each methanolic and 20% hydromethanolic extracts were dissolved in 10 mL of respective solvents. The solutions were diluted to 1mg/mL in particle free Eppendorf tube.

## 2.7   Gas Chromatography-Mass Spectrometry (GC-MS)

GC-MS is a hyphenated analytical technique that exhibits separation properties of GC along with the structural exploration of constituents by MS which provide high efficiency of sample analysis. It is used to identify the volatile, semi-volatile and lipophilic components such as hydrocarbons, steroids and fatty acids etc.
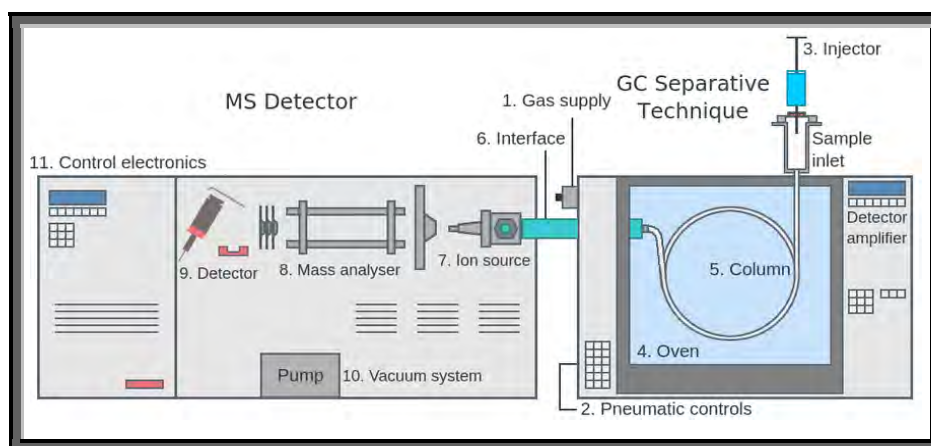
**Figure 1.4** Schematic diagram of GC-MS system

### 2.7.1 Instrumental Specifications

Agilent Technologies GC-MS with model No. 6890 N and Agilent JW Scientific DB-5MS column with dimensions (30 m × 0.25 mm internal diameter × 0.25 $\mu$m film thickness) with stationary phase composed of 5% phenyl-methyl poly siloxane was used. There was a split-less capillary inlet and the mode of injection was manual. Temperature of oven was maintained within the range of 120 ℃ to 280 ℃ having an increment of 10 ℃ per minute. Helium was used as carrier gas at a flow rate of 1 mL/minute. MS having EI mode with 0-1000 *a.m.u.* mass range was employed for GC-MS analysis.

### 2.7.2 Sample Preparation for GC-MS Analysis

1 g crude *n*-hexane extract was dissolved in 10 mL of respective solvent and filtered to remove suspended particles. It was diluted to 1 mg/mL concentration of solution in a clean and dried Eppendorf tube.

24

# 3 CHAPTER 3: RESULTS AND DISCUSSIONS

## 3.1 Percentage Extraction Yield

The calculation of percentage extraction yield is quantitative assessment of constituents dissolved in different solvents used during extraction procedure. Percentage extraction yields for leaves" extracts of *Rhaphidophora decursiva* by reflux using *n*-hexane, methanol and 20% hydromethanol was calculated which is tabulated below in **table 1.3**. Variation in the percentage extraction yields of different extracts depicted the solubility of phytochemicals with the corresponding solvents. Constituents like flavonoid glycosides, phenolics and sugars are highly soluble in polar solvents while lipophilic chemical constituents are preferably more soluble in less polar solvents.

**Table 1.3** Extraction yields of RDL

| Extracts | Mass of leaves taken (g) | Mass of dried extract (g) | Extraction yield (%) |
|---|---|---|---|
| RDH | 10 | 1.2 | 12 |
| RDM | 10 | 2.0 | 20 |
| RDHM | 10 | 3.5 | 35 |

The solubility of constituents depends upon the structure of constituents, nature of the solvent and affinity of constituents with different solvents. It was inferred from the percentage extraction yields that leaves of *Rhaphidophora decursiva* are richer in hydrophilic constituents than lipophilic components as they showed the maximum percentage extraction yield in polar solvents and minimum percentage extraction yield in non-polar solvents.
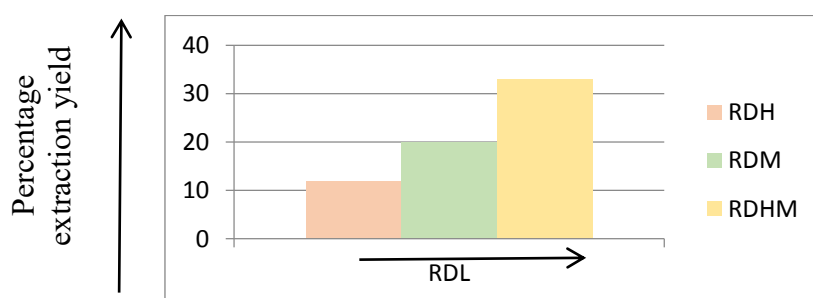


**Figure 1.5** Graphical representation of percentage extraction yields of RDL extracts

## 3.2  Two-Dimensional Paper Chromatography

Preliminary analysis was done by using two-dimensional paper chromatography for the identification of possible phytoconstituents especially phenolic components in the extracts. BAW and 15% acetic acid were used as a mobile phases for the assessment of level of hydroxylation and glycosylation of present constituents. The color of spots and $R_f$ values helped in the recognition of subgroups of flavonoids family. The components separated were visualized under UV lamp4. **Figure 1.6** depicts the 2D PCs of methanolic and 20% hydromethanolic extracts.
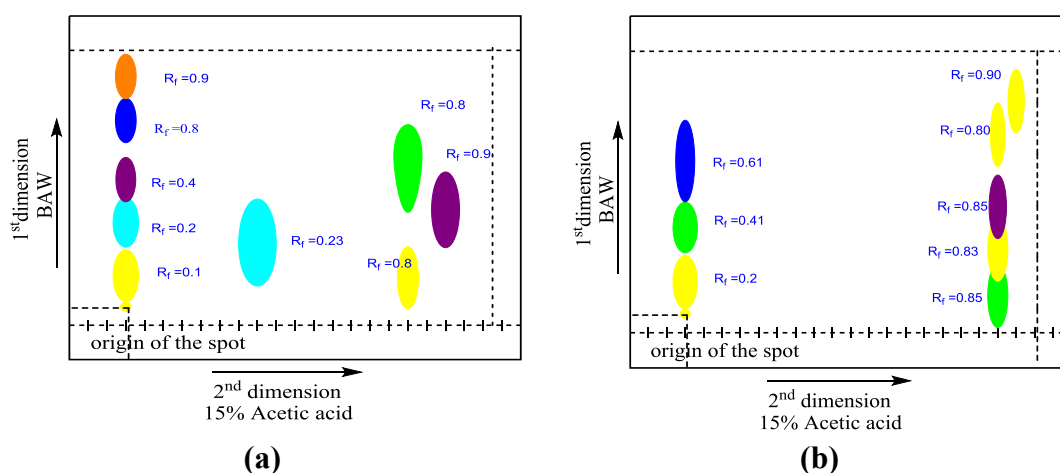


**Figure 1.6** Visualization of colors of spots on 2D PC of methanolic (a) and 20% hydromethanolic extract (b)

The colors of the spots and possible inferences about the structures of flavonoid glycosides present in the methanolic and 20% hydromethanolic extracts are given below in the **table 1.4**.

**Table 1.4** Interpretation of 2D PC results of methanolic extract

| Color of the spots | Color of spots after ammonia exposure | Inference |
|---|---|---|
| **Yellow**  **Yellow orange**  **Yellow green** | No change in color | Flavonols with free 3-hydroxy and with or without a free 5-hydroxy |

| Sky blue | No change in color | Isoflavones lacking free 5-hydroxy |
|---|---|---|
| **Purple** | No change in color | a. Flavones or 3-*O*-substituted flavonols with 5-hydroxy but lacking a free 4′-hydroxy<br>b. Some 6 or 8-hydroxy flavones and 3-*O*-substituted flavonols with 5-hydroxy<br>c. Isoflavones, dihydroflavonols, biflavonyls and some 5-hydroxy flavanones<br>d. Chalcones with 2′-or 6′-hydroxy but without a free 2 or 4-hydroxy |

In first dimension, separation was based upon the number of free –OH groups attached on the aglycone moiety. Higher the number of –OH groups, lesser was the $R_f$ values and vice versa. Separation in second dimension was based upon the level of glycosylation, greater the number of sugars linked to the flavonoid moiety higher was the $R_f$ value and vice versa. It was inferred from the paper chromatograms that both extracts were enriched with various flavonoid glycosides. Methanolic extract showed yellow, purple and sky blue spots on 2D paper chromatogram that indicated the existence of flavones, isoflavones and flavonols. The 20% hydromethanolic extract showed the yellow spots in both dimensions that indicated the presence of flavonols with 3-hydroxy and with or without free 5-hydroxy majorly. The $R_f$ values predicted the existence of dihydoxy, trihydroxy and monohydroxy flavonoids and monoglycosides, diglycosides, triglycosides and tetraglycosides in both the extracts.

## 3.3   Acid Hydrolysis

The acid hydrolysis for methanolic extract of *Rhaphidophora decursiva* was performed to visualize and identify the nature of glycone moieties by co-chromatography. It is evident from the literature that *O*-linked sugar moieties are more prone to acid hydrolysis than *C*-linked sugar moieties. By comparing $R_f$ values of hydrolysate and standard sugars it was concluded that two sugars namely glucose and xylose were present in the hydrolysate of methanolic extract. **Figure 1.7** showed the results of co-chromatogram.
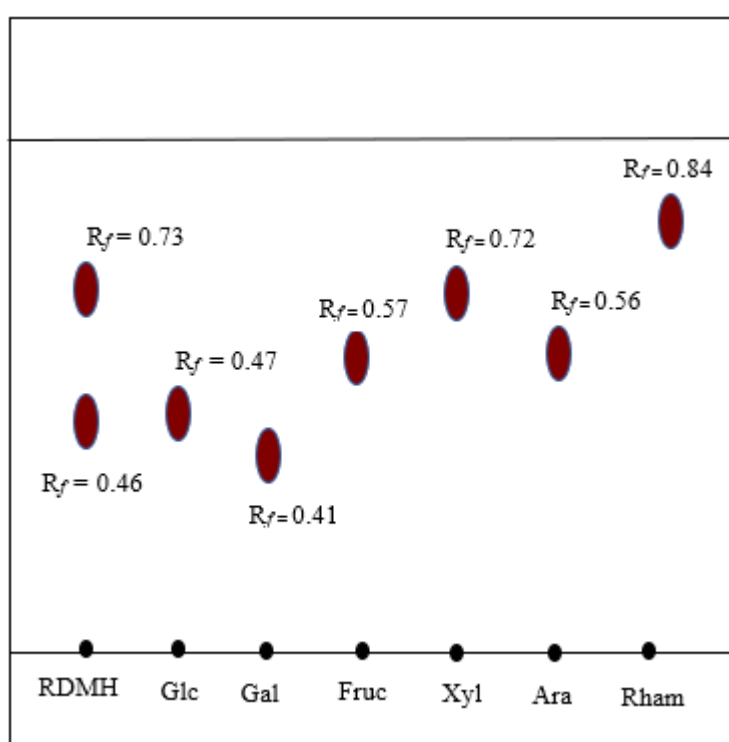


**Figure 1.7** Co-chromatogram of hydrolysate and standard sugars

It was observed in **table 1.5** that the $R_f$ values of hydrolysate were close to the $R_f$ values of standard glucose and xylose sugar. Hence, the results of acid hydrolysis suggested that the methanolic extract enriched in glucose and xylose.

**Table 1.5** R$_f$ values of standard sugars and hydrolysate

| Standard sugars | R$_f$ value of standard sugars | R$_f$ value of sugars identified in RDMH |
|---|---|---|
| Glucose | 0.47 | 0.46 |
| Galactose | 0.41 | - |
| Fructose | 0.55 | - |
| Xylose | 0.69 | 0.69 |
| Arabinose | 0.56 | - |
| Rhamnose | 0.84 | - |

## 3.4 HPLC-DAD-ESI-MS Analysis of RDM

HPLC profile of methanolic extract of *Rhaphidophora decursiva* leaves depicted the elution of compound based on their retention times. Chromatographic profile described the elution of compounds starting from highly hydrophilic constituents such as phenolic acids and polyglycoside compounds followed by tetraglycosides, triglycosides, diglycosides and ultimately monoglycosides to aglycones Compounds were certified on the basis of their DAD and mass spectrum. Diode Array Detector predicted the absorption bands of compounds corresponding to different wavelengths in UV-Visible region. Mass Spectrum gave an idea about the masses and the fragmentation patterns.

### 3.4.1 Identification of RDM-1

The compound eluted from the HPLC column at the retention time of 2.9 minutes was labeled RDM-1 as shown in the **figure 1.8**. At this retention, the composition of mobile phase was 10 % acetonitrile in deionized water. It indicated the presence of highly hydrophilic constituent like polyphenolic or polyglycosidic compound.
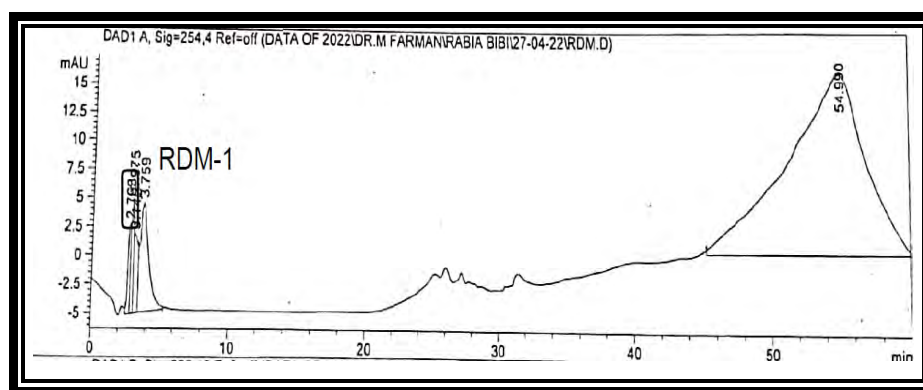
**Figure 1.8** HPLC profile of RDM-1

Diode array spectrum of RDM-1 showed only one prominent band at 265 *nm* which resembled the significant UV absorption band of gallic acid as reported by **Asfaram et al., (2017)**. The DAD spectrum of the RDM-1 is given below in the **figure 1.9**.
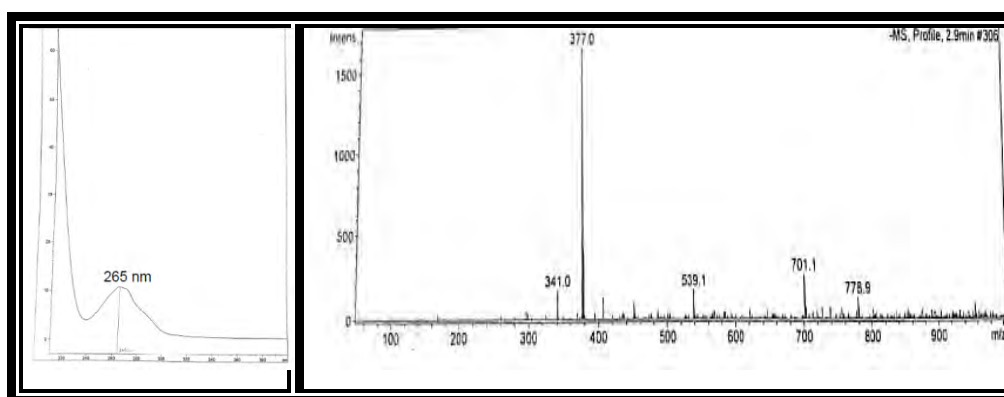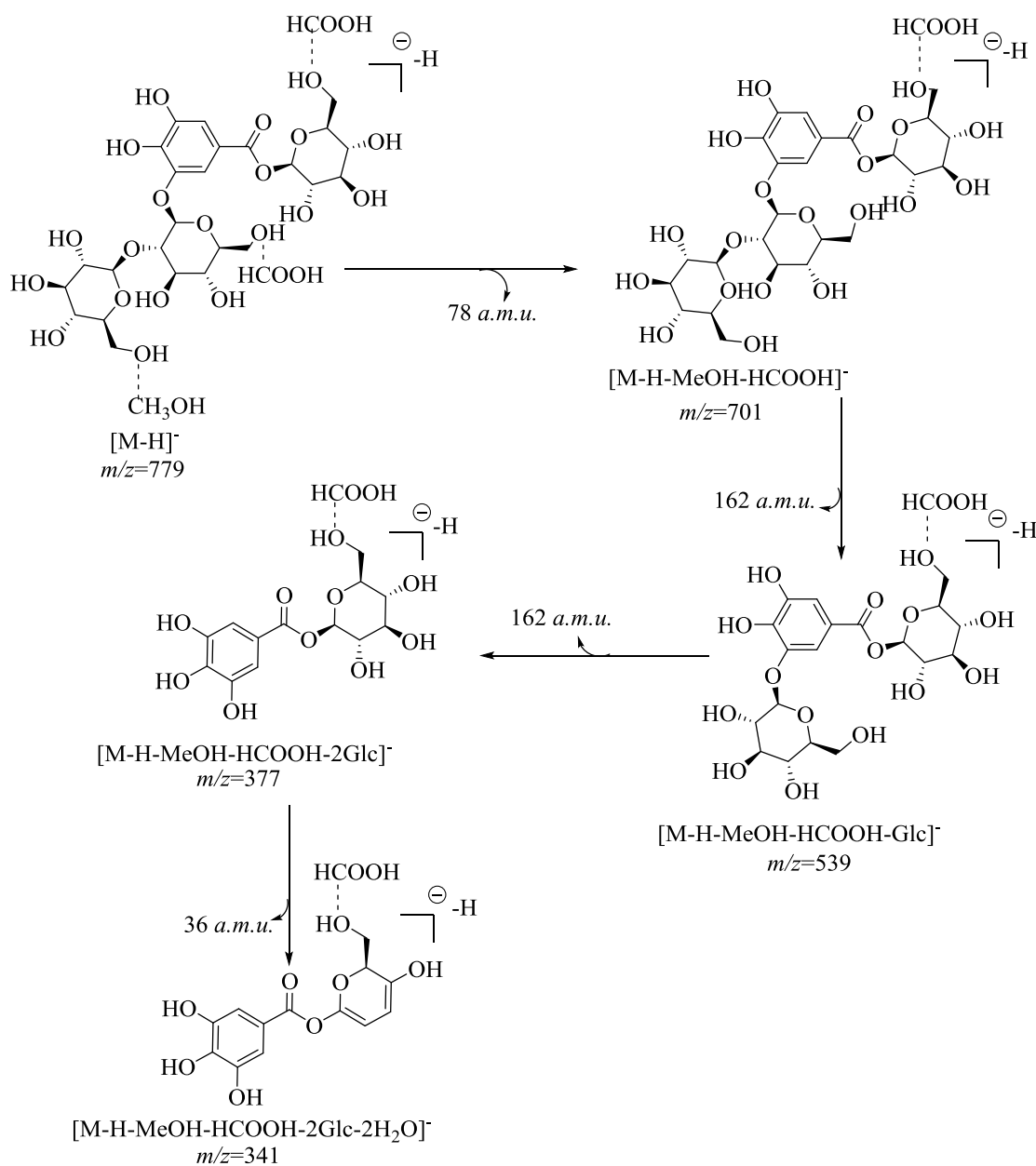


**Figure 1.9** DAD and mass spectrum of RDM-1

Mass spectrum exhibited the molecular ion peak in deprotonated mode at *m/z* 779 so the actual mass of the compound was inferred as 780 *a.m.u.* The molecular ion peak at *m/z* 779 [M-H]⁻ corresponding to 3-O-[*β*-D-glucopyranosyl-(1→2)-β-D-glucopyranoside]-1-O-*β*-D-glucopyranosyl gallate forming adduct along with two formic acid molecules and one methanol molecule. The removal of formic acid and methanol from the molecular ionic peak resulted in the peak at *m/z* 701. By the subsequent loss of two glucose moieties from peak at *m/z* 701, the base peak appeared at *m/z* 377 as mentioned by **Anttonen and Karjalainen (2006)**. This confirmed the presence of two hexose moieties on gallic acid **(Asfaram *et al.*, 2017)**. The peak at *m/z* 377 corresponded to [M-H+HCOOH-2(Glc)-MeOH-HCOOH]⁻. The elimination of 36 *a.m.u.* from peak at *m/z* 377 gave rise to the peak at *m/z* 341. It corresponded to the ejection of two water molecules from the hexose moiety connected to the carboxyl

position of gallic acid **(Krenek _et al.,_ 2014)**. The fragmentation scheme of RDM-1 compound is given below in the **scheme 1.1**.



**Scheme 1.1** Fragmentation scheme of RDM-1

The retention time, UV and mass spectrum of RDM-1 assured the name of the proposed structure as 3-_O_-[_β_-D-glucopyranosyl-(1→2)-_β_-D-glucopyranosyl]-1-_O_-_β_-D-glucopyranosyl gallate.
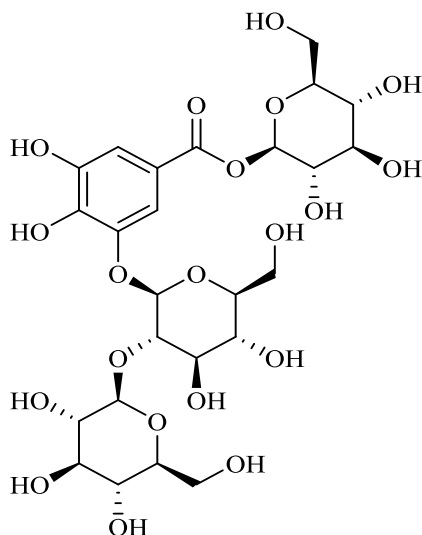
**3-*O*-[*β*-D-glucopyranosyl-(1→2)-*β*-D-glucopyranoside]-1-*O*-*β*-D-glucopyranosyl gallate**

### 3.4.2   Identification of RDM-2

The compound eluted from the HPLC column at retention time of 4.0 was labeled as RDM-2 as shown in the **figure 1.10**.
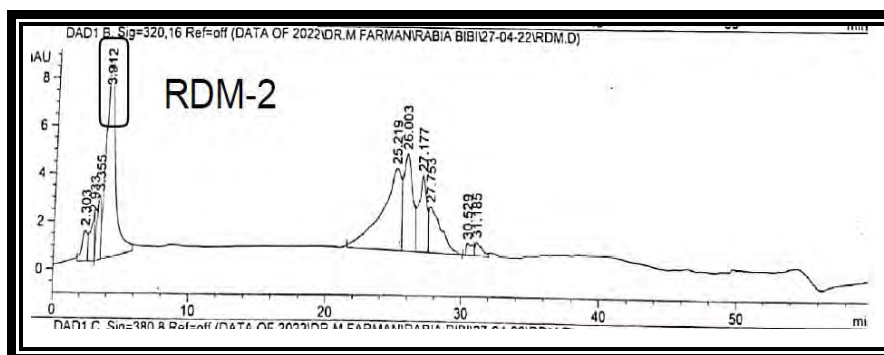


**Figure 1.10** HPLC profile of RDM-2

The composition of mobile phase at that time was 10% acetonitrile in deionized water. These composition of mobile phase certified the highly hydrophilic character of the eluted compound.

DAD spectrum of RDM-2 disclosed the two absorption bands. Band-II appeared at 270 *nm* and band-I appeared to be at 330 *nm*. The intensity of the band-II is a bit higher than the intensity of band-I. These bands were very closely related to the UV bands of the derivative of benzoic acid that is gentisic acid **(Sakushima *et al.*, 1995)**.

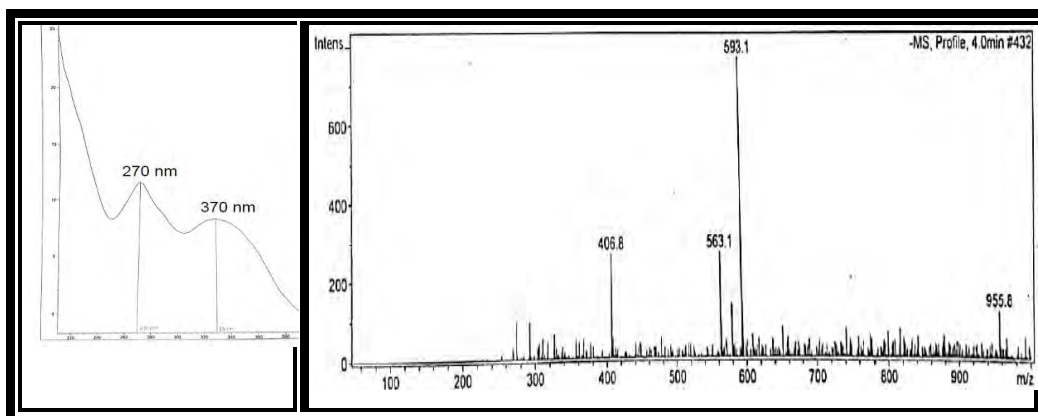**Figure 1.11** DAD and mass spectrum of RDM-2

The analysis of RDM-2 was probed in a deprotonated mode. The molecular ion peak was detected at $m/z$ 956. So, the actual mass of the compound was 957 *a.m.u.* The molecular ionic peak was validated by the adduct molecule *i.e.,* [M-H+2H$_2$O]$^-$. The peak at $m/z$ 593 [M-H-2H$_2$O-Xyl-gallyl-acetyl]$^-$ originated by the loss of 363 *a.m.u.* from the molecular ionic peak. The loss of 363 *a.m.u* was justified by the elimination of 132 *a.m.u* .along with 152 *a.m.u.* from parent ion peak which indicated the presence of gallic acid at xylose sugar **(Taylor *et al.,* 1998)**. Along with this the removal of two water molecules that were present in the form of adduct and loss of acetyl group from molecular ionic peak **(Wang *et al.,* 2004)**. The next fragment ion peak emerged to be at $m/z$ 563 due to the removal of 30 *a.m.u.* corresponding to $^{2,3}$X cleavage from the xylose sugar **(Salpin and Tortajada 2002)**. The fragment ion observed at $m/z$ 407 [M-H-2H$_2$O-2(xyl)-gallyl-acetyl-3H$_2$O]$^-$ appeared by the loss of 186 *a.m.u.* from the peak at $m/z$ 593. The loss corresponded to the removal of xylose r and three water molecules, one water molecule from gallic acid as mentioned by **Fabregat *et al.,* (2013)** and two water molecules from the xylose sugar attached at the 5$^{th}$ position of gentisic acid. The fragmentation pathway is shown in the **scheme 1.2**.
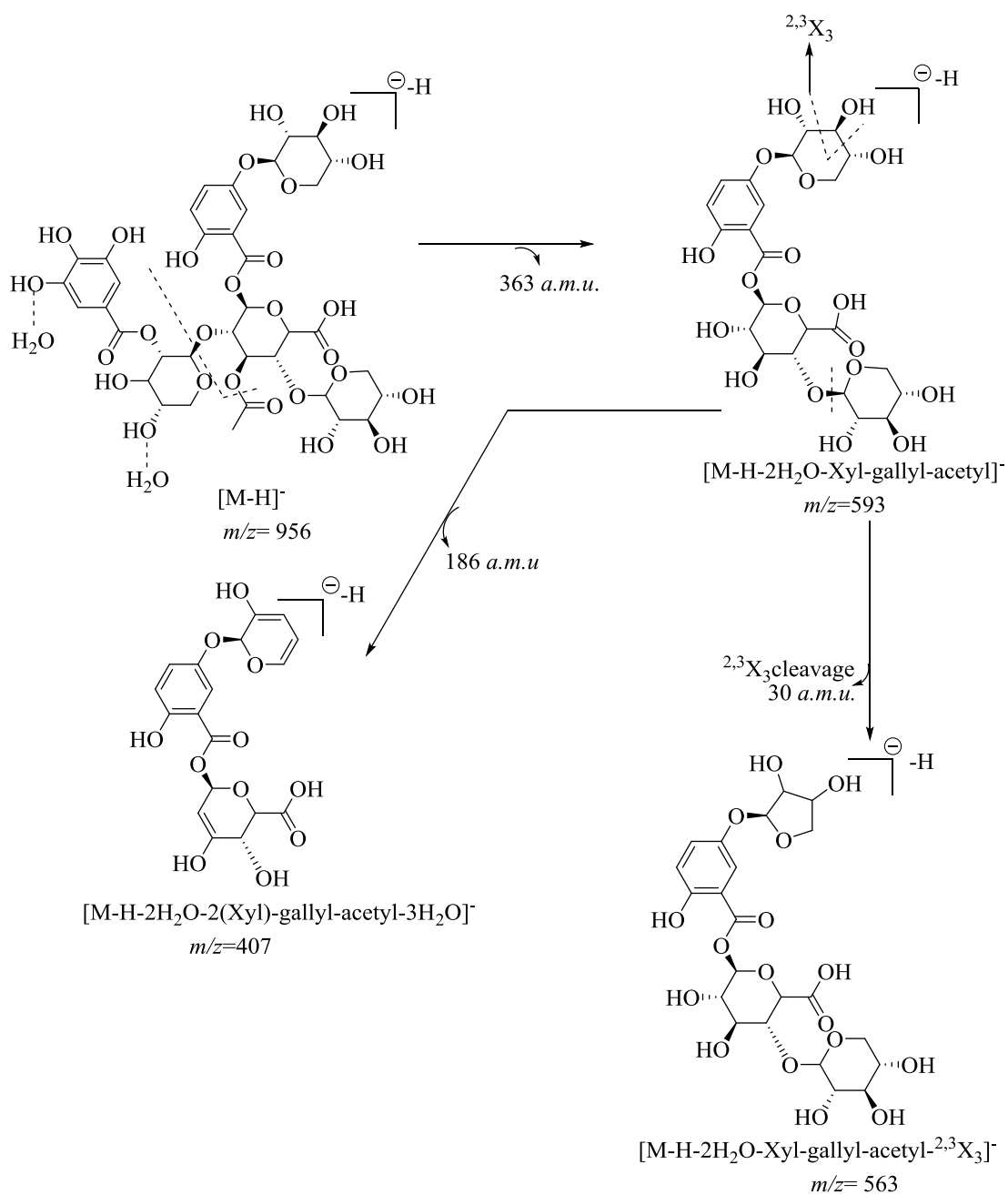
**Scheme 1.2** Fragmentation pathway of RDM-2

The compound was identified as 5-*O*-*β*-D-xylopyranoside-1-*O*-[2′-(2′′-gallyl)-*β*-D-xylopyranosyl-(1→2)]-3′-*O*-acetyl-4′-*O*-*β*-D-xylopyranosyl-(1→4)-glucuronosyl gentisate.
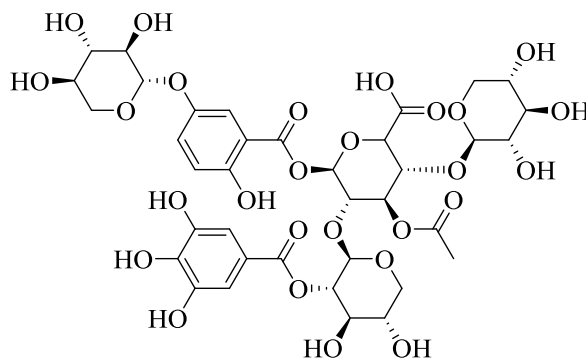
**5-*O*-*β*-D-xylopyranoside-1-*O*-[2´-(2´´-gallyl)- *β*-D-xylopyranosyl-(1→2)]-3´-*O*-acetyl-4´-*O*- *β*-D-xylopyranosyl-(1→4)-glucuronosyl gentisate**

### 3.4.3   Identification of RDM-3

The compound eluted from the HPLC column at retention time of 25.2 minutes is labeled as RDM-3 as shown in the **figure 1.12**.
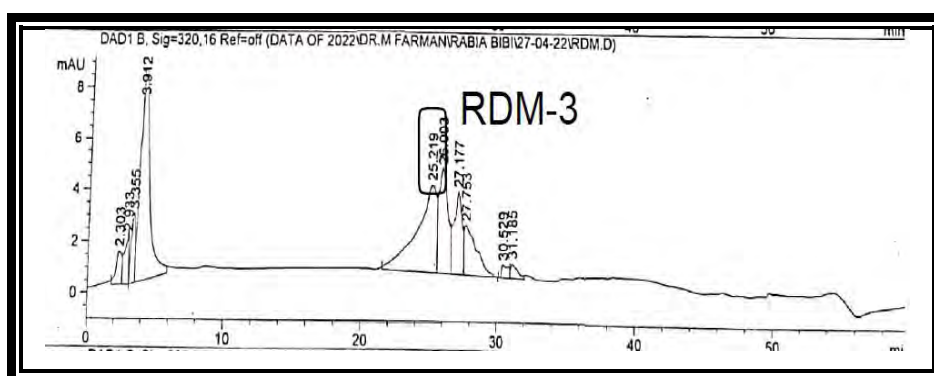


**Figure 1.12** HPLC profile of RDM-3

The compound eluted from the HPLC column exhibited a retention time of 25.2 minutes. The composition of mobile phase at this retention time was 20% acetonitrile in 80% of deionized water. At this retention time tetraglycosidic, triglycosidic or diglycosidic compound might be eluted which was further confirmed by the UV and mass spectrum.

The UV spectrum of RDM-3 displayed two band patterns. Band-I came out at $\lambda_{max}$ 335 *nm* and band-II emerged to be at $\lambda_{max}$ 270 *nm*. The absorption values on the UV spectrum of the eluted compound showed the characteristic band patterns of flavone moiety. The $\lambda_{max}$ value of absorption band-II indicated the level of hydroxylation on ring-A. It could be tri or di hydroxylated (**Markham *et al.,* 1982)**. The shape of bands

and their corresponding $\lambda_{max}$ values are closely related to the UV spectrum of isovitexin as reported by **Mabry _et al.,_ (1970)**.
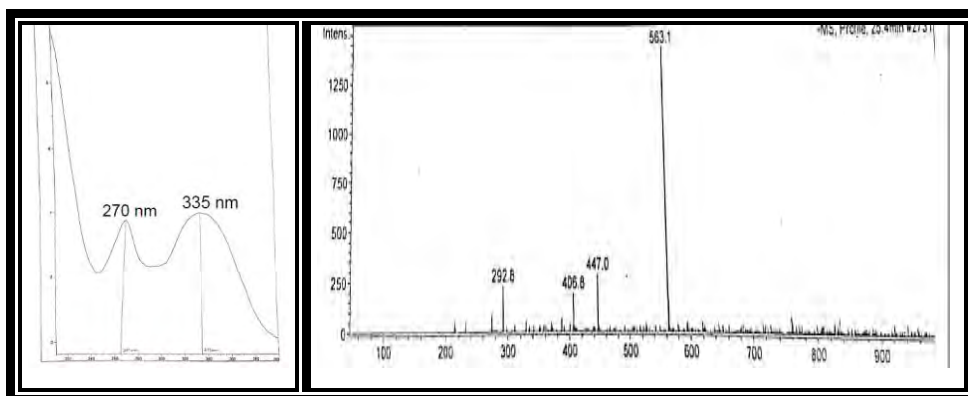


**Figure 1.13** DAD and mass spectrum of RDM-3

Mass spectrum of RDM-3 exhibited the molecular ion peak in negative ionization mode at _m/z_ 563 so the actual mass of the compound was 564 _a.m.u._ The peak at _m/z_ 447 [M-H-$^{0,3}$X-2CO]$^-$ indicated the presence of xylose moiety at 4′ position of aglycan nucleus as reported by **Mashima _et al.,_ (2019)**. It was formed by the $^{0,3}$X cleavage along with the loss of two CO from the aglycan moiety. The next peak at _m/z_ 407 [M-H-2H$_2$O-$^{0,2}$X]$^-$ originated by the loss of 156 _a.m.u._ corresponded to the loss of two water molecules from the _O_-linked xylose and $^{0,2}$X cleavage from _C_-linked glucose. The removal of two water molecules from xylose sugar as documented by **Chapagain _et al.,_ (2007)** and $^{0,2}$X fragment show the presence of glucose moiety at 6$^{th}$ position via _C_-linkage **(Cao _et al.,_ 2014)**. The last peak originated at _m/z_ 293 [M-H-xylose-H$_2$O-$^{0,2}$X]$^-$ by the loss of 270 _a.m.u._ $^{0,2}$X cleavage was observed from glucose moiety upon condensation with the OH group on the fifth position of ring-A as a result five membered ring was formed by the elimination of water **(Cuyckens and Claeys 2004)**. The fragmentation pattern for RDM-3 is given below in the **scheme 1.3**.
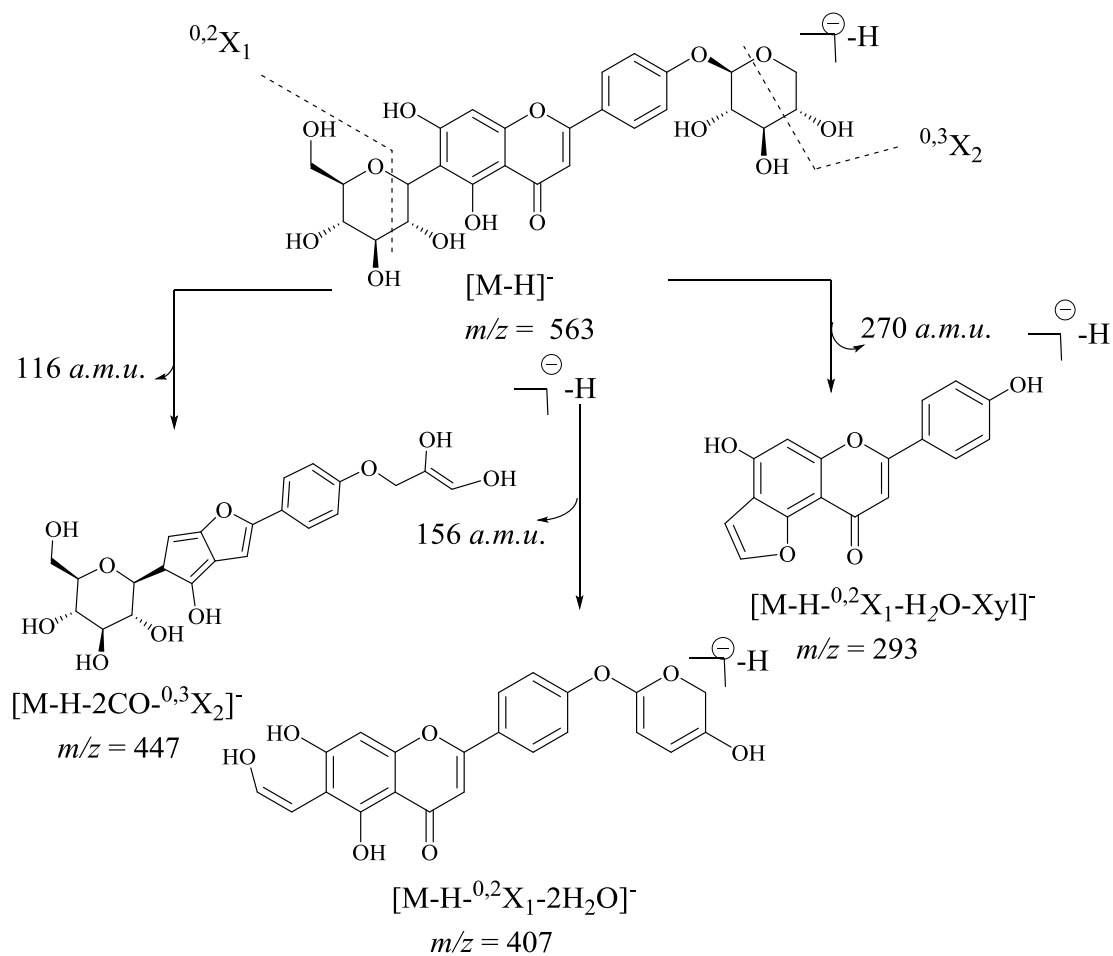
**Scheme 1.3** Fragmentation pathway of RDM-3

Information from retention time, DAD spectrum and mass fragmentation revealed the eluted compound as 4′-*O*-*β*-D-xylopyranosyl-6-*C*-*β*-D-glucopyranosyl apigenin.
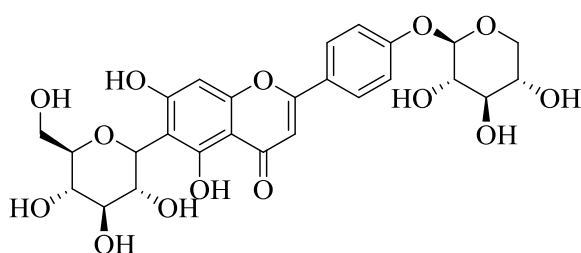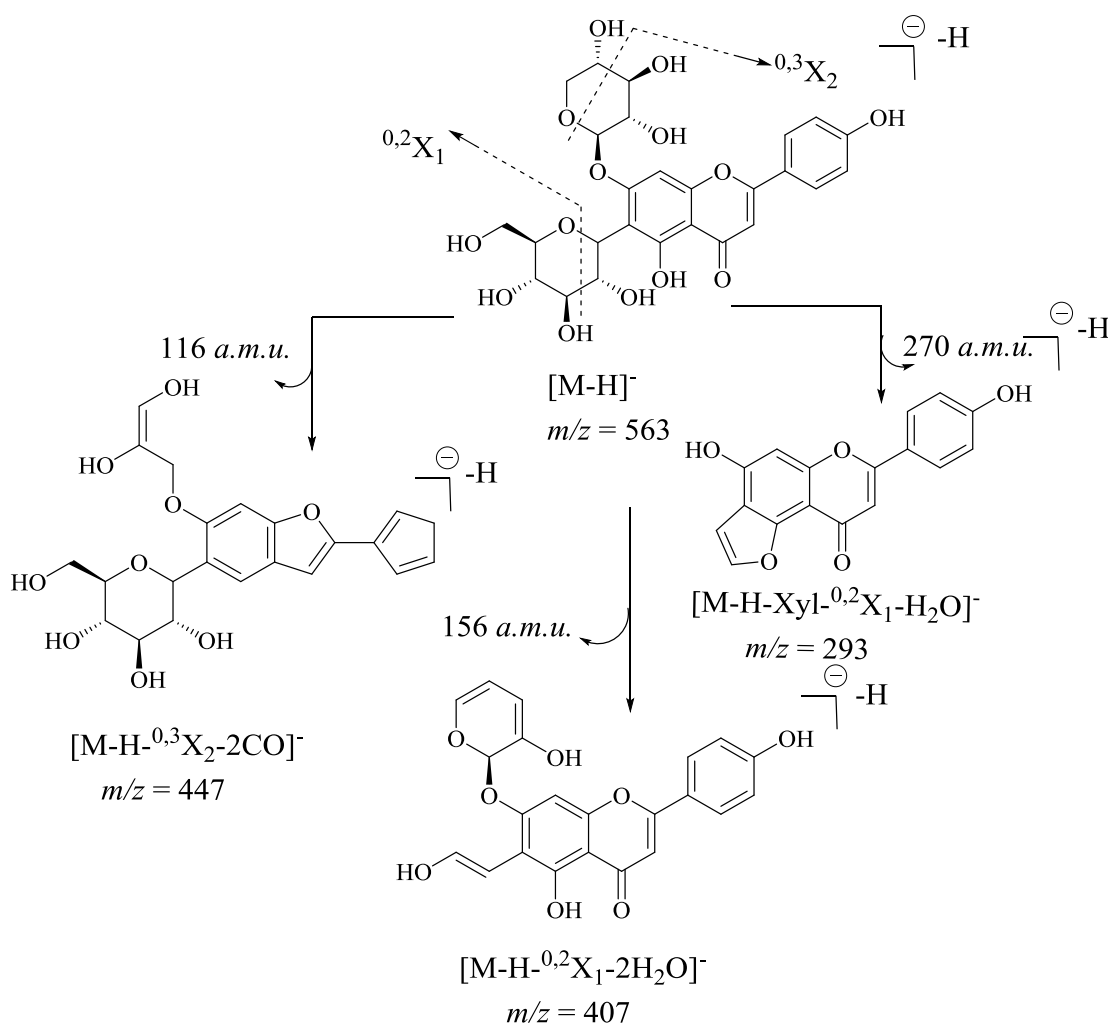


**4′-*O*-*β*-D-xylopyranosyl-6-*C*-*β*-D-glucopyranosyl apigenin**
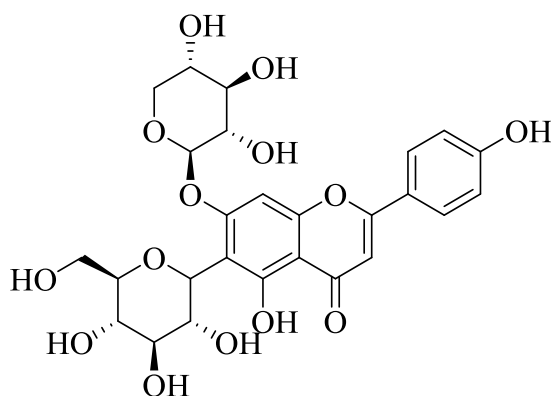
### 3.4.4 Identification of RDM-4

The signal highlighted below in the HPLC chromatogram was labeled as RDM-4 which is below in the **figure 1.14**.

**Figure 1.14** HPLC profile of RDM-4

The compound eluted from the HPLC column at retention time of 26.2 minutes. At this time, the composition of mobile phase was 21% acetonitrile in 79% of water. It predicted the presence of hydrophilic compound.

The DAD spectrum revealed the two band pattern. Band-I appeared at $\lambda_{max}$ 335 *nm* and band-II at $\lambda_{max}$ 265 *nm* as shown in the **figure 1.15**. The UV spectrum resembled the *C* glycoside *i.e.,* isovitexin but the hypsochromic shift was observed in the band-I due to the presence of sugar moiety on the ring-A of aglycan molecule **(Mabry *et al.,* 1970)**. The UV spectrum of RDM-4 was similar to that of RDM-3. So, it was inferred that RDM-4 might be an isomer of RDM-3. The DAD spectrum and mass spectrum of RDM-4 is given below in the **figure 1.15**.



**Figure 1.15** DAD and mass spectrum of RDM-4

Mass spectrum data of RDM-4 indicated the molecular ion peak at *m/z* 563 in deprotonated ionization mode. Hence, the actual mass of the compound was 564 *a.m.u.* The daughter ion peak at *m/z* 447 represented as [M-H-2CO-$^{0,3}$X] ⁻, appeared by the loss of two units of carbon monoxide **(Cao *et al.,* 2014)** along with $^{0,3}$X cleavage from the xylose sugar. The next fragment ion peak observed at *m/z* 407 [M-

H-2H$_2$O-$^{0,2}$X]$^-$ by the removal of 156 *a.m.u.* from molecular ionic peak. It corresponded to the loss of two water molecules from the xylose moiety **(Chapagain and Wiesman 2007)** and $^{0,2}$X cleavage (loss of 120 *a.m.u*) suggested the presence of glucose. The last fragment ion peak originated at *m/z* 293. This peak appeared by the elimination of 270 *a.m.u.* corresponding to the removal of pentose group, $^{0,2}$X cleavage and elimination of water molecule as a result formation of five membered ring occurred **(Cuyckens and Claeys 2004)**. It was justified as [M-H-xylosyl-$^{0,2}$X-H$_2$O]$^-$. The fragmentation pathway of RDM-4 is given below in the **scheme 1.4**.



**Scheme 1.4** Fragmentation pathway of RDM-4

From the given information, the nomenclature for the RDM-4 compound could be designated as 6-*C*-*β*-D-glucopyranosyl-7-*O*-*β*-D-xylopyranosyl apigenin.

**6-*C*- *β*-D-glucopyranosyl-7-*O*- *β*-D-xylopyranosyl apigenin**

### 3.4.5 Identification of RDM-5

The compound highlighted in the HPLC chromatogram as shown in the **figure 1.16** was recognized as RDM-5. Further information was acquired from retention time, UV and mass spectrum.
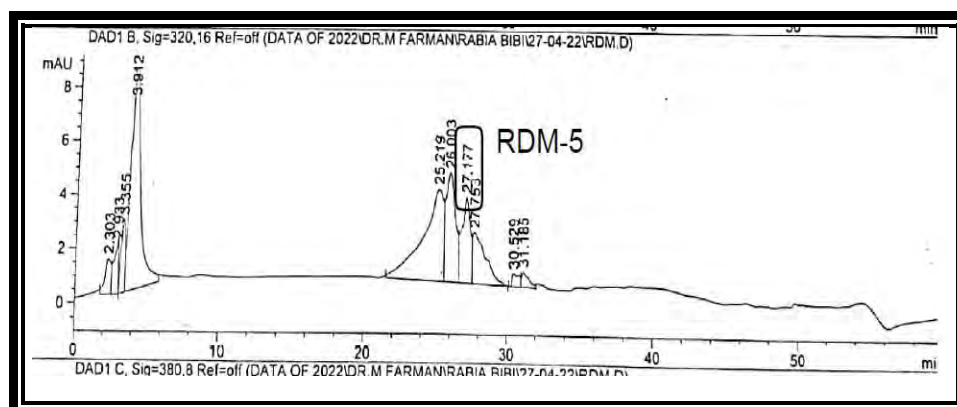


**Figure 1.16** HPLC profile of RDM-5

The HPLC profile displayed the retention time of the compound RDM-5 as 27.2 minutes. At this retention time, the composition of mobile phase as 22% acetonitrile in 78% water indicating the hydrophilic nature of the eluted compound RDM-5.

DAD response displayed the typical two band pattern of flavonoids. Band-I at $\lambda_{max}$ 335 *nm* while band-II at $\lambda_{max}$ value of 265 *nm*. The shape, intensity and the UV spectrum of RDM-5 was similar to the UV spectrum of RDM-4. It was predicted that RDM-5 could be the isomer of RDM-4 and the $\lambda_{max}$ values resembled the UV spectrum of vitexin as reported by **Mabry *et al.,* (2012)**. The UV spectrum of RDM-5 is given below in the **figure1.17**.
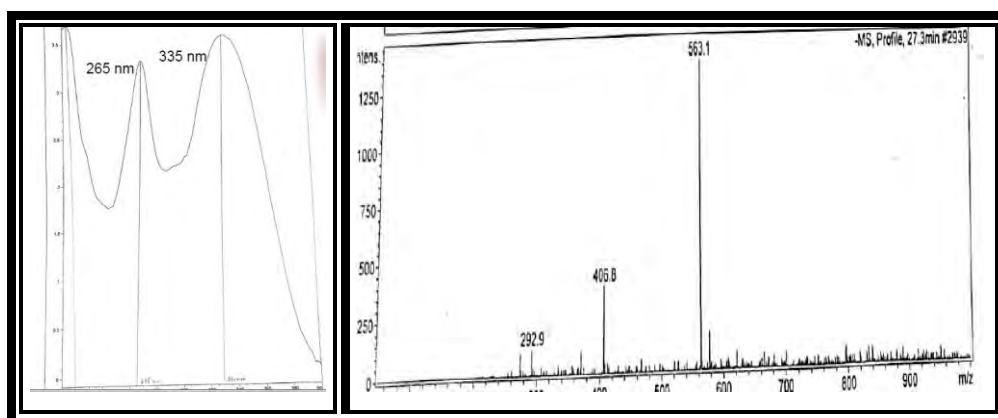
**Figure 1.17** DAD and mass spectrum of RDM-5

Mass spectrum of RDM-5 showed deprotonated molecular ion peak at *m/z* 563 [M-H]⁻ while the neutral mass of the compound was 564 *a.m.u.* The daughter ion peak at *m/z* 407 represented as [M-$^{0,2}$X-2H$_2$O]⁻ appeared on the MS upon the loss of 156 *a.m.u.* It corresponded to the removal of two water molecules **(Chapagain and Wiesman 2007)** from the pentose and inter-glycosidic cleavage that is $^{0,2}$X cleavage from the hexose moiety **(Cuyckens and Claeys 2004).** The last deprotonated peak at *m/z* 293 originated by the removal of 270 *a.m.u* from [M-H]⁻ loss of pentose sugar from 7th position as reported by **Shui and Peng (2004)** along with elimination of water molecule and $^{0,2}$X cleavage confirmed the presence of *C*-linked glucose at 8th position **(Cao *et al.,* 2014)**. It resulted in the formation of five membered ring at 8th position as mentioned by **Tao *et al.,* (2015).** The fragmentation scheme is given below in the **scheme 1.5**.
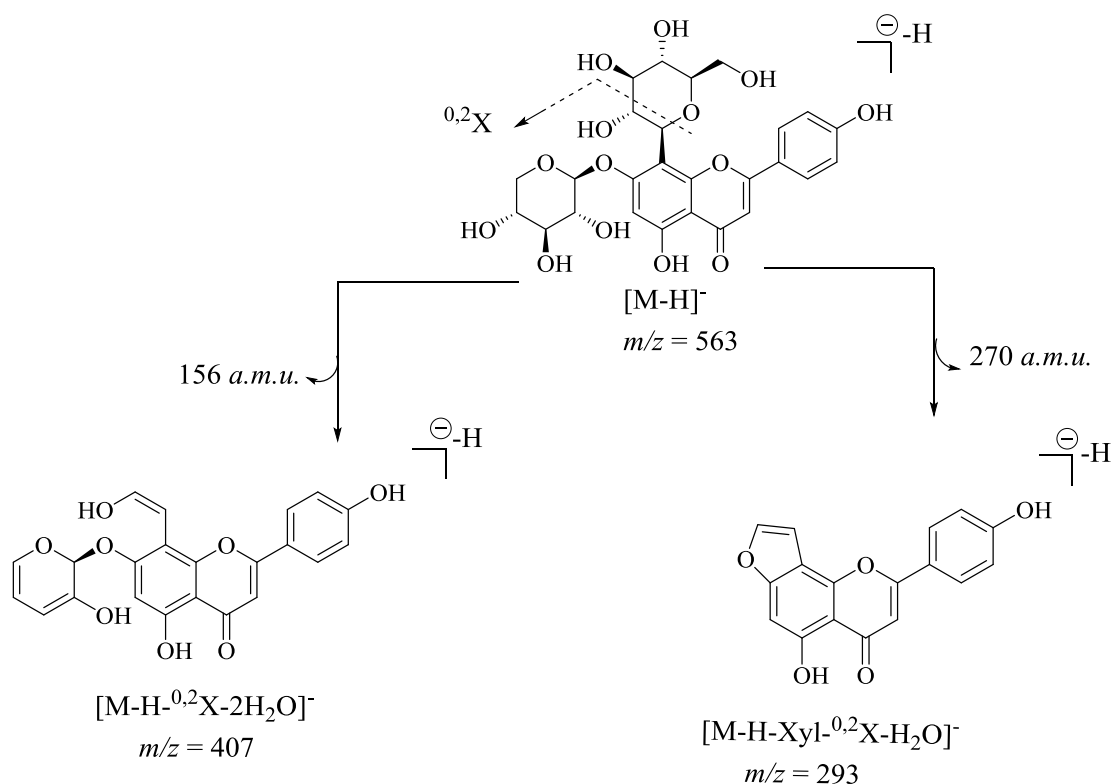
**Scheme 1.5** Fragmentation scheme of RDM-5

Evidences from the HPLC chromatogram, retention time, UV and mass spectrum indicated that the identified compound is the isomer of RDM-3 and RDM-4. The suggested name for this compound is 7-*O*- *β*-D-xylopyranosyl-8-*C*- *β*-D-glucopyranosyl apigenin.
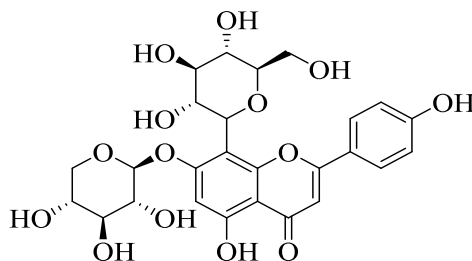


**7-*O*- *β*-D-xylopyranosyl-8-*C*- *β*-D-glucopyranosyl apigenin**

### 3.4.6 Identification of RDM-6

The compound mentioned below on the HPLC profile is RDM-6 as shown in the **figure 1.18**. The retention time, DAD spectrum and MS of RDM-6 is described below.
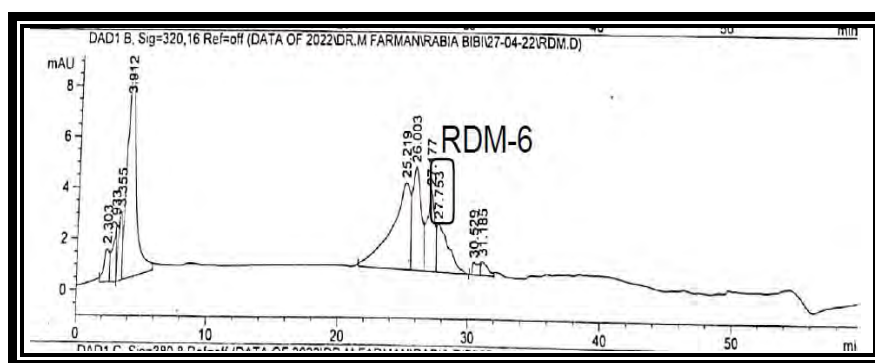
**Figure 1.18** HPLC profile of RDM-6

The compound RDM-6 marked on HPLC profile eluted at retention time of 27.9 minutes. This time corresponded to the mobile phase composition with 22% acetonitrile in 78% of water. This indicated the hydrophilic nature of the compound.

UV spectrum of RDM-6 showed two-band pattern of flavonoid. The $\lambda_{max}$ value of band-I appeared at $\lambda_{max}$ 330 *nm* and band-II at $\lambda_{max}$ 270 *nm*. It showed resembled the UV spectrum of vitexin as mentioned by **Mabry *et al.*, (2012)**. The hypsochromic shift in band-I indicated the glycosylation on ring-B. Mass spectrum and cleavage patterns further confirmed the structure of compound RDM-6.
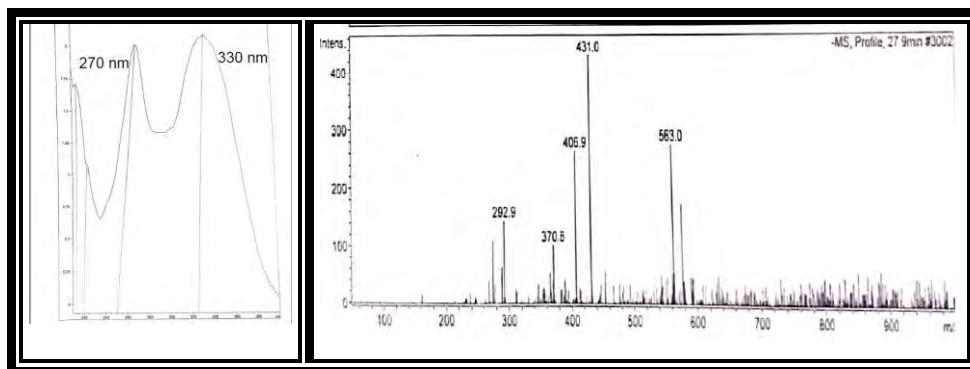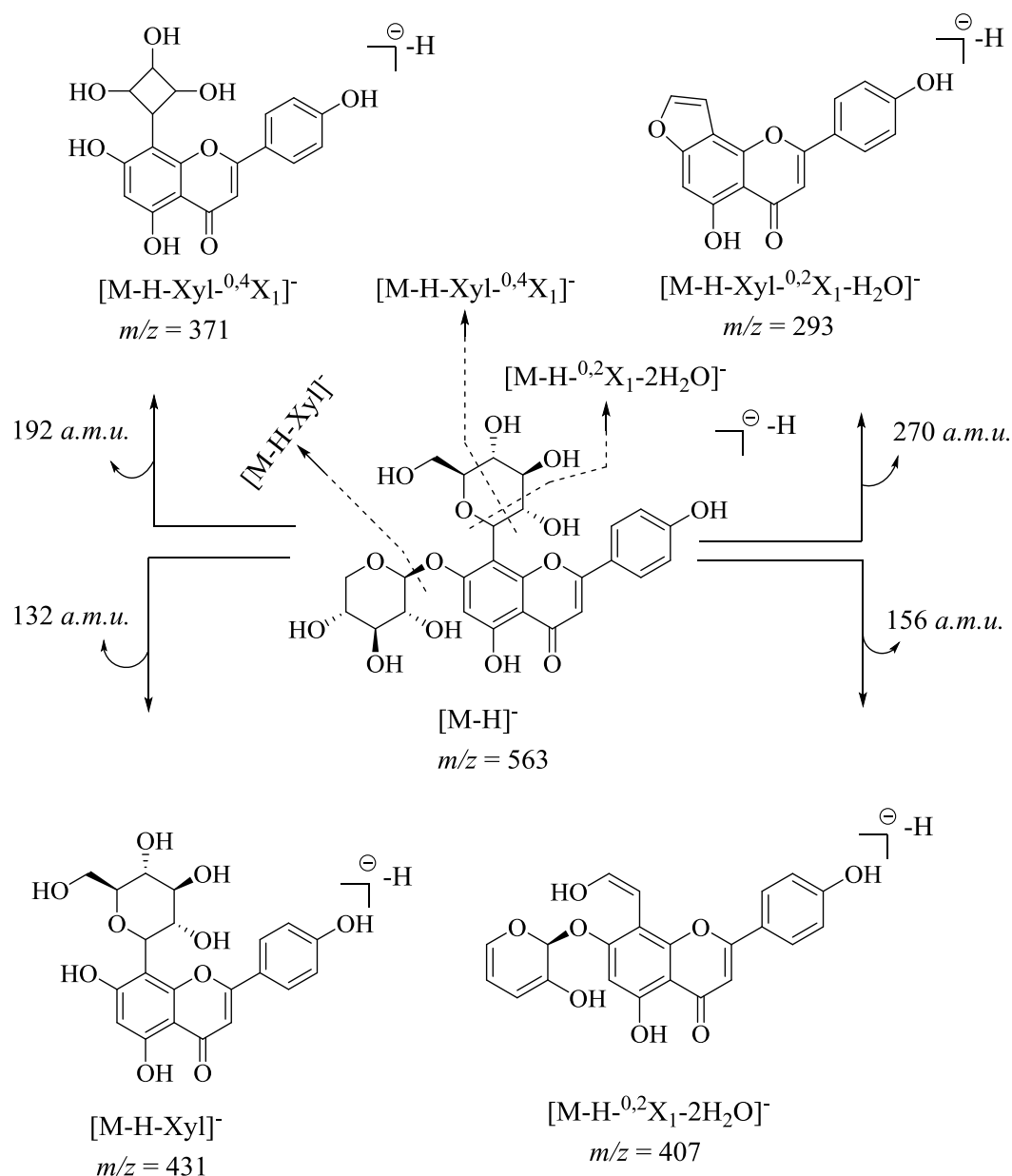


**Figure 1.19** DAD and mass spectrum of RDM-6

Deprotonated molecular ion peak of compound RDM-6 appeared at *m/z* 563 as [M-H]$^-$. Hence, the actual mass of the compound was 564 *a.m.u.* The base peak appeared at *m/z* 431 due to the loss of 132 *a.m.u.* which indicated the presence of xylose moiety **(Mashima *et al.*, 2019)**. This peak is represented as [M-H-Xyl]$^-$. The next fragment ion peak appeared at *m/z* 407 [M-H-2H$_2$O-$^{0,2}$X]$^-$ by the loss of two water molecules from xylose sugar as documented by **Chapagain and Wiesman (2007)** along with $^{0,2}$X cleavage in hexose moiety. The loss of 192 *a.m.u.* occurred from the parent ion peak gave rise to fragment peak at *m/z* 371 as [M-H-Xyl-$^{0,4}$X]$^-$. The loss of 192 *a.m.u.*

corresponded to pentose sugar and $^{0,4}X$ cleavage from the *C*-linked glucose as reported by **Roowi and Crozier (2011)**. The emergence of last fragment ion peak at *m/z* 293 attributed to the loss of 270 *a.m.u.* from the parent ion. The elimination of 270 *a.m.u.* corresponded to the removal of pentose sugar and $^{0,2}X$ cleavage assured the *C*-linked glucose. The five membered furan ring at C-8 position was formed by the loss of water molecule as mentioned by **Toa *et al.,* (2015)**. This led to the peak at *m/z* 293. The fragmentation pathway of RDM-6 is given below in the **scheme1.6**.



$[M-H-Xyl-^{0,4}X_1]^-$
*m/z* = 371

$[M-H-Xyl-^{0,4}X_1]^-$

$[M-H-Xyl-^{0,2}X_1-H_2O]^-$
*m/z* = 293

$[M-H-^{0,2}X_1-2H_2O]^-$

192 *a.m.u.*

$[M-H-Xyl]^-$

270 *a.m.u.*

132 *a.m.u.*

156 *a.m.u.*

$[M-H]^-$
*m/z* = 563

$[M-H-Xyl]^-$
*m/z* = 431

$[M-H-^{0,2}X_1-2H_2O]^-$
*m/z* = 407

**Scheme 1.6** Fragmentation pathway for RDM-6

The evidences from HPLC chromatogram, DAD spectrum and mass spectrum clearly indicated the identified compound as 7-*O*-*β*-D-xylopyranosyl-8-*C*-*β*-D-glucopyranosyl apigenin.
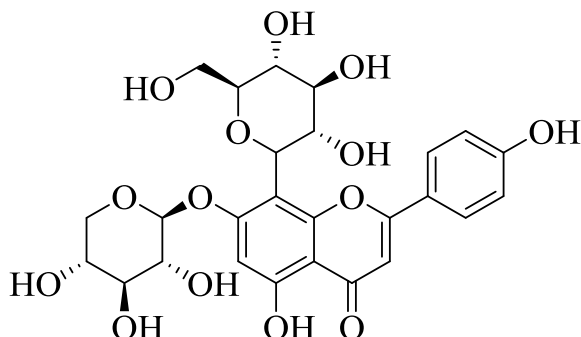


**7-*O*-*β*-D-xylopyranosyl-8-*C*-*β*-D-glucopyranosyl apigenin**

### 3.4.7    Identification of RDM-7

The compound marked on the HPLC profile was mentioned as RDM-7 at retention time of 31.3 minutes shown in the **figure 1.20**. The detailed structure elucidation of compound RDM-7 is stated below.
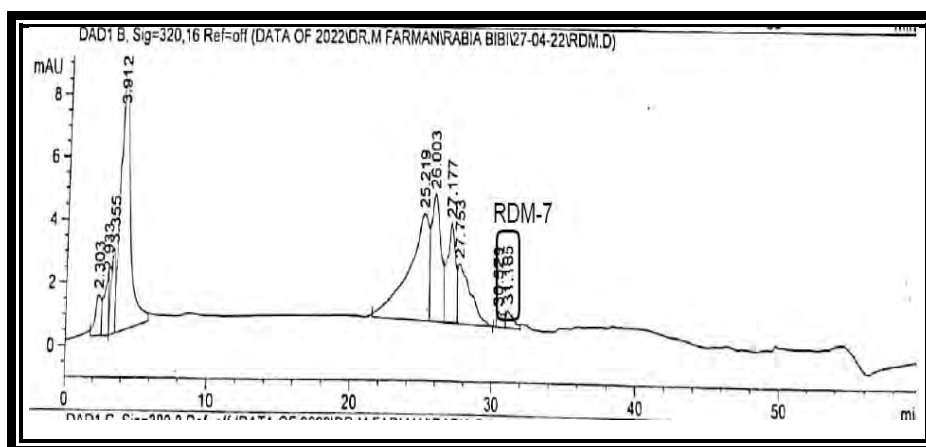


**Figure 1.20** HPLC profile of RDM-7

The mobile phase composition at this time was 24% acetonitrile in 76% deionized water. The mobile phase composition showed the presence of tri or diglycosidic compound.

UV spectrum revealed the two characteristic bands of flavonoid. Band-II of the spectrum showed the $\lambda_{max}$ value at 266 *nm* and band-I at $\lambda_{max}$ 336 *nm*. The shape of the band and their corresponding absorption values resembled the absorption values

of acacetin as reported by **Markovic and Tosovic (2015)**. The DAD spectrum of RDM-7 is given below in the **figure 1.21**.
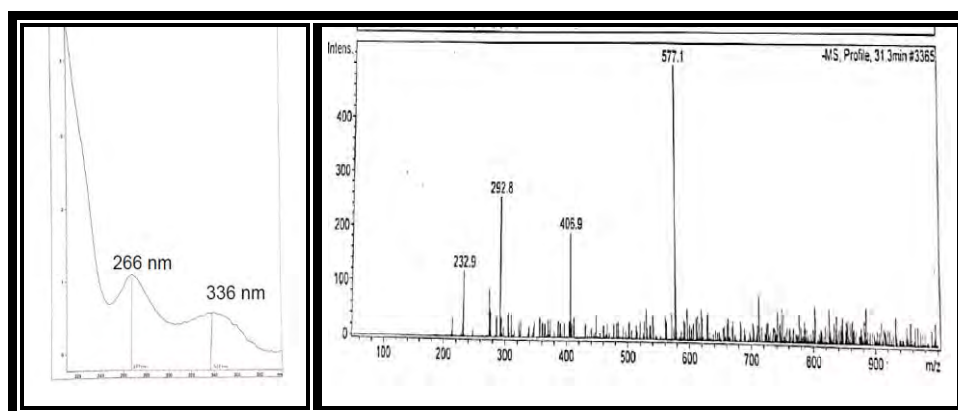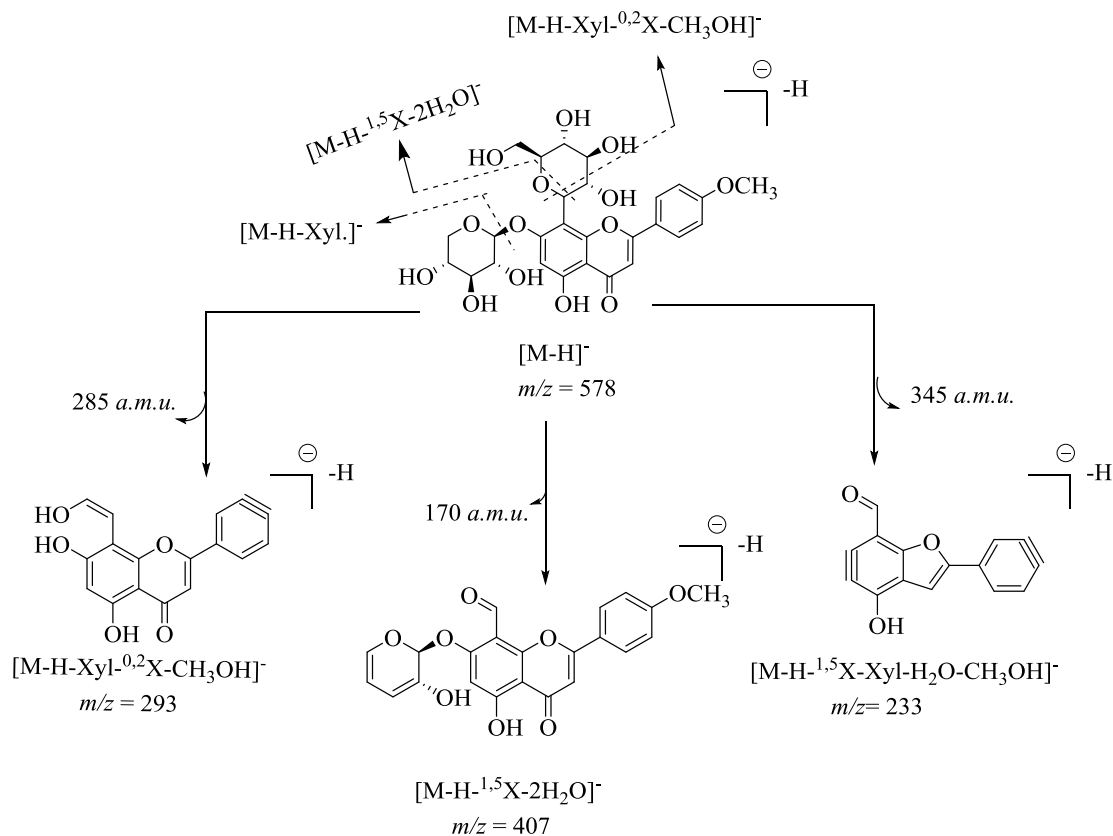


**Figure 1.21** DAD and mass spectrum of RDM-7

Mass spectrum of RDM-7 revealed the molecular ion peak in deprotonated mode at $m/z$ 577 [M-H]⁻. Hence, the actual mass of the compound was 578 *a.m.u.* The first fragment ion peak appeared at $m/z$ 407 [M-H- $^{1,5}$X-2H$_2$O]⁻ by the loss of 170 *a.m.u.* from parent ion that corresponds to the $^{1,5}$X cross ring cleavage of hexose sugar as reported by **Cuyckens *et al.,* (2004)** indicated the presence of glucopyranose along with the removal of two water molecule from the xylose sugar **(Chapagain and Wiesman 2007)**. The next fragment ion peak was observed at $m/z$ 293 [M-H-$^{0,2}$X-Xyl-CH$_3$OH]⁻ by the elimination of 284 *a.m.u.* from molecular ion peak. It was justified by the $^{0,2}$X cleavage of *C*-linked glucose unit, removal of xylosyl sugar and neutral loss of methanol from ring-B. The neutral loss of methanol indicated the existence of methoxy group at 4′ position **(Carbone *et al.,* 2004)**. The removal of 344 *a.m.u.* from the parent molecular ion peak resulted in the formation of fragment ion peak at $m/z$ 233 as [M-H-$^{1,5}$X-Xyl-H$_2$O-CH$_3$OH]⁻. The loss of 344 *a.m.u.* corresponded to the $^{1,5}$X cleavage from glucose and elimination of xylose. The subsequent loss of water molecule resulted in the formation of benzyne ring **(Tao *et al.,* 2015)**. The fragmentation scheme of RDM-7 is given below in the **scheme 1.7**.

$[M-H-Xyl^{0,2}X-CH_3OH]^-$

$[M-H^{1,5}X-2H_2O]^-$

$[M-H-Xyl.]^-$

$[M-H]^-$
$m/z = 578$

285 *a.m.u.*

345 *a.m.u.*

170 *a.m.u.*

$[M-H-Xyl^{0,2}X-CH_3OH]^-$
$m/z = 293$

$[M-H^{1,5}X-2H_2O]^-$
$m/z = 407$

$[M-H^{1,5}X-Xyl-H_2O-CH_3OH]^-$
$m/z= 233$

**Scheme 1.7** Fragmentation scheme of RDM-7

The structure for the compound was suggested according to retention time, DAD spectrum and mass spectrum of RDM-7. The suggested name for RDM-7 is 7-*O*-*β*-D-xylopyranosyl-8-*C*-*β*-D-glucopyranosyl acacetin.
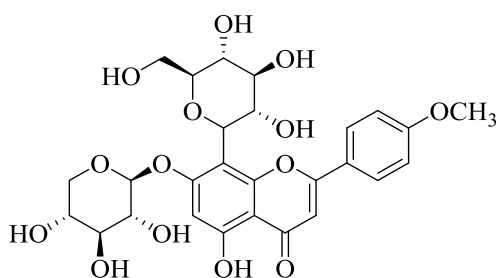


**7-O-*β*-D-xylopyranosyl-8-C-*β*-D-glucopyranosyl acacetin**

The compounds identified from the methanolic extract are enlisted in the **table 1.6**.

**Table 1.6** Compounds identified from RDM extract

| Compounds with codes | Retention time ($R_t$) (minutes) | $\lambda_{max}$ values (*nm*) | Molecular ion peak (*m/z*) [M-H]⁻ | Name of the identified compound |
|---|---|---|---|---|
| **RDM-1** | 2.9 | 265 | 779 | 3-*O*-[*β*-D-glucopyranosyl-(1→2)-*β*-D-glucopyranoside]-1-*O*-*β*-D-glucopyranosyl gallate |
| **RDM-2** | 4.0 | 270, 330 | 956 | 5-*O*-*β*-D-xylopyranoside-1-*O*-[2′-(2′′-galloyl)-*β*-D-xylopyranosyl-(1→2)]-3′-*O*-acetyl-4′-*O*-*β*-D-xylopyranosyl-(1→4)-glucuronosyl gentisate |
| **RDM-3** | 25.2 | 270, 335 | 563 | 4′-*O*-*β*-D-xylopyranosyl-6-*C*-*β*-D-glucopyranosyl apigenin |
| **RDM-4** | 26.0 | 265, 335 | 563 | 6-*C*- *β*-D-glucopyranosyl-7-*O*- *β*-D-xylopyranosyl apigenin |
| **RDM-5** | 27.1 | 265, 330 | 563 | 7-*O*-*β*-D-xylopyranosyl-8-*C*-*β*-D-glucopyranosyl apigenin |
| **RDM-6** | 27.9 | 270, 330 | 563 | 7-*O*-*β*-D-xylopyranosyl-8-*C*-*β*-D-glucopyranosyl apigenin |
| **RDM-7** | 31.1 | 266, 336 | 577 | 7-*O*-*β*-D-xylopyranosyl-8-*C*-*β*-D-glucopyranosyl acacetin |

## 3.5 HPLC-DAD-ESI-MS Analysis of RDHM

The 20% hydromethanolic extract showed the higher percentage extraction yield. It showed the presence of hydrophilic compounds like polyphenolics in a greater amount. These compounds were identified by using HPLC-DAD-ESI-MS technique.

### 3.5.1 Identification of RDHM-1

The signal appeared at retention time of 2.9 minutes was labeled as RDHM-1. The HPLC profile of RDHM-1 is given below in the **figure 1.22**.
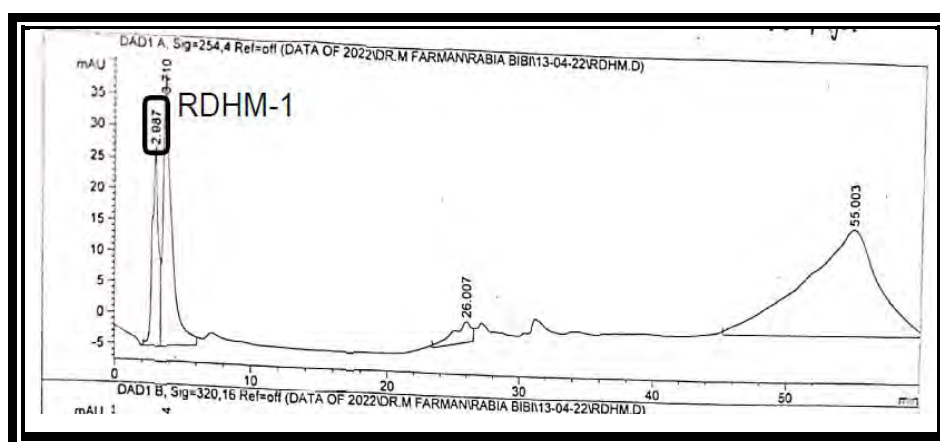


**Figure 1.22** HPLC profile of RDHM-1

The compound was eluted from HPLC column at retention time of 2.9 minutes. At this retention time, the mobile phase composition was 10% acetonitrile and 90% water. It was predicted that the eluted compound was polyphenolic or polyglycosidic compounds in nature. Further confirmation was done by DAD and MS.

DAD spectrum of RDHM-1 compound showed a single absorption band at 270 *nm*. It resembled the significant UV absorption band of Gallic acid as reported by **Asfaram et al.,(2017)**. The DAD spectrum of the RDHM-1 is given below in the **figure 1.23**.
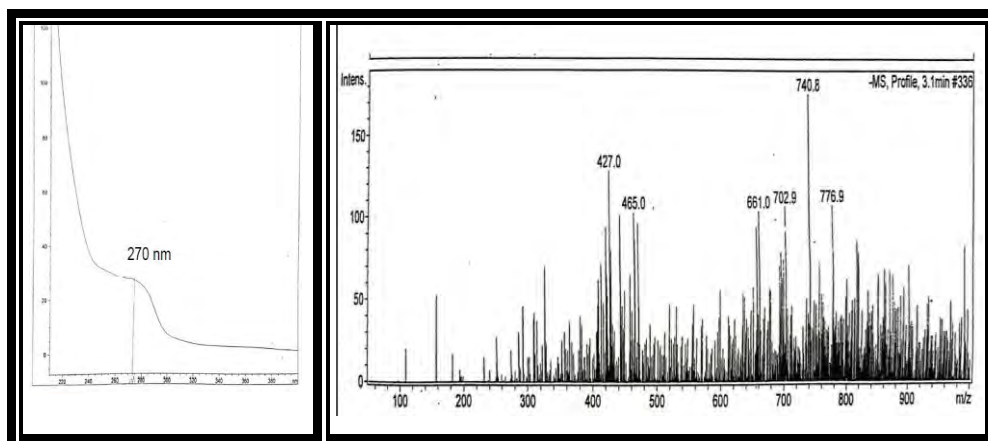
**Figure 1.23** DAD and mass spectrum of RDHM-1

The molecular ion peak of RDHM-1 appeared at *m/z* 777 [M-H+H$_2$O+MeOH]$^-$ in deprotonated mode. So, the actual mass of the compound was 778 *a.m.u.* The signal at *m/z* 741 indicated the removal of two water molecules from the xylose sugar. The fragment peak at *m/z* 703 was observed by the loss of 74 *a.m.u.* from molecular ion peak. It corresponded to the $^{4,5}$X cleavage of glucose sugar along with elimination of formaldehyde group from xylose sugar. The daughter ion peak at *m/z* 661 corresponded to the loss of methanol and water as an adduct along with removal of two water molecules from the xylose sugar and $^{2,3}$X cleavage from glucose sugar attached at the 3$^{rd}$ position of gallic acid. The loss of 312 *a.m.u.* fragment from molecular ion peak resulted in the peak at *m/z* 465. The loss of 312 *a.m.u.* fragment corresponded to the removal of glucose, one xylose sugar and water loss from remaining xylose sugar. The last fragment ion peak at *m/z* 427 was observed by the loss of two xylosyl moieties and loss of two water molecules from the glucose sugar along with the elimination of methanol and water as adducts. The fragmentation pattern for RDHM-1 is given in the **scheme 1.8**.
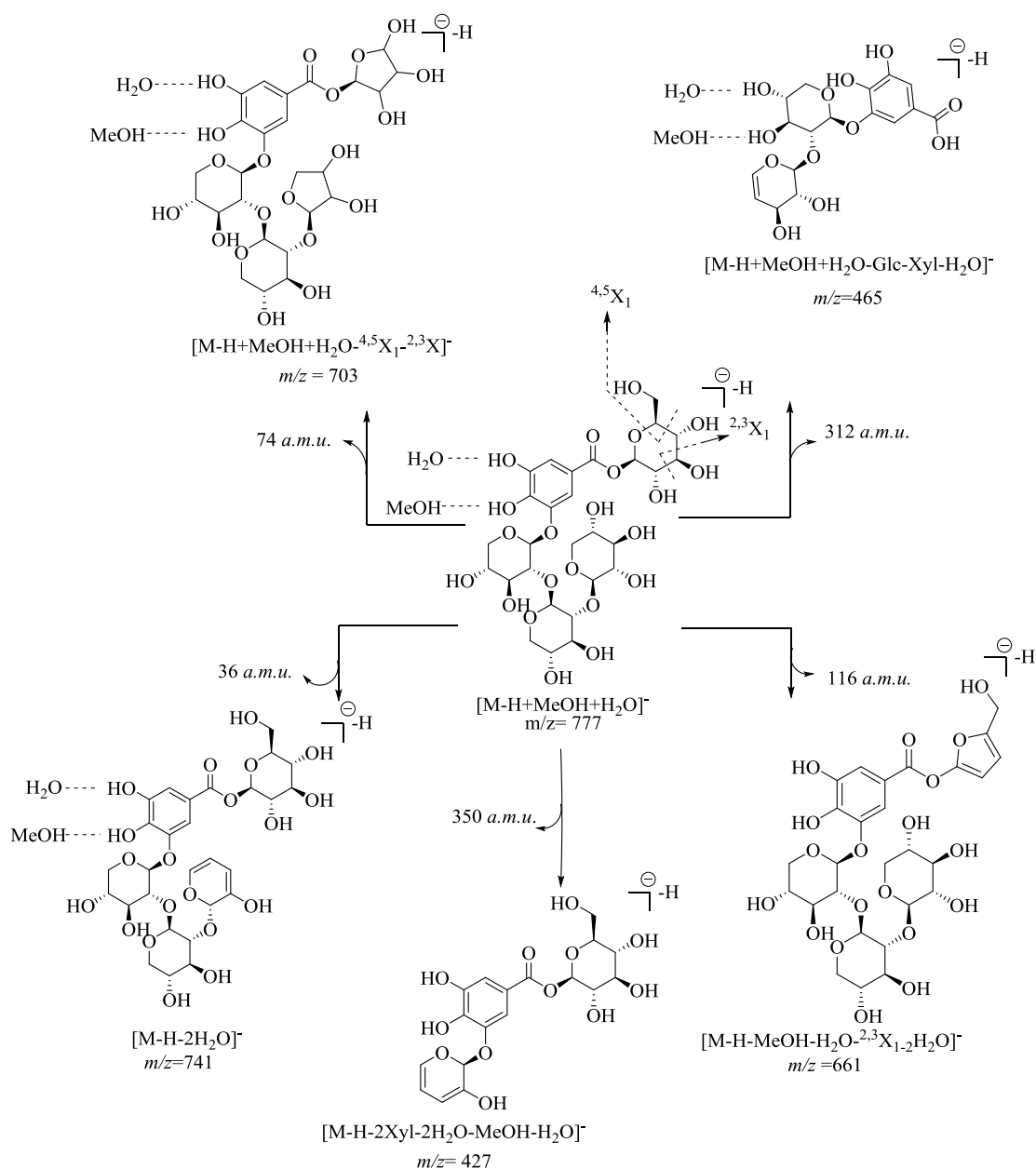
**Scheme 1.8** Fragmentation scheme for RDHM-1

The structure for the compound named as 3-*O*-[β-D-xylopyranosyl-(1→2)-β-D-xylopyranoside]-1-*O*-β-D-glucopyranosyl gallate
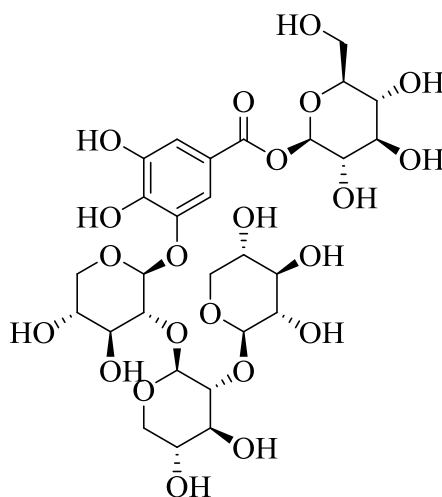
**3-*O*-[*β*-D-xylopyranosyl-(1→2)-*β*-D-xylopyranoside]-1-*O*-*β*-D-glucopyranosyl gallate**

### 3.5.2 Identification of RDHM-2

The compound eluted from HPLC column at retention time of 3.9 minutes was labeled as RDHM-2. The composition of mobile phase at that time was 10% acetonitrile in deionized water. The compositions of mobile phase certified the highly hydrophilic character of the eluted compound. The HPLC profile of the compound is given in the **figure 1.24**.
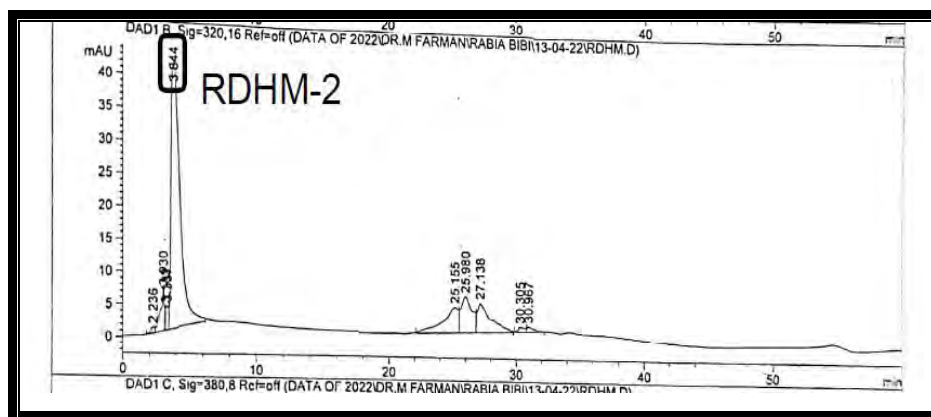


**Figure 1.24** HPLC profile of RDHM-2

The UV spectrum of compound revealed two bands. Band-II appeared at 270 *nm* and band-I appeared to be at 330 *nm*. The intensity of the band-II is slightly higher than the intensity of band-I. These bands were very closely related to the UV bands of the derivative of benzoic acid that is gentisic acid **(Sakushima *et al.*, 1995)**.
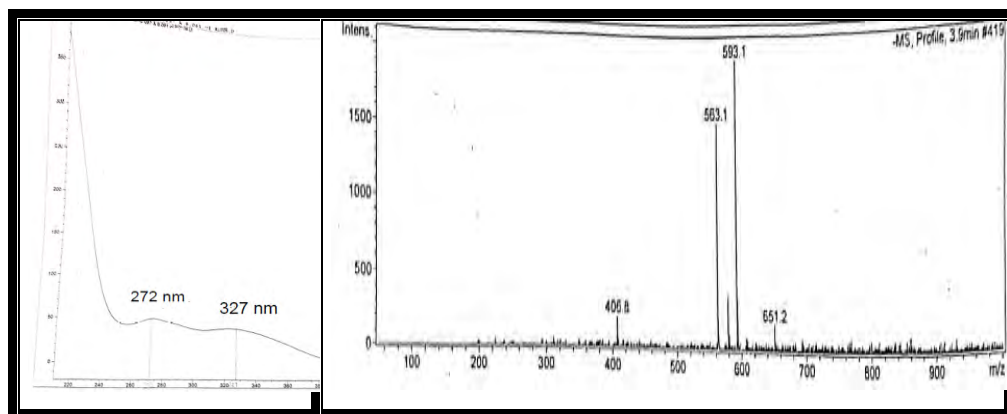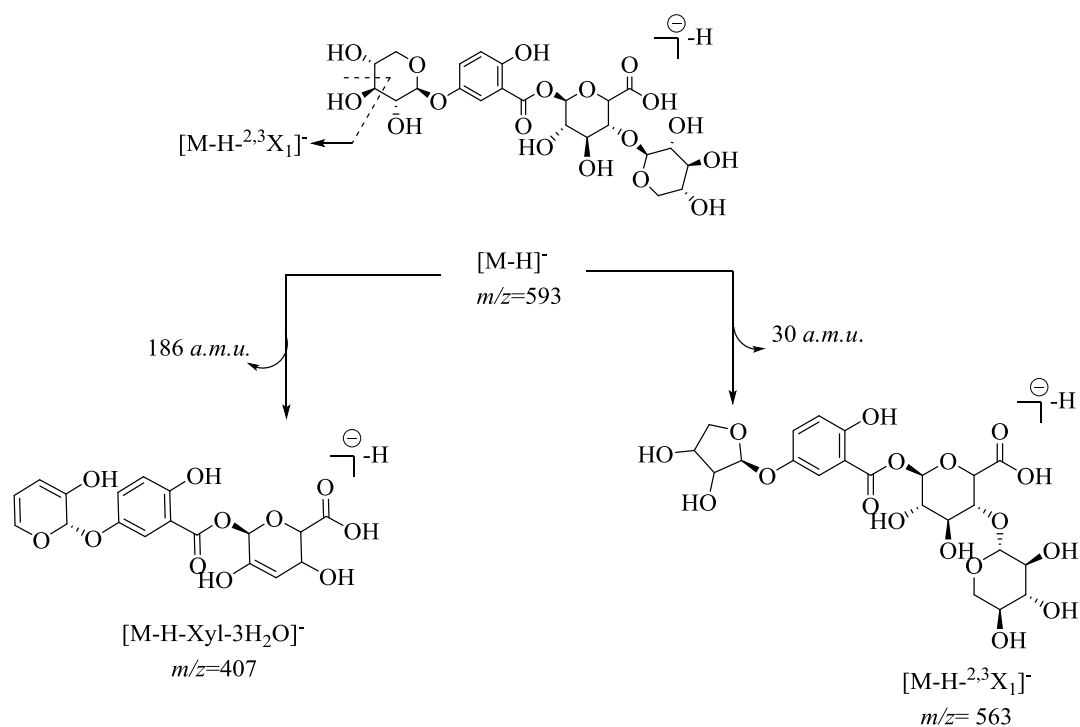
**Figure 1.25** DAD and mass spectrum of RDHM-2

The analysis of RDHM-2 was probed in a negative ionization mode. The molecular ion peak was detected at *m/z* 593[M-H]⁻ while the actual mass of the compound was 594 *a.m.u.* The fragment peak at *m/z* 563 was observed by the loss of formaldehyde as reported by **Salpin and Tortajada (2002)** from the molecular ion peak. So, it was represented as [M-H-formaldehyde]⁻. The peak at *m/z* 407 originated by the loss of one xylose along with the elimination of three water molecules, one from glucuronic acid and two from the remaining xylose sugar. The peak was assigned as [M-H-Xyl-3H₂O]⁻. The fragmentation scheme for RDHM-2 compound is given in the **scheme 1.9**.



**Scheme 1.9** Fragmentation scheme for RDHM-2

53

The retention time, UV and mass spectrum of RDHM-2 confirmed the second proposed structure. The name of the proposed structure was 5-*O*-[*β*-D-xylopyranoside]-1-*O*-[ *β*-D-xylopyranosyl-(1→4)-*β*-D-glucuronosyl] gentisate.
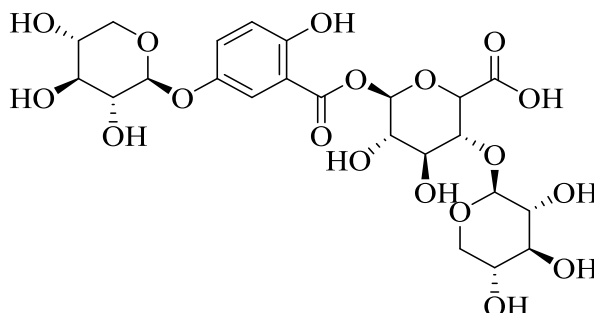


**5-*O*-[*β*-D-xylopyranoside]-1-*O*-[ *β*-D-xylopyranosyl-(1→4)-*β*-D-glucuronosyl] gentisate**

### 3.5.3    Identification of RDHM-3

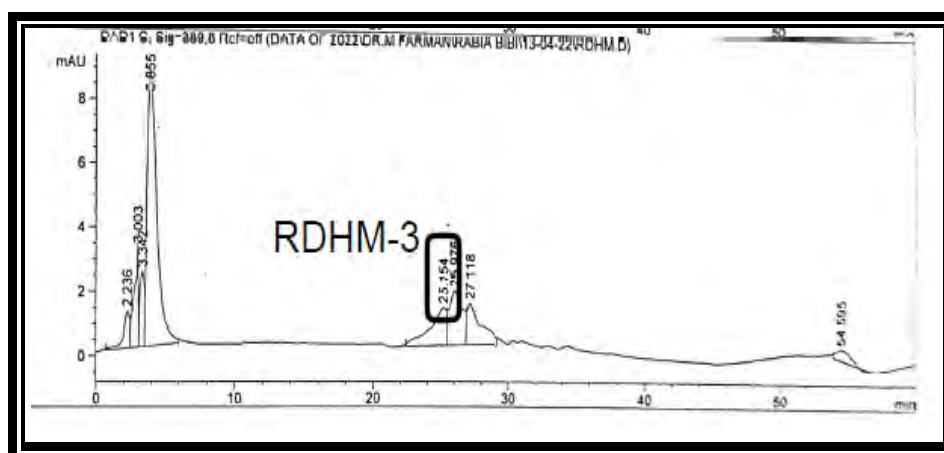The compound eluted from the HPLC column at retention time of 25.2 minutes was labeled as RDHM-3 in the **figure 1.26**.



**Figure 1.26**  HPLC profile of RDHM-3

The composition of mobile phase at this retention time was 20% acetonitrile in 80% of water. At this retention time, tetraglycosidic, triglycosidic or diglycosidic compound might be eluted which was further assured by the UV and mass spectrum.

UV spectrum of RDHM-3 showed two-band pattern of flavonoid. The absorption value of band-I appeared at $\lambda_{max}$ 335 *nm* and band-II at $\lambda_{max}$ 270 *nm*. It showed resemblance to the UV spectrum of vitexin as mentioned by **Mabry *et al.,* (2012)**.

The hypochromic shift in band-I indicated the glycosylation on ring-B. Mass spectrum and cleavage pattern further confirmed the structure of compound RDHM-3.
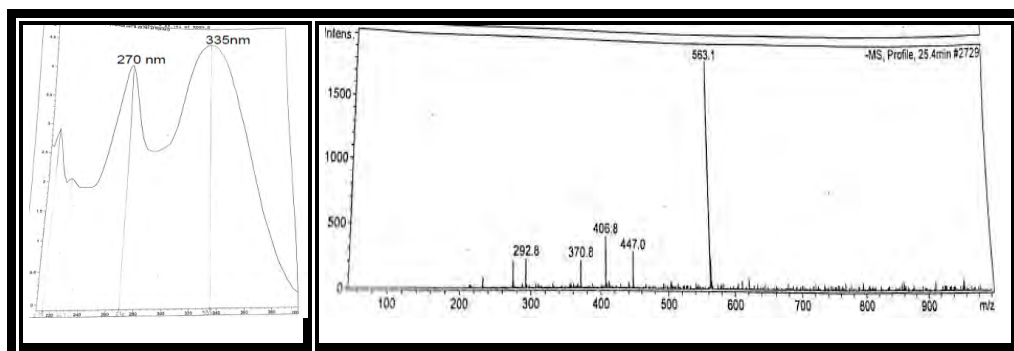


**Figure 1.27** DAD and mass spectrum of RDHM-3

Deprotonated molecular ion peak of compound RDHM-3 appeared at *m/z* 563 as [M-H]$^-$ while the actual mass of the compound was 564 *a.m.u.* The fragment ion peak appeared at *m/z* 447 [M-H-$^{0,3}$X-2CO]$^-$ by the loss of 116 *a.m.u.* It corresponded to the $^{0,3}$X cleavage from xylose sugar **(Mashima *et al.*, 2019)** and loss of two CO from the aglycan. The next fragment ion peak appeared at *m/z* 407 [M-H-2H$_2$O-$^{0,2}$X]$^-$ by the loss of two water molecules from xylose as documented by **Chapagain and Wiesman (2007)** along with $^{0,2}$X cleavage from hexose moiety. The loss of 192 *a.m.u.* occurred from the parent ion peak gave rise to fragment peak at *m/z* 371 as [M-H-Xyl-$^{0,4}$X]$^-$. This loss corresponded to the pentose sugar along with removal of $^{0,4}$X from the *C*-linked glucose as reported by **Roowi and Crozier (2011)**. The emergence of last fragment ion peak at *m/z* 293 attributed to the loss of 270 *a.m.u.* from the parent ion. The elimination of 270 *a.m.u.* corresponded to the removal of pentose sugar. The $^{0,2}$X cleavage confirmed the *C*-linked glucose and then five membered furan ring was formed at *C*-8 position by the loss of water molecule as mentioned by **Toa *et al.*, (2015)**. The fragmentation pathway of RDHM-3 is given below in the **scheme 1.10**.
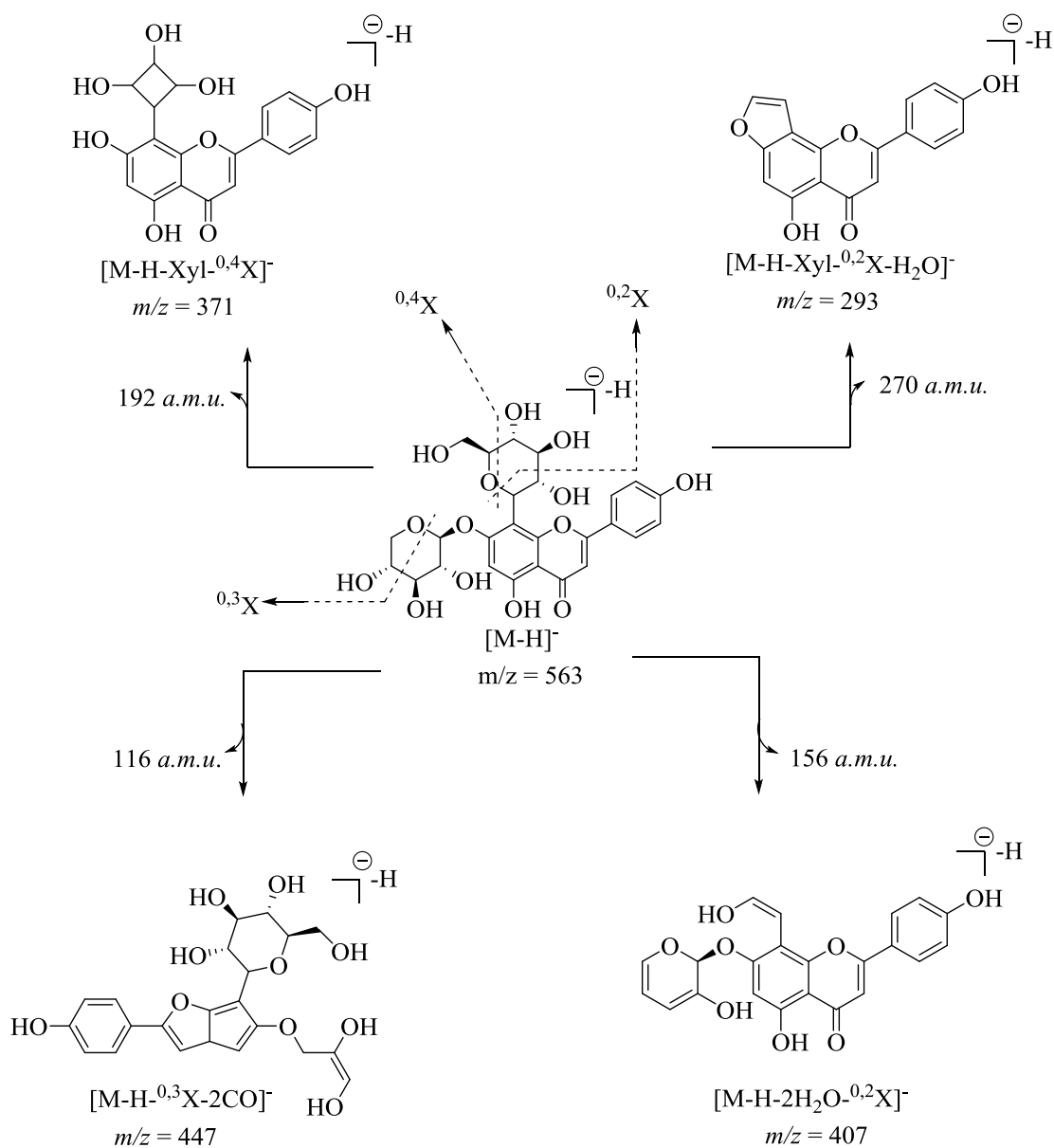
**Scheme 1.10** Fragmentation scheme of RDHM-3

The evidences from HPLC chromatogram, DAD spectrum and mass spectrum clearly indicated the identified compound is 7-*O*-β-D-xylopyranosyl-8-*C*-β-D-glucopyranosyl apigenin.
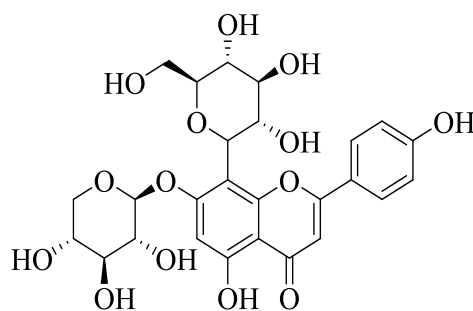
**7-*O*- *β*-D-xylopyranosyl-8-*C*-*β*-D-glucopyranosyl apigenin**

### 3.5.4 Identification of RDHM-4

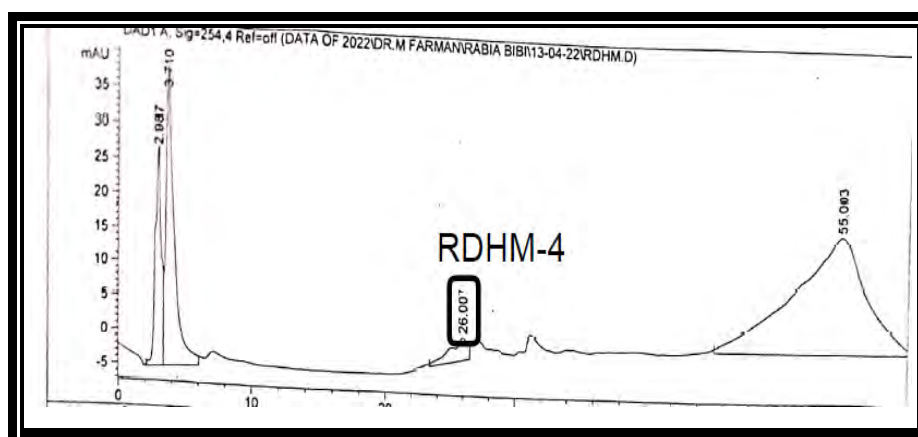The signal highlighted below in the HPLC profile was labeled as RDHM-4 which is shown below in the **figure 1.28**.



**Figure 1.28** HPLC profile of RDHM-4

The compound was eluted from the HPLC column at retention time of 26.1 minutes. At this time, the composition of mobile phase was 21% acetonitrile in 79% of deionized water. It predicted the presence of hydrophilic compound.

The DAD spectrum revealed the characteristic two band pattern of flavonoid. The given UV spectrum showed the band-I at $\lambda_{max}$ 335 *nm* and band-II at $\lambda_{max}$ 265 *nm* as shown in the **figure 1.29**. The UV spectrum of RDHM-4 resembled the UV spectrum of isovitexin but the hypsochromic shift was observed in the band-I due to the presence of sugar moiety on the ring-A of aglycan molecule **(Mabry *et al.,* 1970)**. The UV spectrum of RDHM-4 was similar to that of RDHM-3. So, it was inferred that RDHM-4 might be considered as an isomer of RDHM-3.
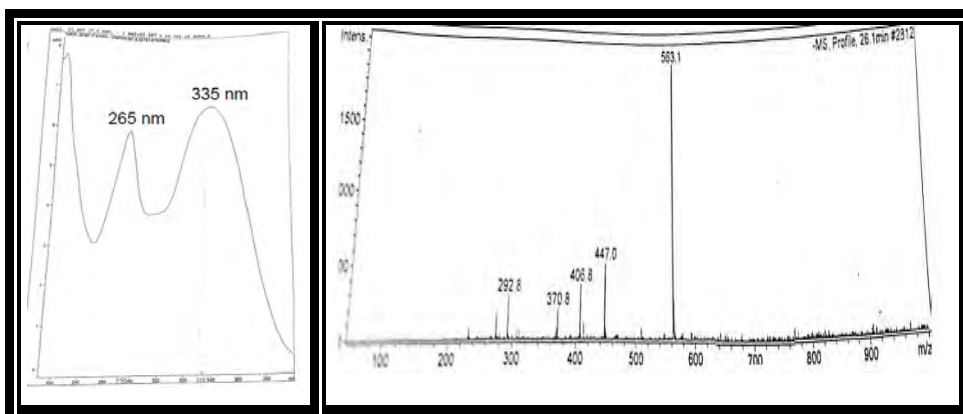
**Figure 1.29** DAD and mass spectrum of RDHM-4

Mass spectrum data of RDHM-4 indicated the molecular ion peak at *m/z* 563 in deprotonated mode. Hence, the actual mass of the compound was 564 *a.m.u.* The daughter ion peak appeared at *m/z* 447 represented as [M-H-2CO-$^{0,3}$X] $^-$, due to loss of two carbon monoxide units **(Cao *et al.,* 2014)** along with $^{0,3}$X cleavage from the xylose sugar. The loss of 192 *a.m.u.* occurred from the parent ion peak which gave rise to fragment peak at *m/z* 371 as [M-H-Xyl-$^{0,4}$X]. This predicted the loss of pentose sugar along with removal of $^{0,4}$X from the *C*-linked glucosyl as reported by **Roowi and Crozier (2011)**. The next fragment ion peak observed at *m/z* 407 [M-H-2H$_2$O-$^{0,2}$X]$^-$ by the removal of 156 *a.m.u.* Loss of two water molecules from the xylose as **(Chapagain and Wiesman 2007)**. The $^{0,2}$X cleavage, loss of 120 *a.m.u.* suggested the presence of glucose. The last fragment ion peak appeared at *m/z* 293. This peak appeared by the elimination of 270 *a.m.u.* corresponding to the removal of pentose group, $^{0,2}$X cleavage and loss of water molecule as a result formation of five member ring was occurred **(Cuyckens and Claeys 2004)**. It was justified as [M-H-Xyl-$^{0,2}$X-H$_2$O]$^-$. The fragmentation pathway of RDHM-5 is given below in the **scheme 1.11**.
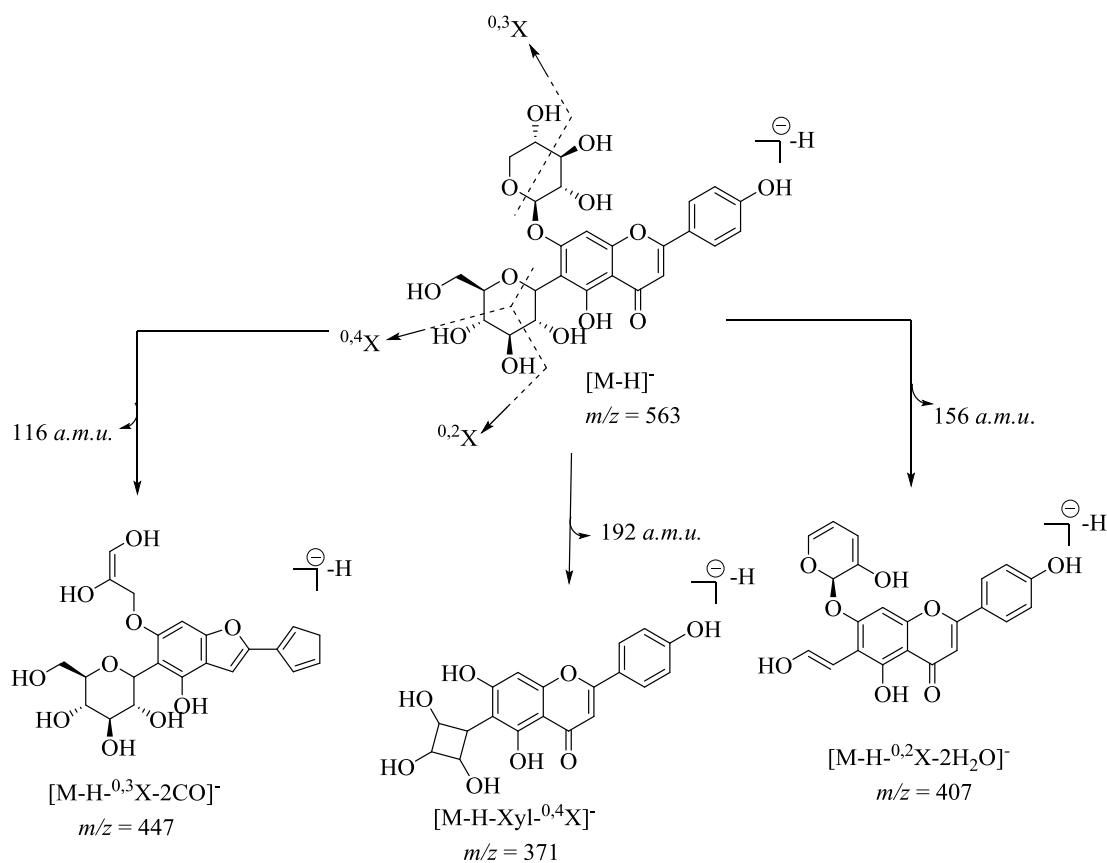
**Scheme 1.11** Mass fragmentation scheme of RDHM-4

From the given information, the name of the compound designated as 6-*C*-β-D-glucopyranosyl-7-*O*- β-D-xylopyranosyl apigenin.
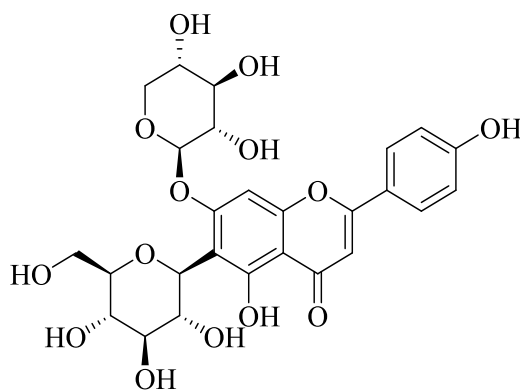


**6-*C*-β-D-glucopyranosyl-7-*O*-β-D-xylopyranosyl apigenin**

### 3.5.5 Identification of RDHM-5

The compound highlighted on the HPLC profile as shown in the **figure 1.30** was marked as RDHM-6. Further information was acquired by retention time, UV and mass spectrum.
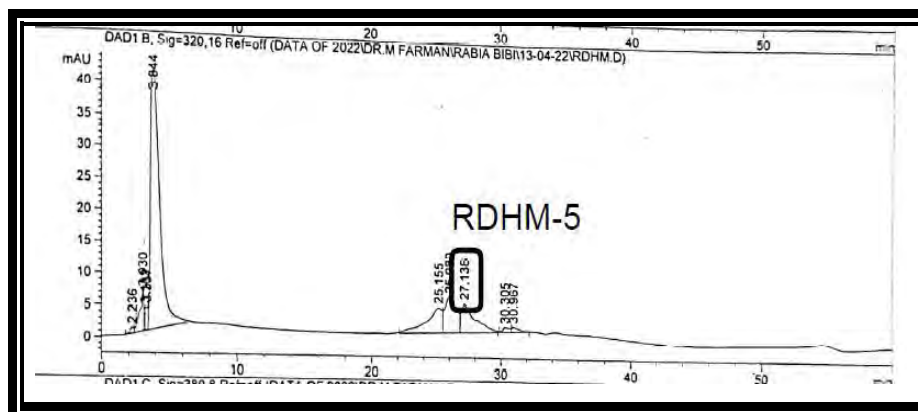


**Figure 1.30** HPLC profile of RDHM-5

The HPLC chromatogram displayed the retention time of the compound RDHM-5 at 27.2 minutes. This retention time showed that the mobile phase composition was 22% acetonitrile in 78% water. It indicated the hydrophilic nature of the eluted compound.

The UV spectrum of RDHM-6 displayed two band patterns. Band-I appeared at $\lambda_{max}$ 335 *nm* and band-II appeared at $\lambda_{max}$ 268 *nm*. The absorption values of the eluted compound showed the characteristic band patterns of flavone moiety. The $\lambda_{max}$ value of absorption band-II represented the level of hydroxylation on ring-A **(Markham *et al.,* 1982)**. It could be trihydroxylated or dihydroxylated. The shape of bands and their corresponding $\lambda_{max}$ values are closely related to the UV spectrum of isovitexin reported by **Mabry *et al.,* (2012)**.
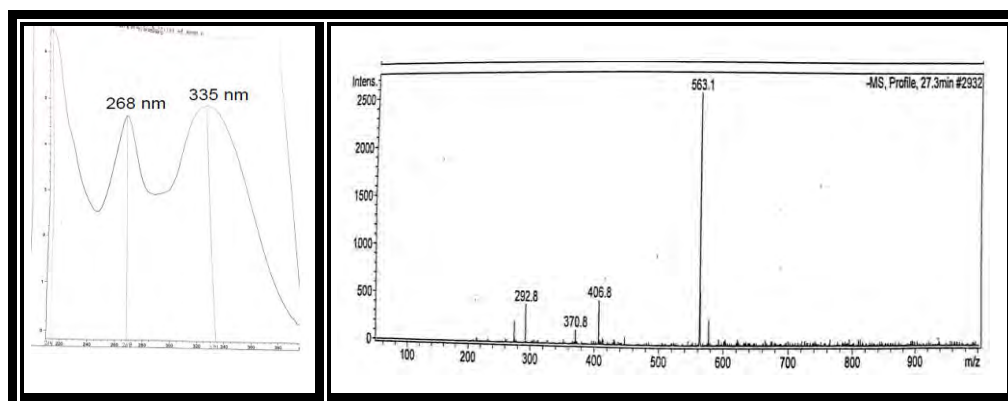


**Figure 1.31** DAD and mass spectrum of RDHM-5

Mass spectrum of RDHM-5 exhibited the molecular ion peak in deprotonated mode at $m/z$ 563 so the actual mass of the compound was 564 *a.m.u.* The peak at $m/z$ 447 [M-H-$^{0,3}$X-2CO]$^-$ indicated the presence of xylose moiety at 4′ position of aglycan moiety as reported by **Mashima *et al.,* (2019)**. It appeared due to $^{0,3}$X cleavage along with the loss of two CO from the aglycan moiety. The next peak at $m/z$ 407 [M-H-2H$_2$O-$^{0,2}$X]$^-$ originated by the loss of 156 *a.m.u.* The removal of two water molecules from xylose sugar as documented by **Chapagain and Wiesman (2007)** and $^{0,2}$X cleavage showed the existence of glucose moiety at 6th position via *C*-linkage **(Cao *et al.,* 2014)**. The loss of 192 *a.m.u.* occurred from the parent ion peak gave rise to the fragment peak at $m/z$ 371 as [M-H-Xyl-$^{0,4}$X]$^-$. The 192 *a.m.u* loss corresponded the removal of pentose sugar along with $^{0,4}$X cleavage from the *C*-linked glucose as reported by **Roowi and Crozier (2011)**. The last peak appeared at $m/z$ 293 [M-H-Xyl-H$_2$O-$^{0,2}$X]$^-$ by the loss of 270 *a.m.u.* It corresponded to $^{0,2}$X cleavage from glucose moiety which was condensed with the OH group on the fifth position of ring A as a result five membered ring was formed by the elimination of water molecule **(Cuyckens *et al.,* 2004)**. The fragmentation pattern for RDHM-5 is given below in the **scheme 1.12**.
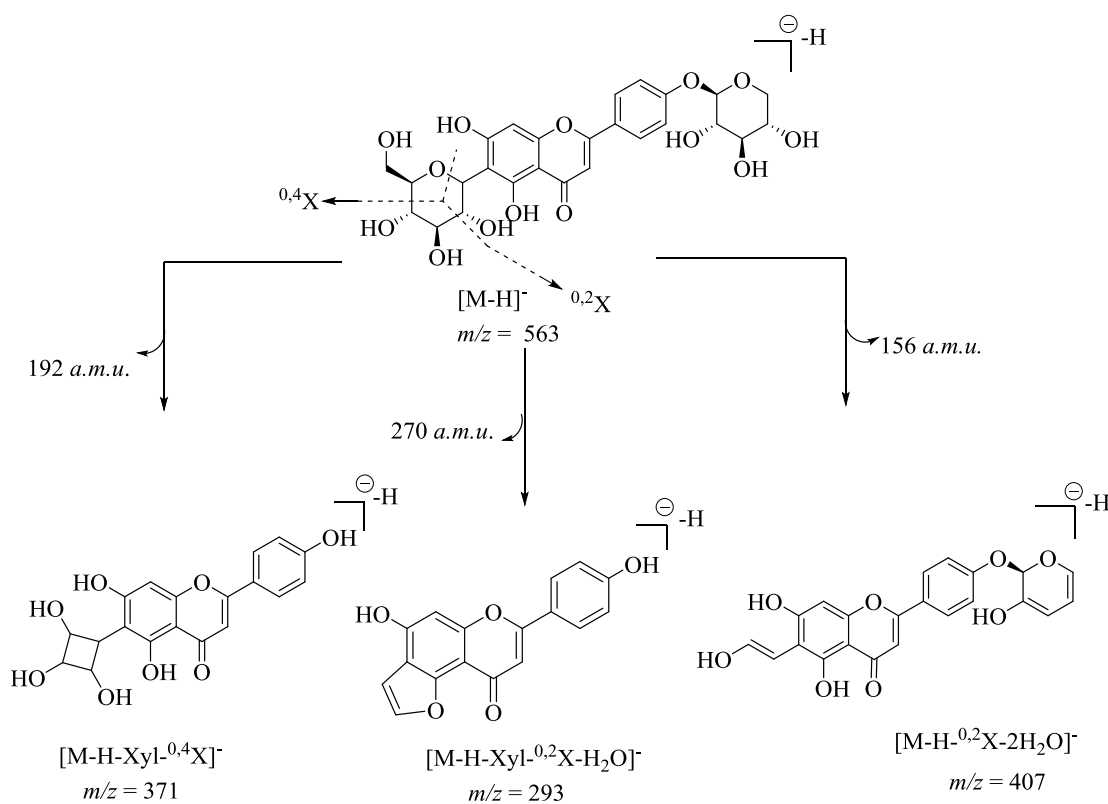


**Scheme 1.12** Fragmentation scheme of RDHM-5

Information from retention time, DAD spectrum and mass fragmentation revealed the eluted compound as 4′-*O*-β-D-xylopyranosyl-6-*C*-β-D-glucopyranosyl apigenin.
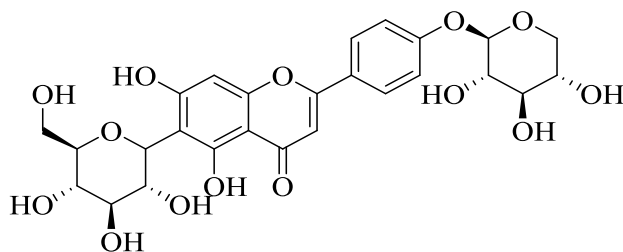


**4′-*O*-β-D-xylopyranosyl-6-*C*-β-D-glucopyranosyl apigenin**

### 3.5.6  Identification of RDHM-6

The compound mentioned on the HPLC profile was marked as RDHM-6 at retention time of 31.3 minutes as shown in the **figure 1.16**.
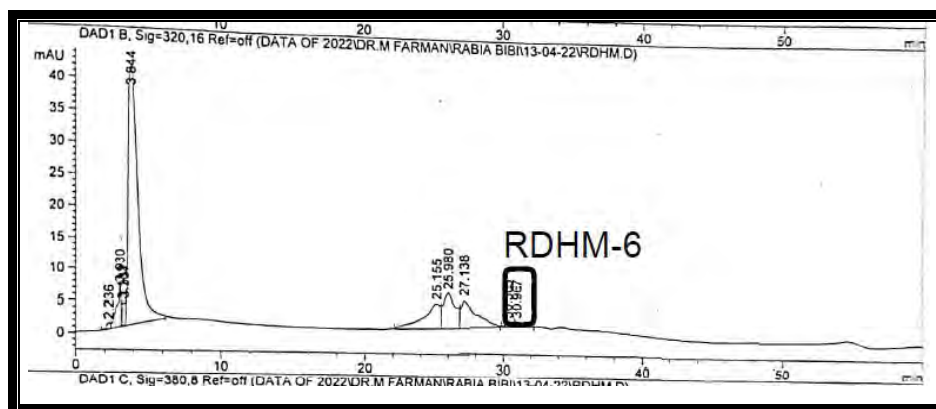


**Figure 1.32** HPLC profile of RDHM-6

The mobile phase composition at this time was 24% acetonitrile in 76% deionized water. The mobile phase composition predicted the presence of triglycosidic or diglycosidic compound.

UV spectrum revealed the two characteristic bands. Band-II of the spectrum showed the $\lambda_{max}$ value at 270 *nm* and band-I at $\lambda_{max}$ 337 *nm*. The shape of the band and their corresponding absorption values resembled the absorption values of acacetin as reported by **Markovic and Tosovic (2015)**. The DAD spectrum of RDHM-6 is given below in the **figure 1.33**.
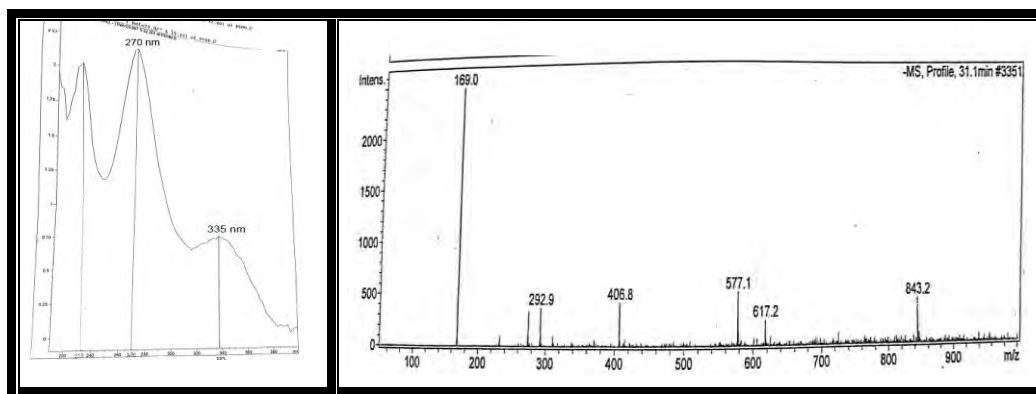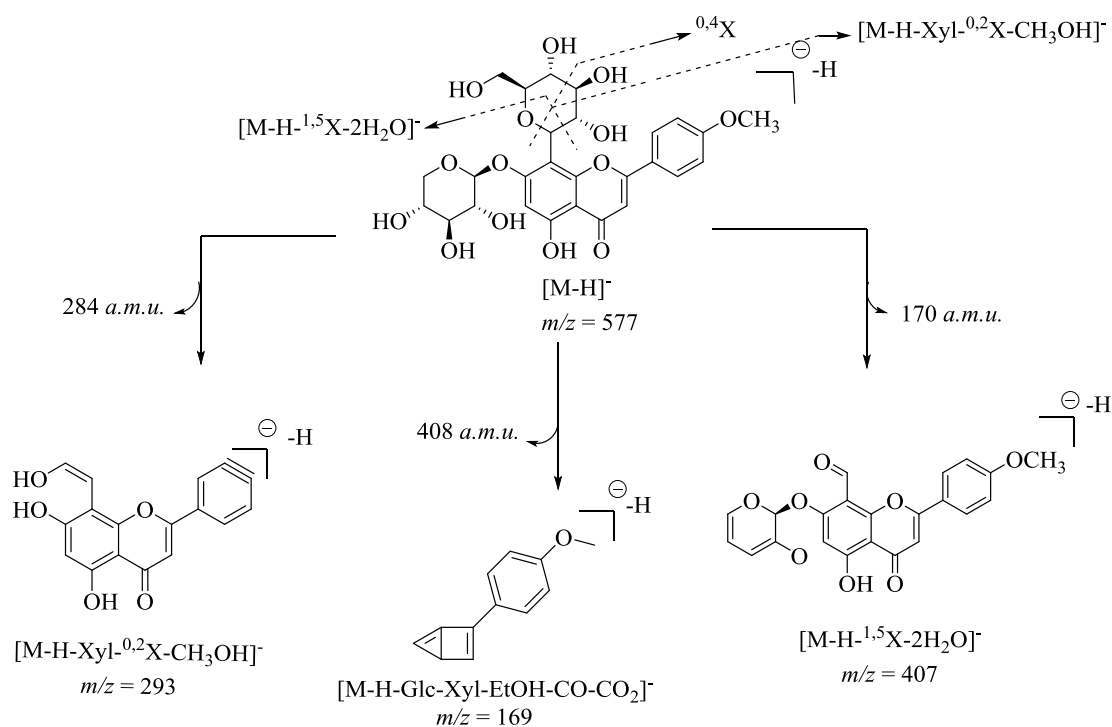
**Figure 1.33** DAD and mass spectrum of RDHM-6

Mass spectrum of RDHM-6 revealed the molecular ion peak in deprotonated mode at $m/z$ 577 [M-H]$^-$. Hence, the actual mass of the compound was 578 *a.m.u.* The first fragment ion peak originated at $m/z$ 407 by the loss of 170 *a.m.u.* from parent ion that corresponded the $^{1,5}$X cross ring cleavage of hexose sugar as reported by **Cuyckens and Claeys (2004)**. It assured the presence of glucopyranose alongside the removal of two water molecule from the xylose sugar **(Chapagain and Wiesman 2007)**. This peak was represented as [M-H- $^{1,5}$X-2H$_2$O] $^-$. The next fragment ion peak was observed at $m/z$ 293 [M-H-$^{0,2}$X-Xyl-CH$_3$OH]$^-$ by the elimination of 284 *a.m.u.* from molecular ion peak. It corresponded to $^{0,2}$X cleavage of *C*-linked glucose unit, removal of xylose moiety and neutral loss of methanol from ring-B. The neutral loss of methanol indicated the presence of methoxy group at 4′ position **(Carbone *et al.*, 2004)**. The peak at $m/z$ 169 appeared by the loss of 408 *a.m.u.* from molecular ion peak. It corresponded to the loss of glucosyl, xylosyl, ethynyl alcohol moiety and CO from ring-A which resulted in the formation of 3-membered ring. The elimination of CO$_2$ from ring-C led to the formation of 4-membered ring. The fragmentation scheme of RDHM-6 is given below in the **scheme 1.13**.

**Scheme 1.13** Fragmentation scheme of RDHM-6

The structure of the compound was predicted according to retention time, DAD spectrum and mass spectrum of RDHM-6. The name suggested for RDHM-6 is 7-O-$\beta$-D-xylopyranosyl-8-C-$\beta$-D-glucopyranosyl acacetin.
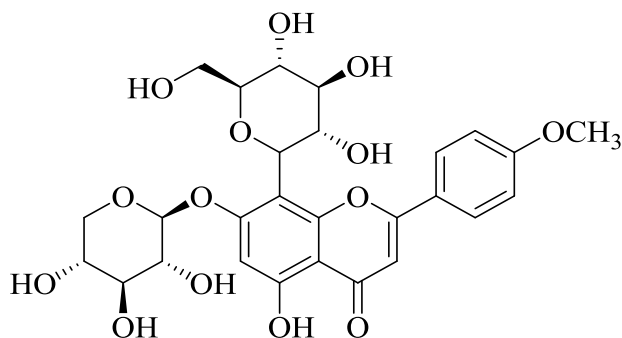


**7-O-$\beta$-D-xylopyranosyl-8-C-$\beta$-D-glucopyranosyl acacetin**

### 3.5.7 Identification of RDHM-7

The compound eluted from the HPLC column at retention time of 55.2 minutes was labeled as RDHM-7. It is given in the **figure 1.34**.
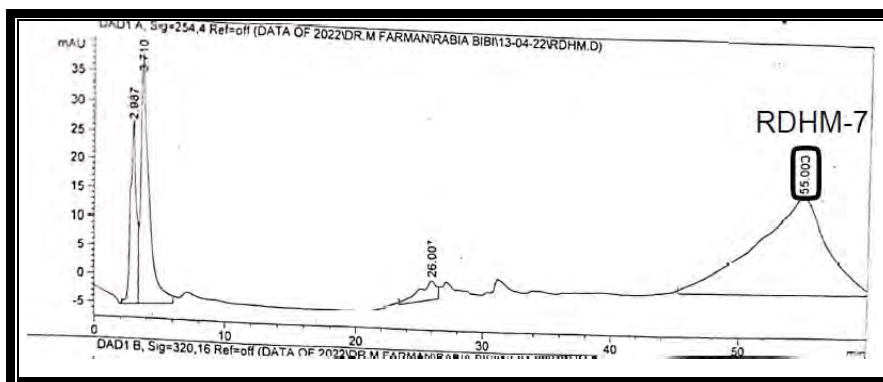
**Figure 1.34** HPLC profile of RDHM-7

The mobile phase composition at this retention time was 40% water and 60% acetonitrile. It predicted the hydrophobic nature of eluted compound.

The UV spectrum of compound showed only one absorption band at $\lambda_{max}$ 240 *nm*. The $\lambda_{max}$ value was evaluated by using Woodward-Fieser rule. According to this rule, the base value of $\alpha,\beta$-unsaturated cyclic ketones showed absorption band at $\lambda_{max}$ 215 *nm*. The two ring residues at $\beta$-position gave the $\lambda_{max}$ value at 24 *nm*. The one exocyclic double bond added 5 *nm* to the remaining value. So, the calculated $\lambda_{max}$ value for RDHM-7 was 244 *nm*. The UV spectrum of compound resembled the cholestane type molecule. The UV and mass spectrum of RDHM-7 is given in the **figure 1.35**.
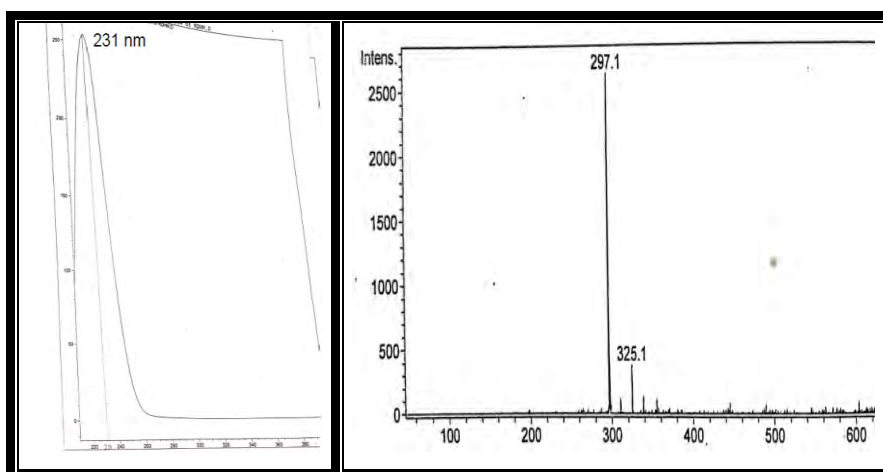


**Figure 1.35** DAD and mass spectrum of RDHM-7

The molecular ion peak of RDHM-7 appeared at *m/z* = 325 in negative ionization mode. So, the exact mass of the compound was 326 *a.m.u.* The molecular ion corresponded to the alkenyl substituted steroids with $\alpha$, $\beta$-unsaturated cyclic ketones.

The loss of 28 *a.m.u.* resulted in the peak at *m/z* 297. The fragmentation scheme for RDHM-7 is given in the **scheme 1.14**.
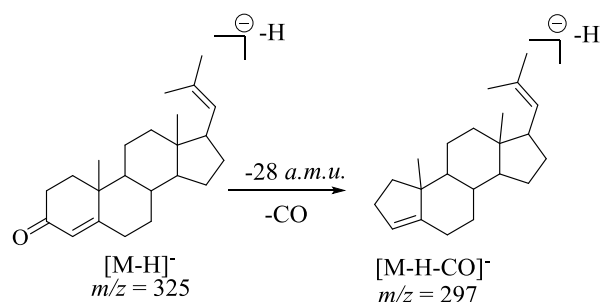


**Scheme 1.14** Mass fragmentation scheme of RDHM-7

The structure of the compound was predicted according to retention time, DAD spectrum and mass spectrum. It was named as 10,13-Dimethyl-17-butenyl dodeca hydrocyclopentanephthren-3-one.
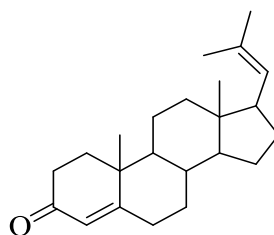


**10,13-Dimethyl-17-butenyldodecahydrocyclopentanephthren-3-one**

List of the compounds identified by 20% hydromethanolic extract are given below in the **table 1.7**.

**Table 1.7** Compounds identified from RDHM extract

| Compounds with codes | Retention time ($R_t$) (minutes) | $\lambda_{max}$ values (*nm*) | Molecular ion peak (*m/z*) [M-H]$^-$ | Name of the identified compound |
|---|---|---|---|---|
| **RDHM-1** | 2.9 | 265 | 777 | 3-*O*-[$\beta$-D-glucopyranosyl-(1 →2)-$\beta$-D-xylopyranoside]-1-*O*-$\beta$-D-glucopyranosyl gallate |

| RDHM-2 | 4.0 | 270, 330 | 593 | 3-*O*-[*β*-D-xylopyranoside]-1-*O*-[ *β*-D-xylopyranosyl-(1→4)-*β*-D-glucuronosyl] benzoate |
|--------|-----|----------|-----|------------------------------------------|
| RDHM-3 | 25.2 | 270, 335 | 563 | 7-*O*- *β*-D-xylopyranosyl-8-*C*- *β*-D-glucopyranosyl apigenin |
| RDHM-4 | 26.0 | 265, 335 | 563 | 6-*C*- *β*-D-glucopyranosyl-7-*O*- *β*-D-xylopyranosyl apigenin |
| RDHM-5 | 27.1 | 265, 330 | 563 | 4′-*O*-*β*-D-xylopyranosyl-6-*C*- *β*-D-glucopyranosyl apigenin |
| RDHM-6 | 27.9 | 270, 330 | 577 | 7-O-*β*-D-xylopyranosyl-8-*C*-*β*-D-glucopyranosyl acacetin |
| RDHM-7 | 31.1 | 266, 336 | 325 | 10,13-Dimethyl-17-butenyl dodecahydrocyclopenta-nephthren-3-one |

## 3.6   GC-MS Analysis of *Rhaphidophora decursiva*

Volatile organic constituents from the *n*-hexane extract of *Rhaphidophora decursiva* were determined using GC-MS technique. The elution of components from gas chromatographic column occurred in such a way that more volatile compounds eluted first followed by less volatile compounds. The TIC profile of RDH extract is given below in the **figure 1.36**
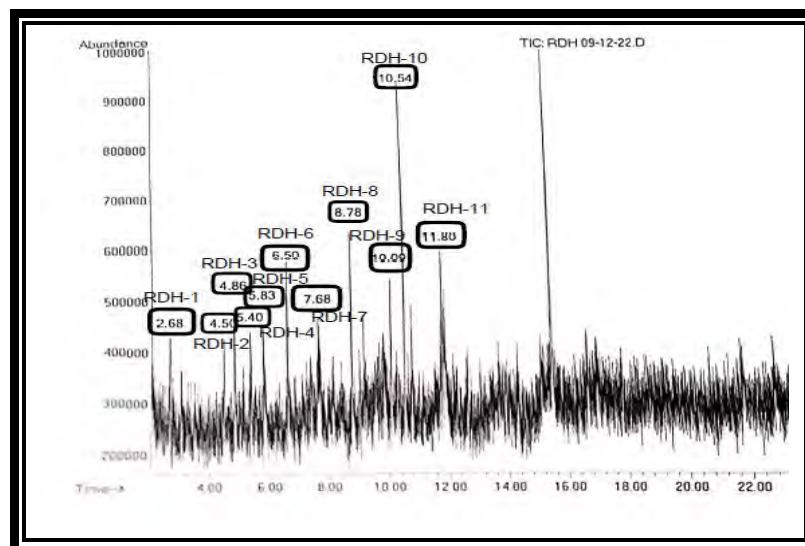
**Figure 1.36** TIC profile of RDH

### 3.6.1 Identification of RDH-1

The compound with retention time of 2.6 minutes was labeled as RDH-1. The lowest retention time predicted the presence of highly volatile nature of eluted compound the mass spectrum of RDH-1 which is in the **figure 1.37**.
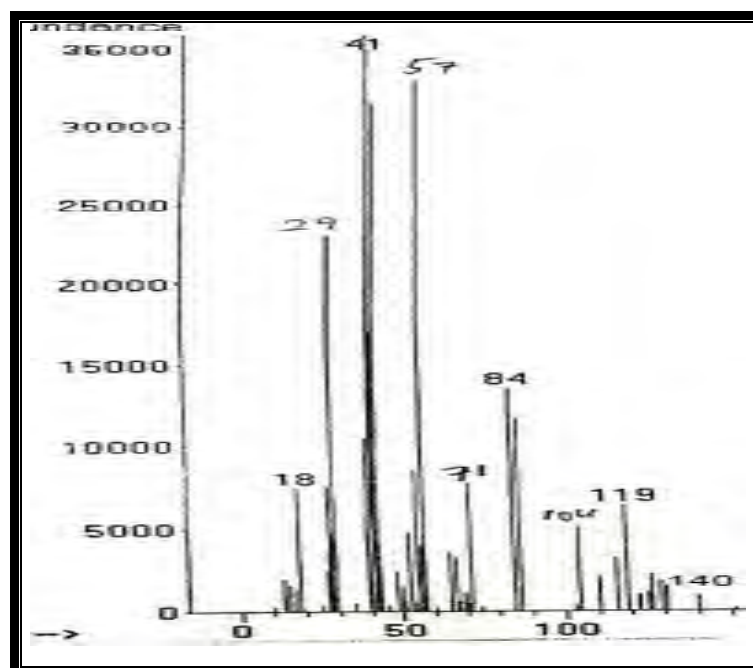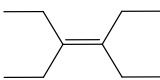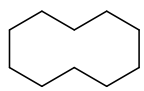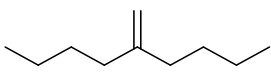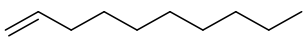


**Figure 1.37** Mass spectrum of RDH-1

The molecular ion peak was analyzed at *m/z* 140. The even molecular ion peak suggested the presence of either even number of nitrogen atoms or the absence of nitrogen atom. The base formula was generated as $C_{10}H_{20}$ by applying the rule of
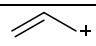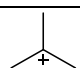
thirteen. It might be alkenes as the base formula justify the general formula of alkenes $CnH_2n$. So, the base formula was not modified. The IHD of 1 was calculated for RDH-1 compound. The possible structures for RDH-1 are given in the **table 1.8**.

**Table 1.8** Possible structures for RDH-1

| Sr. No. | Possible structures for RDH-1 |
|---|---|
| 1. | 3,4-Diethyl-3-hexene |
| 2. | Cyclodecane |
| 3. | 2-Butyl-1-hexene |
| 4. | Dec-1-ene |

First structure was ruled out as base peak of the given spectrum appeared at *m/z* 41 which was not observed in the mass spectrum of 3, 4-Diethyl-3-hexene. The second possible structure for RDH-1 is cyclodecane. It was excluded as the characteristic base peak of cycloalkanes was observed at *m/z* 56 which was not found in the given mass spectrum. The third possible structure for RDH1 was ruled out because its mass fragmentation pattern did not justify the peaks on the given spectrum of RDH1 compound. The characteristic fragment peaks of mass spectrum of RDH1 with considerable intensities are given in the **table 1.9**.

**Table 1.9** Characteristic fragments in the mass spectrum of RDH-1

| Peak (*m/z*) | Structure of fragment |
|---|---|
| 41 | |
| 57 | |

The fragment ion peaks supported the dec-1-ene to be the tentative structure for RDH-1 compound. The molecular ion peak of dec-1-ene was observed at *m/z* 140. The base peak appeared at *m/z* 41 resulted due to allylic cleavage and the cation was formed in resonance with double bond. This indicated the position of double bond on terminal position. The second highest peak appeared by the simple *C-C* cleavage into an isobutyl cation by the 1,2-hydride shift **(Castro-Perez *et al.,* 2011)** and methyl shift **(Terheijden *et al.,* 1985)**. The mechanism is given below in the **scheme 1.15**.
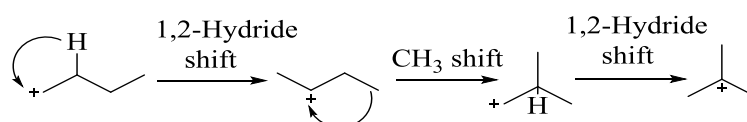


**Scheme 1.15** Formation of t-butyl cation at *m/z* 57

The rest of the signals appeared at *m/z* 29, 71, 84 and 85 corresponding to the alkyl part of the compounds. The peak at *m/z* 29 appeared by the loss of octenyl radical from the molecular ionic peak at *m/z* 140. The peak at *m/z* 71 and 85 originated by the removal of pentenyl and butenyl radical respectively from the parent ion. The *m/z* 84 appeared by the loss of hydrogen radical from the fragment ion *m/z* 85. The mass fragmentation scheme of RDH-1 compound is given in the **scheme 1.16**.
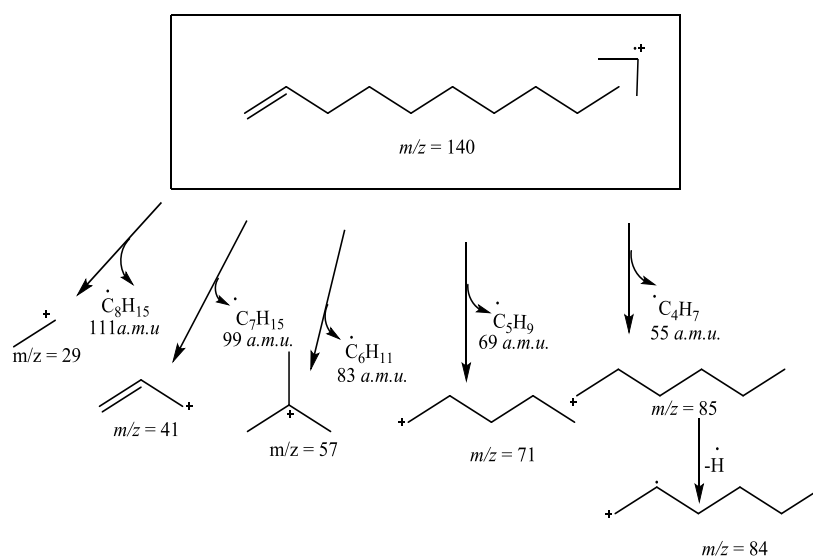


**Scheme 1.16** Mass fragmentation scheme for RDH-1

### 3.6.2 Identification of RDH-2

The signal which appeared on TIC profile at retention time of 4.50 minutes was labeled as RDH-2. The retention time predicted the volatile nature of RDH-2 as it

eluted initially from the column. The mass spectrum of RDH-2 is given in the **figure 1.38**.
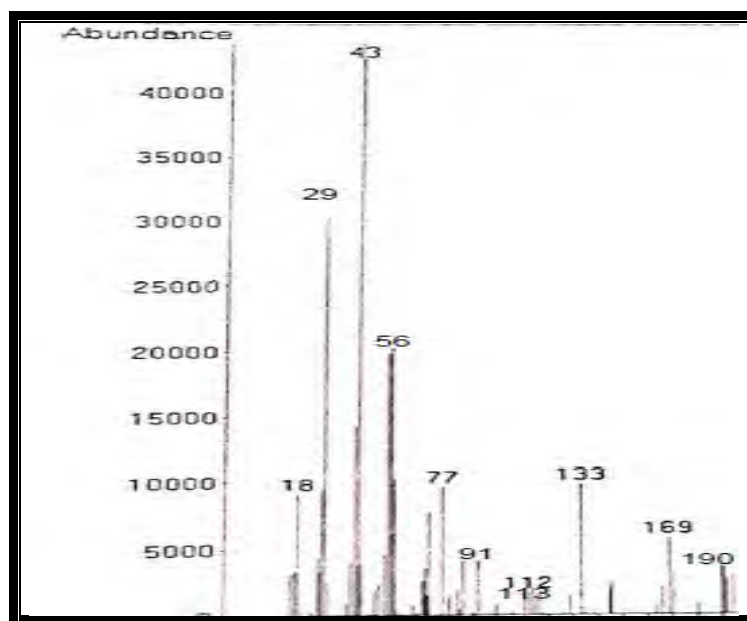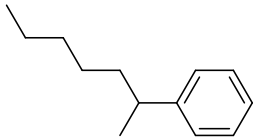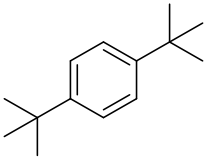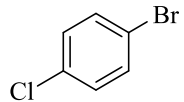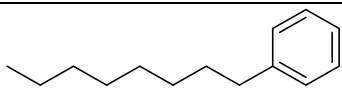


**Figure 1.38** Mass spectrum of RDH-2

The molecular ion peak recognized at *m/z* 190. The even molecular ion peak suggested the presence of either even number of nitrogen atoms in the compound or the absence of nitrogen atom according to nitrogen rule. The base formula of the compound was designed by applying rule of thirteen as $C_{14}H_{22}$. The IHD of four was calculated for RDH-2. The possible structures for molecular ion peak at *m/z* 190 are given in the **table 1.10**.
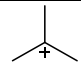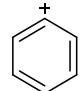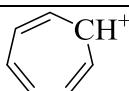
**Table 1.10** Possible structures for RDH-2

| Sr. No. | Possible structures |
|---------|---------------------|
| 1. |  1-Methyl hexyl benzene |
| 2. |  1,4-Di-ter-butyl benzene |

| 3. | 1-Bromo-4-chloro benzene |
|---|---|
| 4. | Octyl benzene |

The possibility of first compound was eliminated as the formation of tropylium cation was not observed on this mass spectrum. The second compound did not justify the characteristic fragmentation peaks observed on the given mass spectrum for RDH-2. The third compound was ruled out as the isotopic peak of bromine did not appear on the given mass spectrum. The characteristic fragment ion peaks supported the Octyl benzene as RDH-2 compound. The characteristic fragment peaks and their structures are given below in the **table 1.11**.

**Table 1.11** Characteristic fragment peaks and their structures

| Peak (*m/z*) | Structure of fragment peak |
|:---:|:---:|
| 57 |  |
| 77 |  |
| 91 |  |

It was concluded that the tentative structure for RDH-2 is Octyl benzene because it justified the maximum number of peaks appeared on the given mass spectrum. The base peak appeared at *m/z* 43 that corresponded to the propyl cation by the loss of hexyl benzene radical. The peak at *m/z* 56 of butyl radical cation appeared by the loss of butyl benzene radical along with the hydrogen radical. The fragment peak at *m/z* 71 corresponding to the pentyl cation was originated by the loss of propyl benzene radical. The peak at *m/z* 113 indicated the heptyl cation formed upon the loss of methyl benzene radical from the molecular ion peak. The peak at *m/z* 112 corresponded to the heptyl radical cation. By the loss of octyl radical, fragment ion peak of phenyl cation was observed at *m/z* 77. The peak at *m/z* 91 correspondent to

the tropylium ion appeared by the loss of heptyl radical from molecular ionic peak. The fragmentation scheme of RDH-2 compound is given below in the **scheme 1.17**.
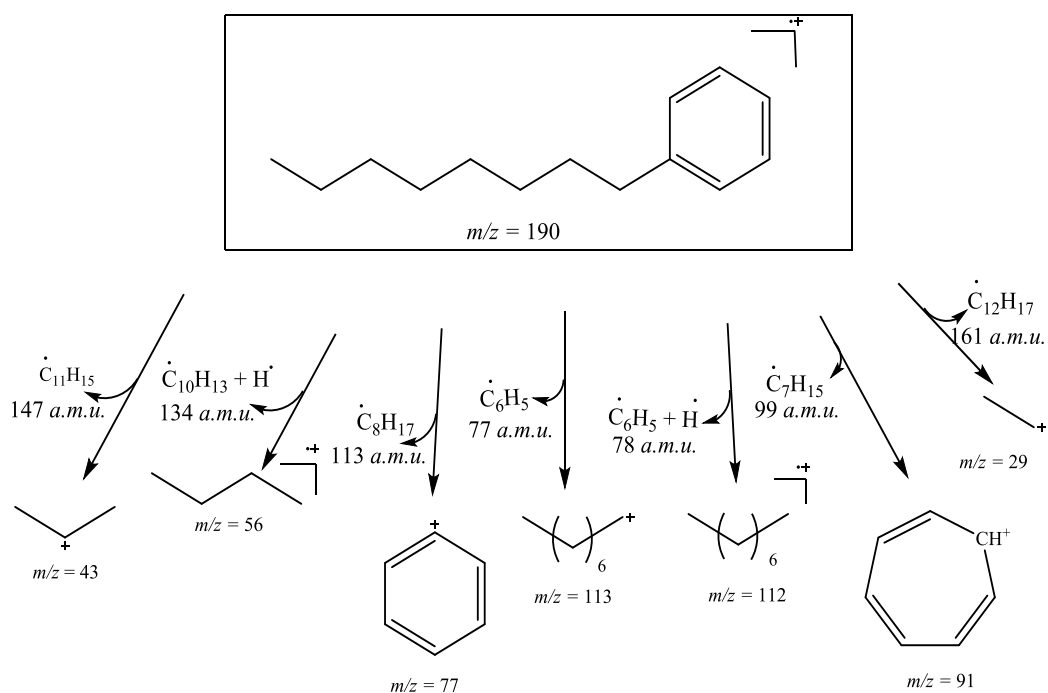


**Scheme 1.17** Fragmentation scheme of RDH-2

### 3.6.3 Identification of RDH-3

The compound eluted from the GC column at retention time of 4.86 minutes was labeled as RDH-3 compound. The less retention time indicated the volatile nature of the compound. The mass spectrum of RDH-3 is given in the **figure 1.39**.
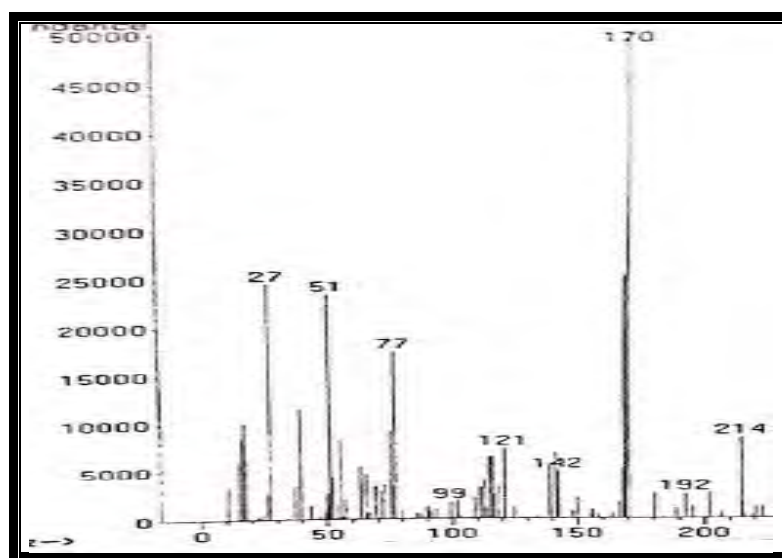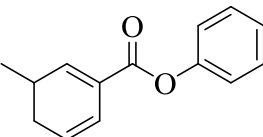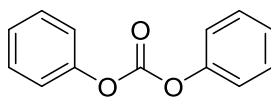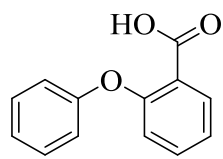


**Figure 1.39** Mass spectrum of RDH-3
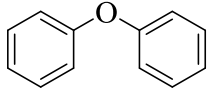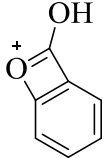
The molecular ion peak was observed at *m/z* 214. The even numbered molecular mass showed the absence of nitrogen in the compound. The molecular formula was designed as $C_{16}H_{22}$ through rule of thirteen. The base peak appeared at *m/z* 170 which is the characteristic peak of diphenyl ether. By considering the base peaks and fragment ion peaks, the molecular formula was modified as $C_{13}H_{10}O_3$. The IHD of 9 was calculated for the modified base formula. The possible structures for RDH-3 are given in the **table 1.12**.

<div align="center">

**Table 1.12** Possible structures for RDH-3

</div>

| Sr. No. | Possible structures for RDH-3 |
|---|---|
| 1. | <br>Phenyl-3-methyl cyclohexa-1,5-diene-1-carboxylate |
| 2. | <br>Diphenyl carbonate |
| 3. | <br>2-Phenoxy benzoic acid |

The first structure was ruled out as the peak at *m/z* 119 resulting from α –cleavage did not appear on the mass spectrum. The second structure was ruled as the base peak of the compound appears at *m/z* 77 while the base peak in the given spectrum appeared at *m/z* 170. So, the probability of 3$^{rd}$ compound to be suitable compound for RDH-3 is more than the others. The characteristics peaks and their corresponding structures is given in the **table 1.13**.

**Table 1.13** Characteristic fragments in the mass spectrum

| Fragment peak (m/z) | Structure of fragment |
|:---:|:---:|
| **170** |  |
| **121** |  |

The fragment ion peaks and their structure confirmed the structure three as the identified compound for RDH-3. The molecular ion peak of 2-phenoxy benzoic acid observed at *m/z* 214. The neutral loss of carbon dioxide resulted in the generation of radical cation at *m/z* 170 which appeared as base peak on mass spectrum. The peak at *m/z* 121 appeared due to the loss of phenoxy radical from the molecular ion peak and fused rings were formed as reported by **Ballantine and Pillinger (1968)**. Again, the loss of phenoxy radical gave rise to the peak at *m/z* 77 which then upon the loss of acetylene moiety by *retro*-Diels-Alder reaction gave peak at *m/z* 51. From cyclobutyl cation another loss of acetylene molecule occurred which led to the fragment ion peak at *m/z* 27.

The fragment ion peak at *m/z* 141 resulted by the rearrangement of bonds of diphenyl ether as documented by **Guerra *et al.,* (2015)**. The reaction mechanism of formation of fragment ion peak at their respective *m/z* is shown below in the **scheme 1.18**.
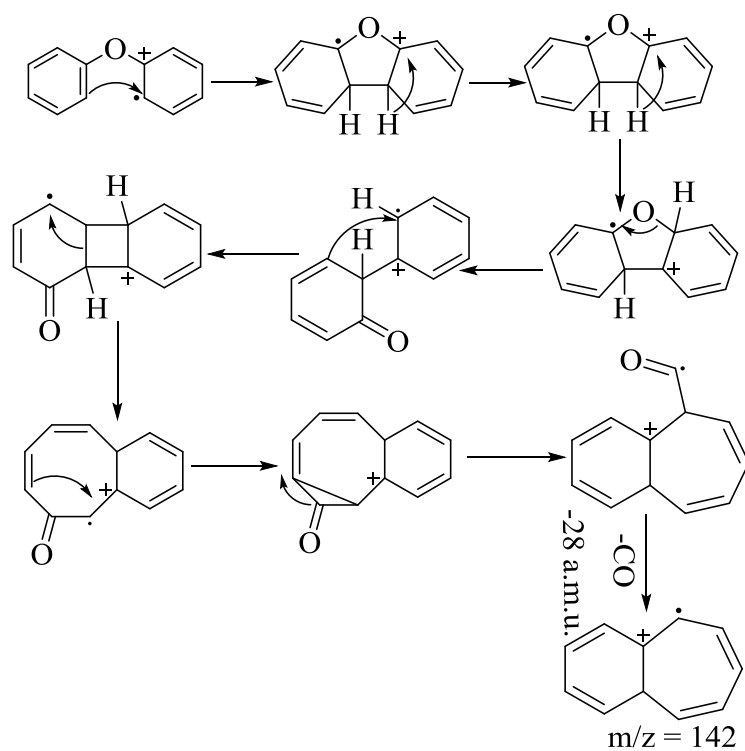
**Scheme 1.18** Scheme for the fragment ion *m/z* 142

The fragmentation scheme for RDH-3 compound is given in the **scheme 1.19** given on the next page.
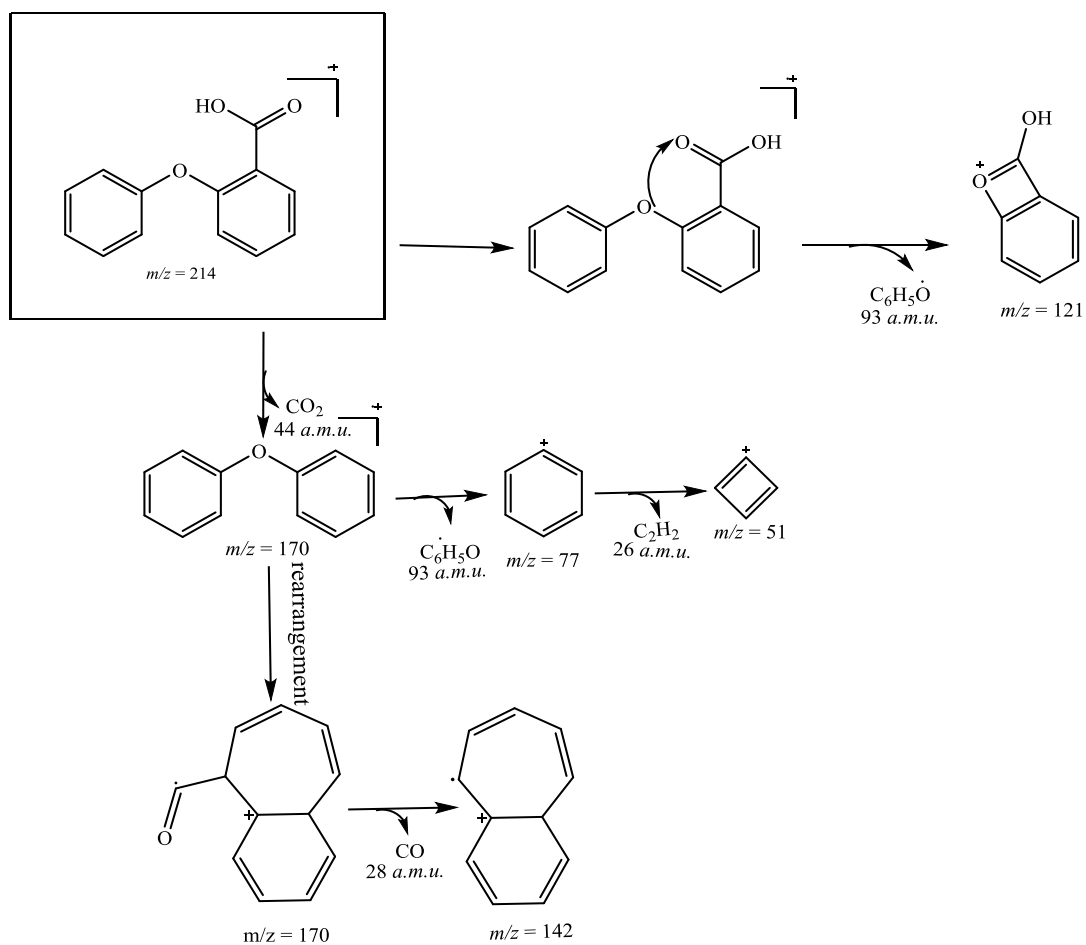
**Scheme 1.19** Fragmentation scheme for RDH-3

### 3.6.4 Identification of RDH-4

The signal that appeared on TIC profile at retention time of 5.40 minutes was labeled as RDH-4. It was predicted that highly volatile compounds eluted at first, so the RDH-4 was volatile in nature. The mass spectrum of RDH-4 is given in the **figure 1.40**.
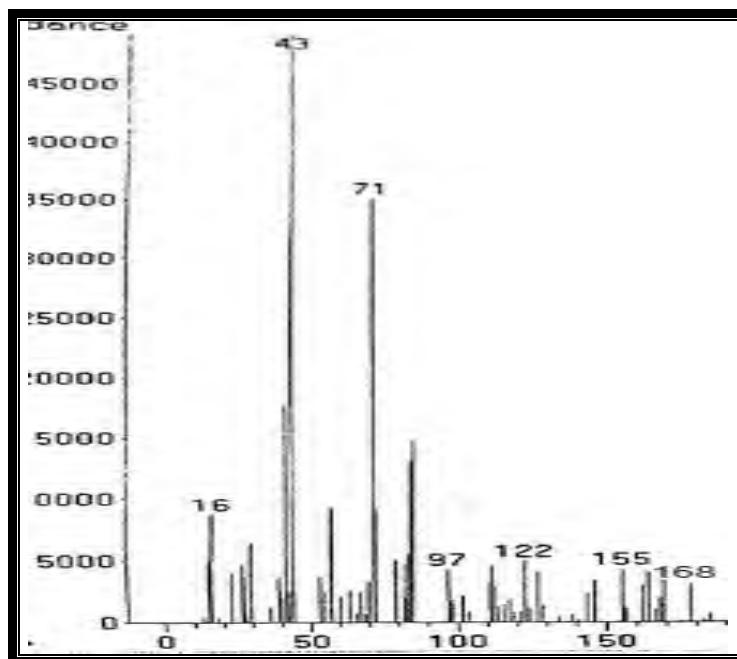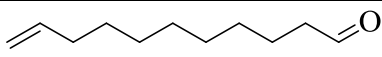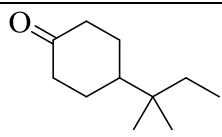
**Figure 1.40** Mass spectrum of RDH-4

The molecular ion peak was recognized at *m/z* 168. The even numbered molecular ion peak suggested that molecule either consisted of even number of nitrogen atoms or absence of nitrogen atom. The base formula RDH-4 was generated as $C_{12}H_{24}$ by the application of rule of thirteen. It suggested that the molecule belonged to the unsaturated aliphatic compounds. The base formula was modified due to the base peak at *m/z* 43. The modified base formula generated was $C_{11}H_{20}O$. The IHD of 2 was calculated for the modified base formula. The possible structures for *m/z* 168 are given in the **table 1.14**.

**Table 1.14** Possible structures for RDH-4

| Sr. No. | Possible structures for RDH-4 |
|---------|-------------------------------|
| 1. |  Undec-10-ene-1-al |
| 2. |  4-(1,1-dimethyl propyl)-cyclo hexanone |
| 3. |  2-Undecenal |

| 4. | Undec-8-ene-2-one |
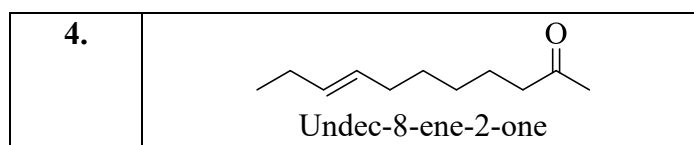
The first structure was ruled out as the base peak of formyl cation was not observed in the mass spectrum of RDH-4. The second structure was excluded as the base peak at *m/z* 43 was not observed in the spectrum of 4-(1,1-dimethyl propyl)-cyclohexanone. The fragmentation ion peaks observed in the given mass spectrum of RDH-4 did not suggest the third compound to be the suitable one structure for RDH-4 compound. The fragment ion peaks of the spectrum justified the undec-8-ene-2-one to be the suitable structure for RDH-4.

The molecular ion peak of undec-8-ene-2-one was observed at *m/z* 168. The base peak at *m/z* 43 was observed by the α-cleavage. The peak at *m/z* 71 was justified by the loss of octenyl radical. By the loss of heptenyl cation, the peak at *m/z* 85 was justified. The peak at *m/z* 97 of heptenyl cation was observed by the loss of butenone radical from molecular ion peak. The fragment ion peak at *m/z* 111 was of octenyl cation was observed by the loss of propenone radical. The fragmentation scheme for RDH-4 is given in **scheme 1.20**.
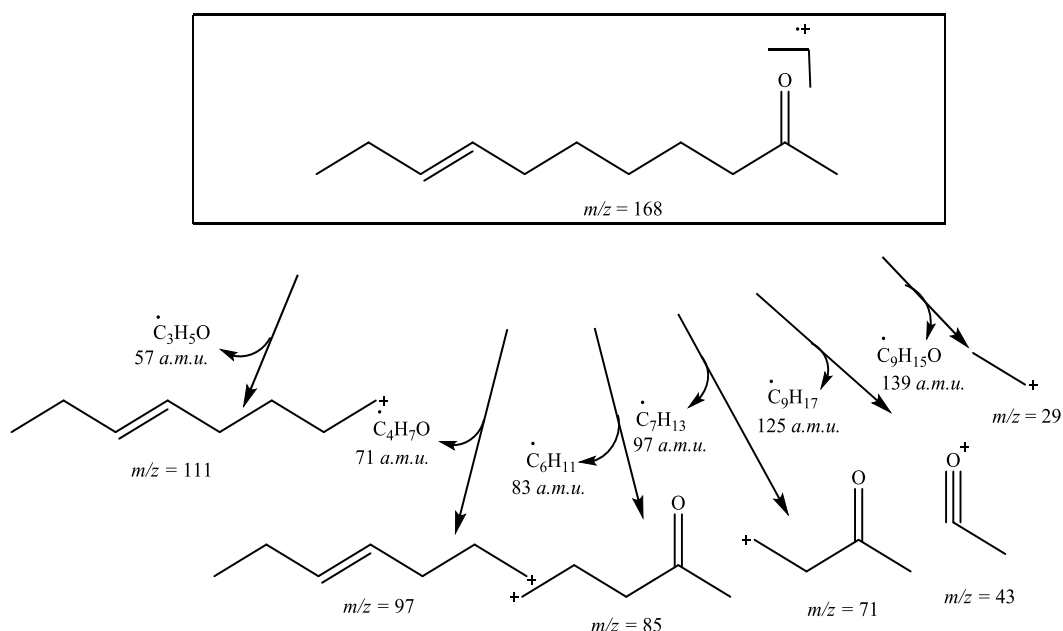


**Scheme 1.20** Fragmentation scheme of RDH-4

79

### 3.6.5 Identification of RDH-5

The compound eluted at retention time of 5.8 minutes was labeled as RDH-5. The less retention time suggested the presence of highly volatile compound. The mass spectrum of RDH-5 is given in **figure 1.41**.
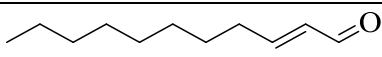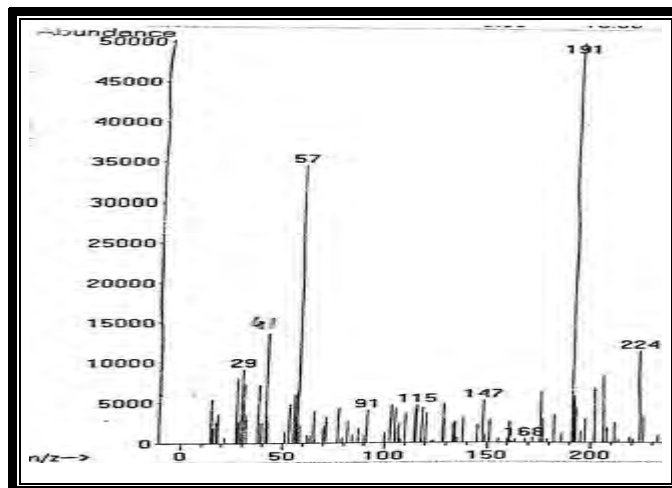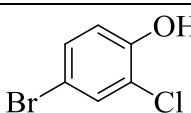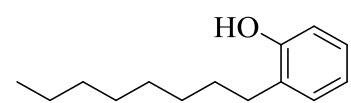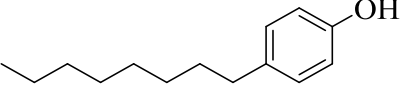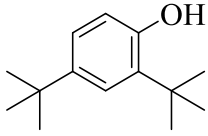


**Figure 1.41** Mass spectrum of RDH-5

The peak at *m/z* 206 was assigned as molecular ion peak. So, the actual mass of the compound was 206 *a.m.u.* The even numbered mass of compound suggested the presence of even number of nitrogen atoms or absence of nitrogen atom. The base formula of the compound was evaluated as $C_{15}H_{26}$ by the implication of rule of thirteen. A modification in the formula was done by considering the base at *m/z* 191. So, the modified base formula of the compound was $C_{14}H_{22}O$ and the IHD of compound was calculated to be 4. The possible structures for the molecular mass are given in the **table 1.15**.
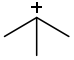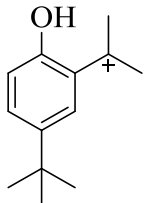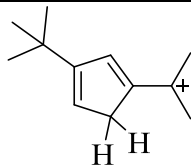
**Table 1.15** Possible structures for RDH-5

| Sr. No. | Possible structure for RDH-5 |
|---------|------------------------------|
| 1. | 4-bromo-2-chlorophenol |
| 2. | 2-octyl phenol |

80

| 3. |  |
|----|----|
|    | 4-octyl phenol |
| 4. |  |
|    | 2,4-di-tert-butyl phenol |

The isotopic peak of chlorine and base peak of first suggested compound was not observed in the given mass spectrum. So, the first compound was ruled out. The second and the third structure exhibited both alkyl and phenyl part. These structures were excluded as mass spectrum of RDH-5 did not show the consecutive losses of $CH_2$ groups. The 3$^{rd}$ compound did not justify the peaks observed on the mass spectrum of RDH-5. The IHD and the fragment peaks supported the 2, 4-di-tert-butyl phenol **(Kharat *et al.*, 2022)** to be the suitable structure for RDH-5. The distinctive peaks and their corresponding structures as identified in the provided mass spectrum of RDH-5 are listed in **table 1.16.**

**Table 1.16** Characteristic fragment peaks in mass spectrum of RDH-5

| Peak (*m/z*) | Structure of the fragment |
|:---:|:---:|
| 57 |  |
| 191 |  |
| 163 |  |

The molecular ion peak of 2, 4-di-t-butyl phenol appeared at *m/z* 206. The base peak appeared at *m/z* 191 corresponding to the removal of methyl radical from the ortho tertiary butyl group which was resonance stabilized with benzene ring. Peak at *m/z*

177 was observed by the loss of carbon monoxide and hydrogen free radical from the parent molecule. The fragment ion peak at *m/z* 163 was observed by the elimination of methyl free radical followed by the loss of neutral carbon monoxide. The tertiary carbocation was observed at *m/z* 57 from parent molecule. The fragmentation scheme of RDH-5 compound is given in the **scheme 1.21**.
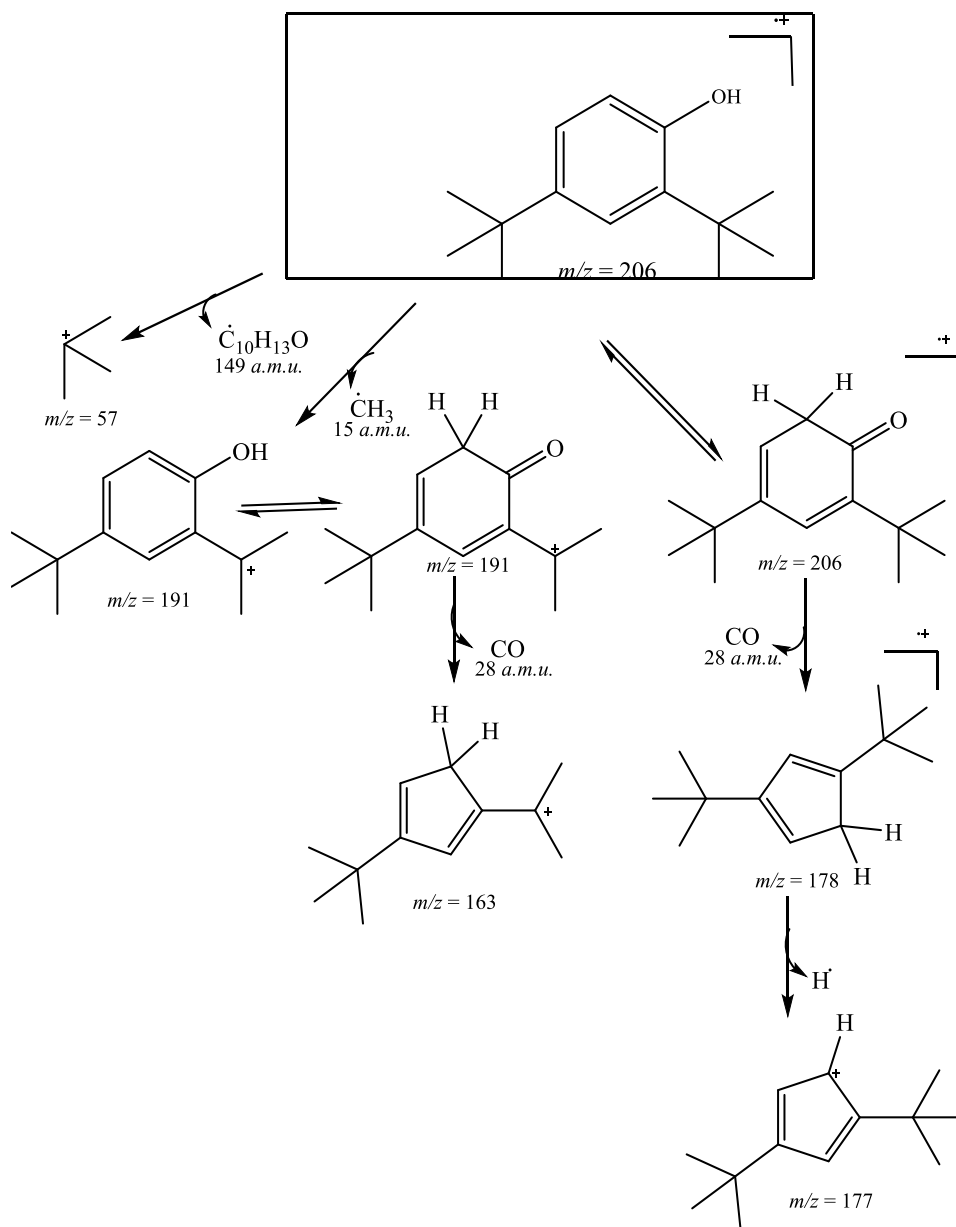


**Scheme 1.21** Mass fragmentation scheme of RDH-5

### 3.6.6   Identification of RDH-6

The signal appeared on TIC profile at 6.65 minutes, was labeled as RDH-6 .Generally the more volatile compounds eluted at first from GC column. It was concluded that

the compound RDH-6 was volatile in nature. The mass spectrum of RDH-6 compound is given below in the **figure 1.42**.
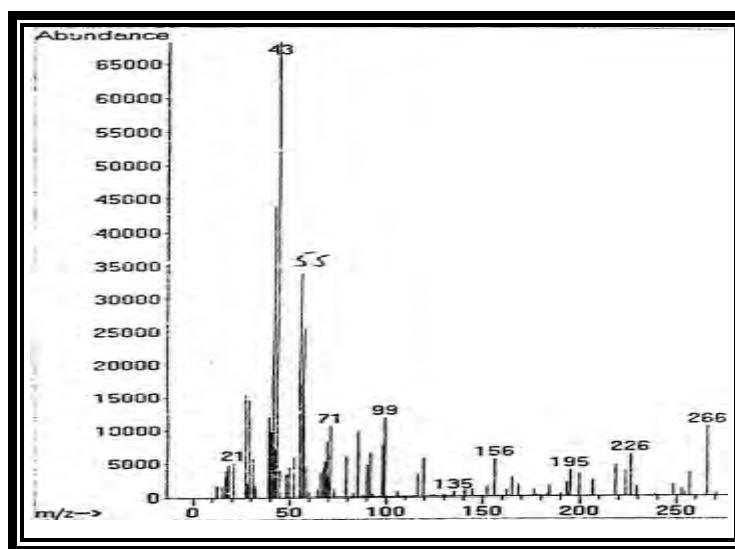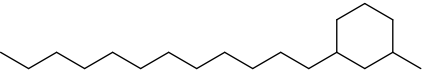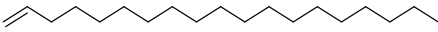


**Figure 1.42** Mass spectrum of RDH-6

In electron ionization mode, mass spectrum of RDH-6 showed the different ion peaks. The peak at *m/z* 266 was recognized as molecular ion peak because it was relatively more intense peak and appeared at higher *m/z* value. The even molecular ionic peak predicted the absence of nitrogen atom in the compound. The base formula of the compound found to be $C_{20}H_{26}$ by applying rule of thirteen. This base formula was modified into $C_{19}H_{38}$. The index of hydrogen deficiency (IHD) was calculated to be one for the modified base formula. The peaks at *m/z* = 27, 55 and 195 justified the presence of one double bond in the compound. The possible structures for modified base formula are given in the **table 1.17**.

**Table 1.17** Possible structures for RDH-6 compound

| Sr.No. | Possible structures according to modified base formula |
|--------|--------------------------------------------------------|
| 1. | Tridecyl cyclo hexane |
| 2. | 7-(methyl cyclo pentyl) tridecane |

| | |
|---|---|
| **3.** | <br>1-Dodecyl-3-methyl cyclo hexane |
| **4.** | <br>Nonadec-1-ene |

First and the third structure was ruled out as the peak at *m/z* 83 of cyclohexyl cation was absent in the mass spectrum of RDH-6 compound. The peak at *m/z* 69 was not observed in the mass spectrum. So, it was predicted that the second structure did not justify the peaks appearing on the mass spectrum of RDH-6 compound. The fourth structure **(Prodhan *et al.,* 2017)** justified the maximum number of fragment ion peaks appeared on the mass spectrum of RDH-6. Therefore, nonadec-1-ene considered to be the correct structure for RDH-6. The base peak at *m/z* 43 of propyl cation appeared by the removal of hexadeca-1-enyl radical from the molecular ion peak. Similarly, peaks at *m/z* 27 and 55 appeared by the loss of heptdecanyl and pentadecanyl radical respectively from the molecular ion peak. Pentyl cation appeared at *m/z* 71 by the *C-C* cleavage of molecular ionic peak. The fragment ion at *m/z* 99 justified the heptyl cation which appeared by the loss of 167 *a.m.u.* from molecular ion peak in the form of dodeca-1-enyl radical. The peak at *m/z* 195 appeared by the loss of Pentyl radical. The loss of nonyl radical resulted in the peak at *m/z* 139 from which the loss of two hydrogen molecules occurred and gave the peak at *m/z* 135. The loss of vinyl radical from molecular ion peak generated the fragment ion at *m/z* 239 with very low intensity peak. It appeared by the cleavage of bond alpha to double bond. The fragmentation scheme for RDH-6 compound is given below in the **scheme 1.22**.
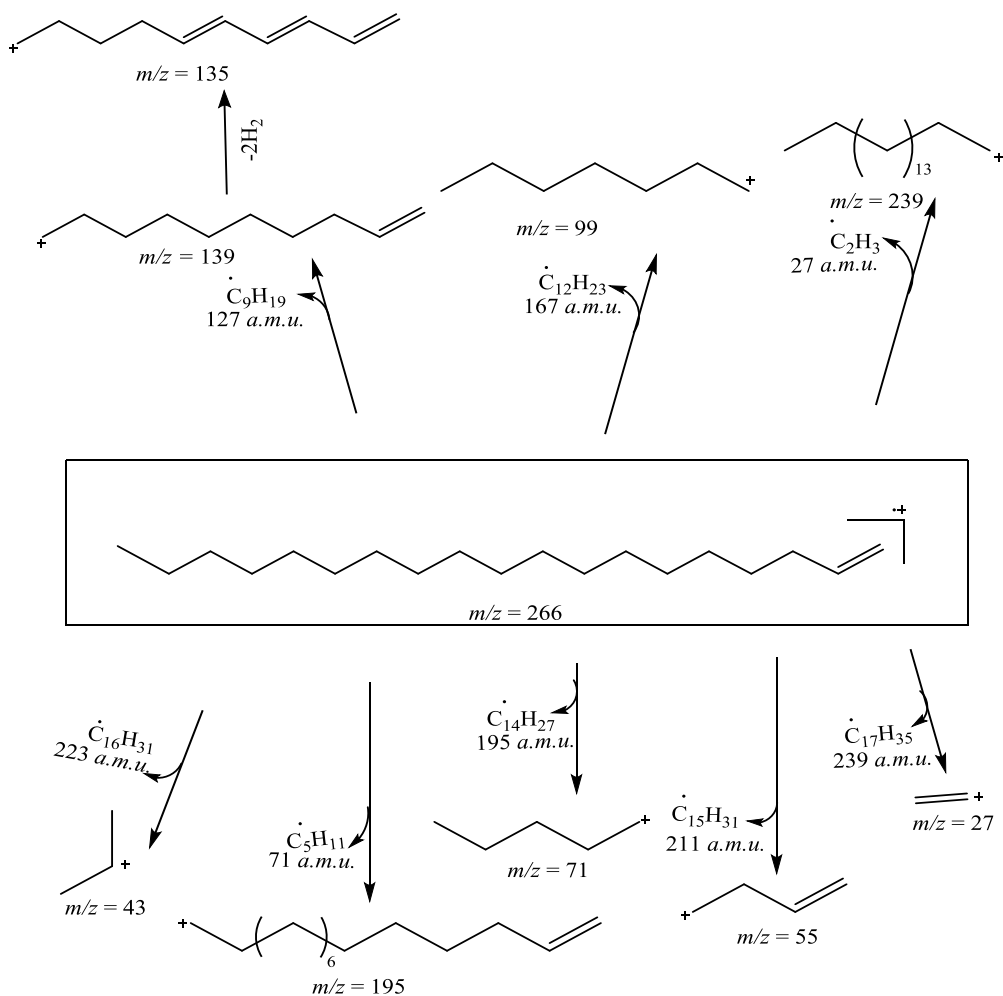
**Scheme 1.22** Fragmentation scheme for RDH-6

### 3.6.7 Identification of RDH-7

The compound labeled as RDH-7 eluted at retention time of 7.6 minutes. So, it was concluded that the RDH-7 compound was highly volatile organic compound. The mass spectrum of RDH-7 in Electron Ionization mode is given in the **figure 1.43**.
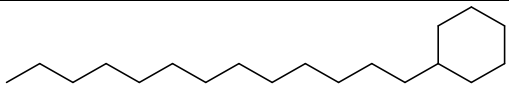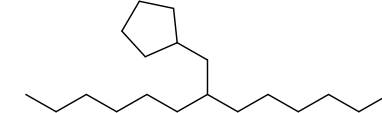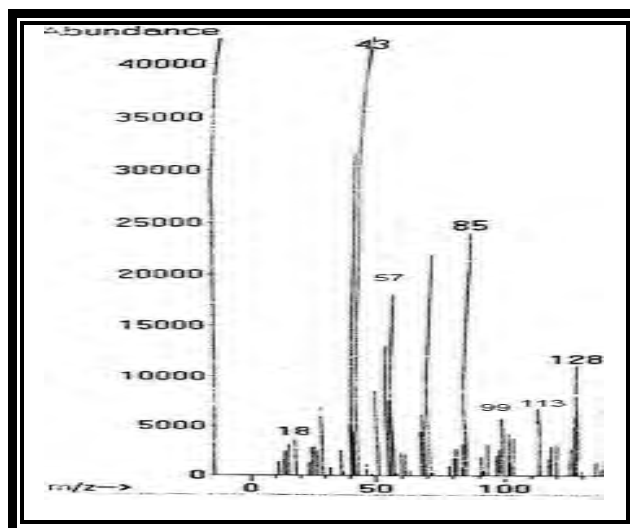
**Figure 1.43** Mass spectrum of RDH-7

The peak at *m/z* 128 was taken as a molecular ion peak due to its significantly higher intensity compared to other peaks. The even numbered molecular ion peak suggested that nitrogen was absent in RDH-7 compound. The base formula for compound was obtained to be $C_9H_{20}$ by applying the rule of thirteen. The base formula was not modified because it indicated that RDH-7 belonged to alkane class of compound. The IHD of the compound was calculated to be one. The possible structures for RDH-7 are given below in the **table 1.18**.

**Table 1.18** Possible structures for RDH-7

| Sr. No. | Possible structures for RDH-7 |
|:---:|:---:|
| 1. | Chloromethyl-2-chlorohexanoate |
| 2. | Octan-2-one |
| 3. | 2-Octene-1-ol |
| 4. | Octan-4-one |

The first structure was ruled out as the isotopic peak of chlorine was not observed on the mass spectrum. The primary alcohol was ruled out as the removal of neutral water

molecule was not observed in the peaks. The fourth structure was ruled out because the base peak of the compound due to acylium cation appeared at *m/z* 71 value which is different to the base peak of the given spectrum appeared at *m/z* 43. The mass fragments peak supported the structure number two as a compound identified for the RDH-7. The characteristics peaks and fragmentation pattern that justified the structure number two for RDH-7 is given in the **table 1.19**.

**Table 1.19** Fragment ion peaks and their inference

| Peaks at (*m/z*) | Inference |
|---|---|
| **29, 57, 71** | Presence of alkyl chain |
| **43 base peak** | Presence of acetylium ion |

The base peak appeared at *m/z* 43 by the loss of hexyl radical by *α*-cleavage from the molecular ion peak. The peak of butyl cation at *m/z* 57 originated by the removal of pentyl radical from the molecular ion peak. The loss of acetyl radical from molecular ion peak resulted in the fragment ion peak at *m/z* 71 of pentyl cation. Similarly, fragment peak at *m/z* 85 resulted by the loss of acetylium radical through *α*-cleavage. The peaks at *m/z* 99 and at *m/z* 113 appeared on mass spectrum of RDH-7 by the loss of ethyl and methyl radical from the molecular ion peak. The peak at *m/z* 29 that corresponded to ethyl cation appeared by the loss of heptyl radical. These fragment peaks fully supported the Octan-2-one a naturally occurring compound **(Damerau *et al.*, 2022)** for RDH-7 compound as a tentative structure. The fragmentation scheme for RDH-7 compound is given below in the **scheme 1.23**.
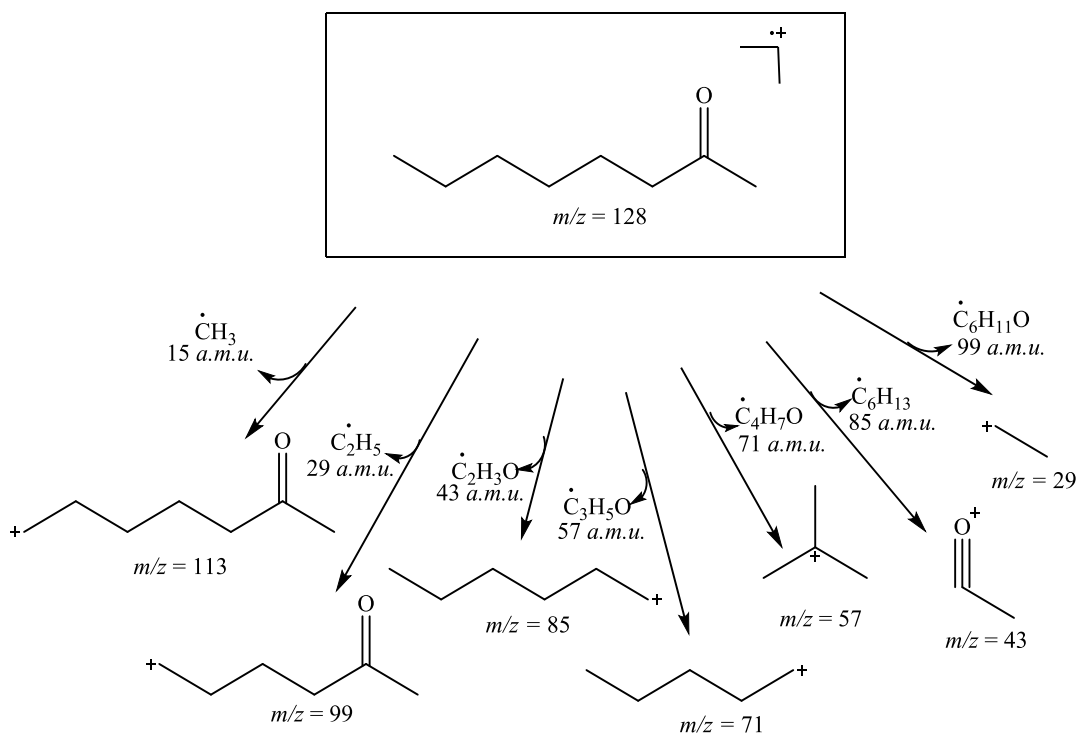
**Scheme 1.23** Fragmentation scheme for RDH-7

### 3.6.8 Identification of RDH-8

The compound eluted at retention time of 8.7 minutes was labeled as RDH-8. The relatively less retention time predicted the high volatility of eluted compound. The mass spectrum of RDH-8 is given in the **figure 1.44**.
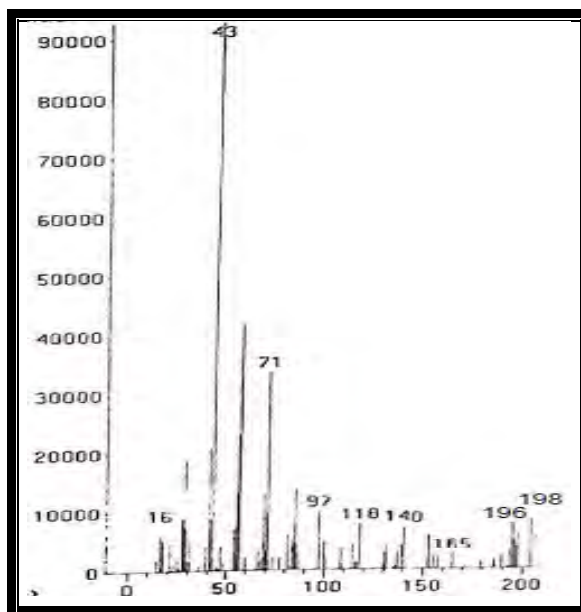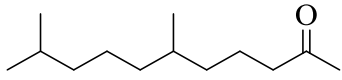


**Figure 1.44** Mas spectrum of RDH-8

The molecular ion peak for RDH-8 was analyzed at *m/z* 198. The even numbered peak suggested that the compound either contained even numbered nitrogen atom or is deprived of nitrogen atom. The base formula for RDH-8 was calculated as $C_{15}H_{18}$. By considering the base peak at *m/z* 43, the base formula was modified into the formula as $C_{13}H_{26}O$. The IHD of 1 was calculated for the compound according to the modified base formula. The structural possibilities for RDH-8 compound are given in the **table 1.20**.

**Table 1.20** Structural possibilities for RDH-8

| Sr. No. | Structural possibilities for RDH-8 |
|---------|-----------------------------------|
| 1. | Br<br>Br<br>1,1-Dibromopropene |
| 2. | O<br>O Cl<br>Cl<br>Chloromethyl-2-chlorohexanoate |
| 3. | O<br>Vinyl undecanyl ether |
| 4. | O<br>6,10-Dimethylundecan-2-one |

The first molecule was ruled out as the isotopic peak of two bromine atoms was not observed in the given spectrum. The second molecule was excluded because the isotopic peak of chlorine atom in peak of chloromethyl-2-chlorohexanoate was missing in the given mass spectral data. The third structure was ruled out due to the absence of the peak at *m/z* 71 due to α-cleavage of ether. So, the structure chosen for RDH-8 was 6, 10-dimethyl undecan-2-one. The fragments peaks are given below in the **table 1.21** that supported the presence of 6,10-dimethylundecan-2-one.

**Table 1.21** Characteristics peaks in the mass spectrum of RDH-8

| Peak (*m/z*) | Structure of the fragments |
|--------------|---------------------------|
| 43 | $O^+$ |

| 57 |  |
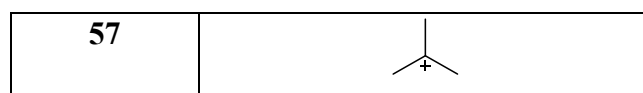
The molecular ionic peak of 6,10-dimethyl undecan-2-one observed at *m/z* 198. The peak at *m/z* 57 indicated the presence of isoprene unit. The base peak at *m/z* 43 indicated the presence of ketone moiety which resulted by the loss of 6,10-dimethyl nonyl radical from the parent ion. The remaining peaks showed the general alkane fragments. The tertiary butyl cation appeared at the *m/z* 57 by the loss of octanoyl radical from parent ion. Similarly, the peaks originated at *m/z* 71 and 85 with the difference of $CH_2$ unit assured the presence of alkanes. Due to the loss of neutral hydrogen molecule from the parent molecule resulted in the peak at *m/z* 196. The loss of pentanoyl radical from *m/z* 196 peak produced the fragment ion at *m/z* 97. The fragmentation peaks of RDH-8 are shown in the **scheme 1.24**.
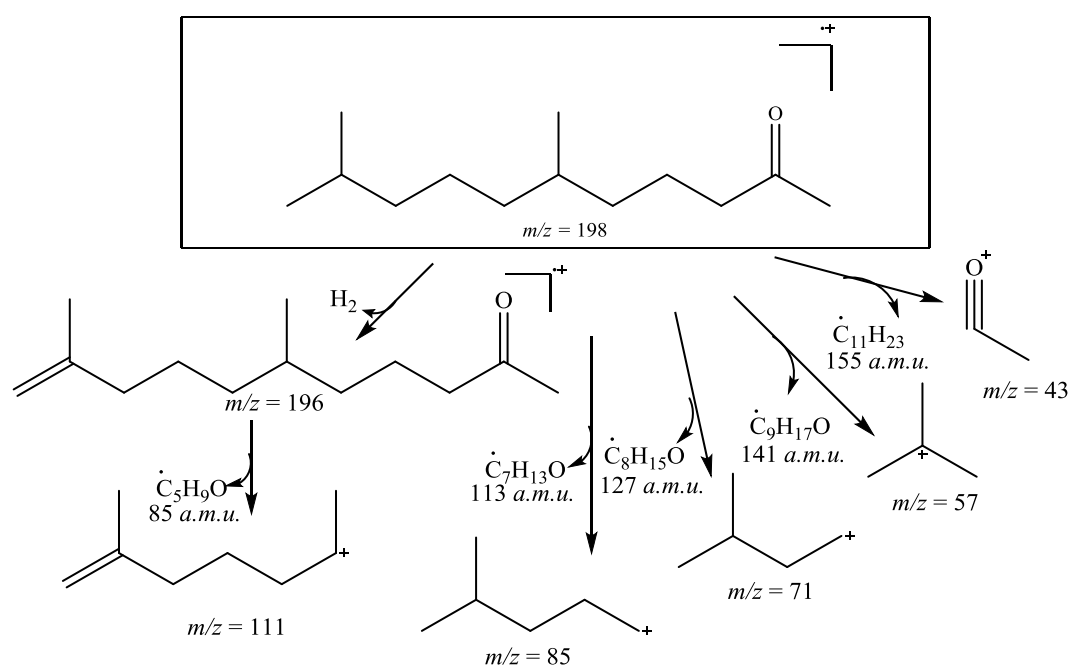


**Scheme 1.24** Mass fragmentation scheme for RDH-8

## 3.6.9  Identification of RDH-9

The compound eluted at retention time of 10.09 minutes was labeled as RDH-9. The relatively high retention time predicted the less volatility of RDH-9 compound. The mass spectrum of RDH-9 is given below in the **figure 1.45**.
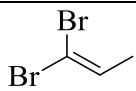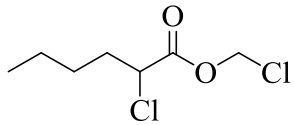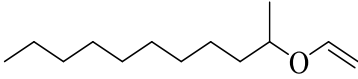
90
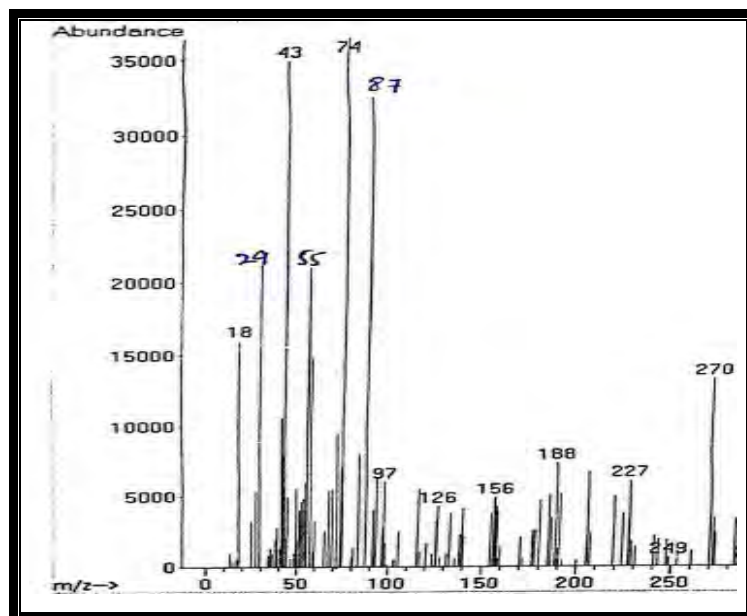
**Figure 1.45** Mass spectrum of RDH-9
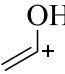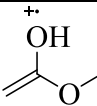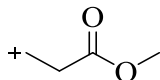
In electron impact ionization, the peak at *m/z* 270 appeared as molecular ion peak because of its noticeable intensity. The even molecular ion peak suggested that the compound was deprived of nitrogen. The application of rule of thirteen resulted in the generation of base formula as $C_{20}H_{30}$. The base formula was modified by considering the base peak which appeared at *m/z* 74. This represents the distinctive base peak of the methyl ester resulting from McLafferty rearrangement. So, the modified base formula was $C_{17}H_{34}O_2$. The IHD for the modified base formula was calculated to be 1.The possible structures for molecular ion peak are given below in the **table 1.22**.

**Table 1.22** Possible structures of RDH-9

| Sr. No. | Possible structures |
|---------|---------------------|
| 1. | <br>Propyl decanoate |
| 2. | <br>Heptanoic acid |
| 3. | <br>1-Octadecanol |
| 4. | <br>Methyl hexadecanoate |

The first structure was ruled out because the mass spectrum of RDH-9 did not exhibit the presence of base peak at *m/z* 102. The peak at *m/z* 60 which is the base peak of acids was not observed in the RDH-9 spectrum. So, the second spectrum was dismissed in this way. The primary alcohols showed the distinct peak at *m/z* 31 of oxonium ion which was not observed in this spectrum. Methyl hexadecanoate was chosen as the correct structure for RDH-9. The peaks observed in the mass spectrum of RDH-9 are given below in the **table 1.23**.

**Table 1.23** Characteristics peaks observed in the mass spectrum of RDH-9

| Peak (*m/z*) | Structure of fragment |
|---|---|
| 43 |  |
| 74 |  |
| 87 |  |

The molecular ion peak of methyl palmitate appeared at *m/z* 270. The base peak of methyl ester originated at *m/z* 74 through McLafferty rearrangement as shown in the **scheme 1.25**.
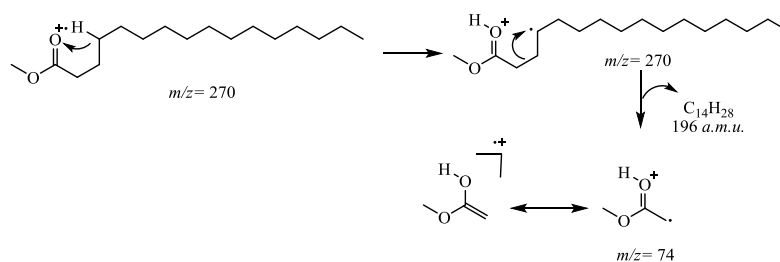


**Scheme 1.25** Mechanism for McLafferty rearrangement

The second highly intense peak at *m/z* 43 resulted by the loss of methoxy free radical in a homolytic cleavage of base peak. The peak at *m/z* 55 appeared by the 1,3-hydride shift along with removal of methoxy radical. The mechanism for *m/z* 55 is given below in the **scheme 1.26**.

*m/z* = 270

C$_{13}$H$_{26}$ + H$_2$
185 *a.m.u.*

ȮCH$_3$
31 *a.m.u.*
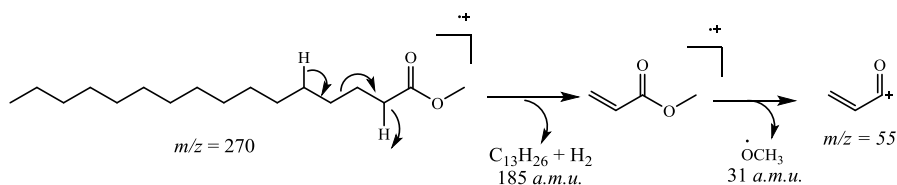
*m/z* = 55

**Scheme 1.26** Mechanism for peak *m/z* 55

By the γ-cleavage, a fragment at *m/z* 87 was detected with considerably high intensity. The fragment ion peak at *m/z* 97 of heptenyl cation originated by the *C-C* bond cleavage from molecular ion peak followed by the neutral loss of hydrogen molecule from heptyl cation occurred. The next fragment peak at *m/z* 129 appeared by the loss of decyl radical from molecular ion peak. The removal of hydrogen radical gave rise to the peak at *m/z* 126. The elimination of the octane fragment from the molecular ion peak revealed a radical cation at *m/z* 156. The heptenyl cation was observed at *m/z* 97 by the loss of 173 *a.m.u.* from molecular ion peak. The peak at *m/z* 227 was observed by the loss of methyl radical from the parent molecule. The fragmentation scheme for RDH-9 is given in the **scheme 1.27**.
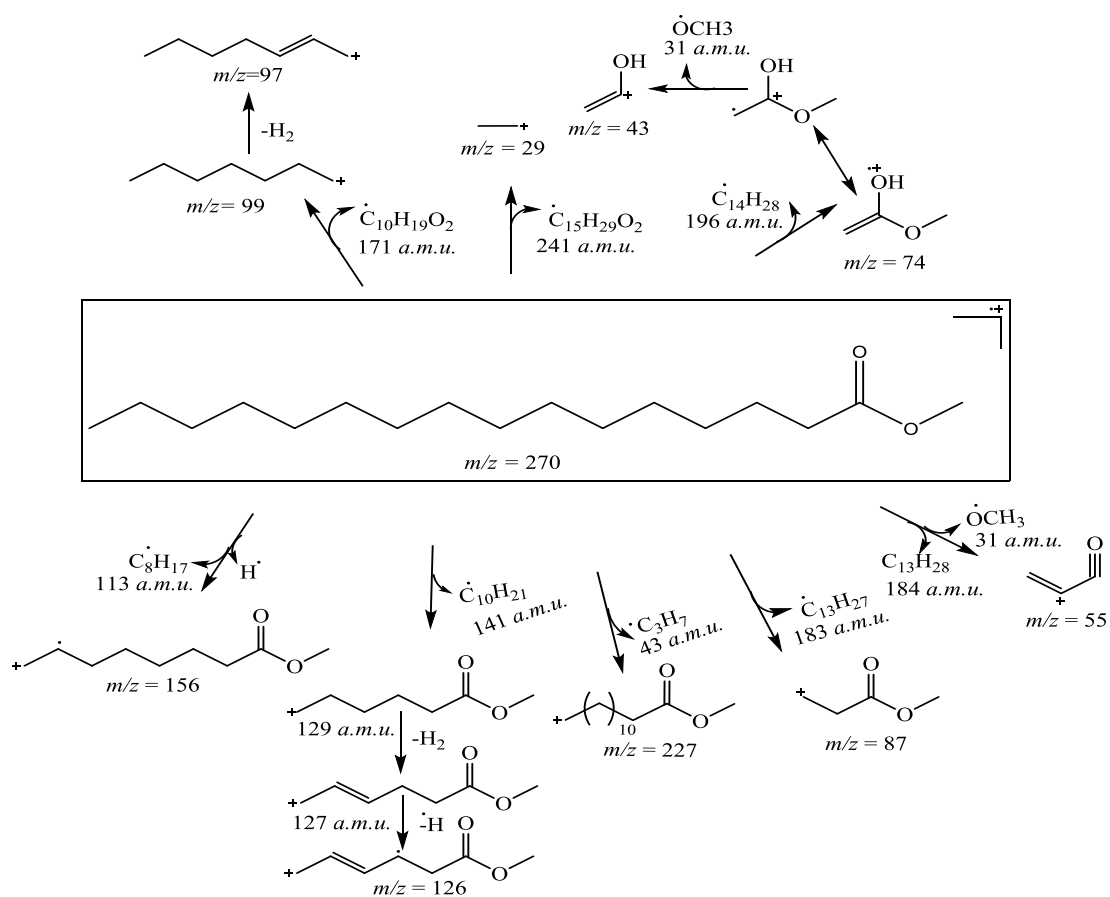
**Scheme 1.27** Mass fragmentation scheme for RDH-9

## 3.6.10 Identification of RDH-10

The compound identified at retention time of 10.5 minutes was labeled as RDH-10. The relatively high retention time indicated that the eluted compound is relatively less volatile in nature. The mass spectrum of RDH-10 is given below in the **figure 1.46**.
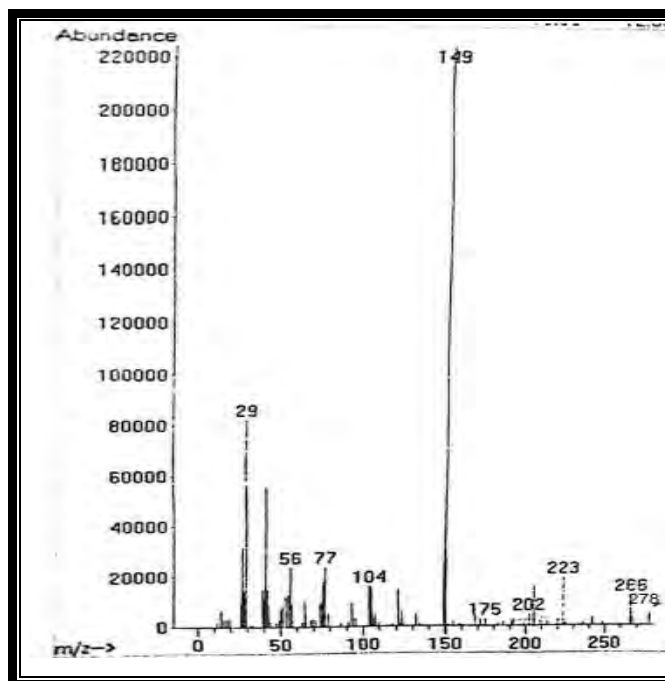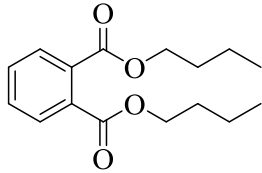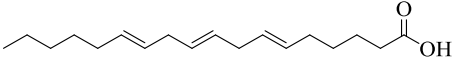
**Figure 1.46** Mass spectrum of RDH-10

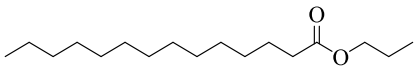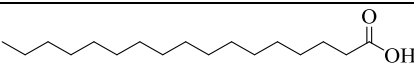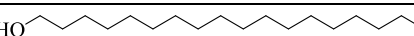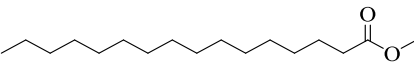Under electron impact ionization mode, the RDH-10 compound exhibited a notable intensity with its molecular ion peak originating at *m/z* 278. The even molecular mass showed the absence of nitrogen atom in compound. The modified formula for RDH-10 compound was calculated as $C_{16}H_{22}O_4$. The highest intensity peak at *m/z* 149 was considered as a base peak of phthalate as reported by **Yin *et al.,* (2014)**. The IHD of 6 was calculated for the modified base formula. The possible structures for RDH-10 are given below in the **table 1.24**.

**Table 1.24** Possible structures for RDH-10 compound

| Sr. No. | Possible structures for RDH-3 compound |
|---------|----------------------------------------|
| 1. |  Dibutyl phthalate |
| 2. |  Octadeca-6,9,12-trienoic acid |

| 3. |  |
|---|---|
| | Benzoic acid-4-methoxy nonyl ester |
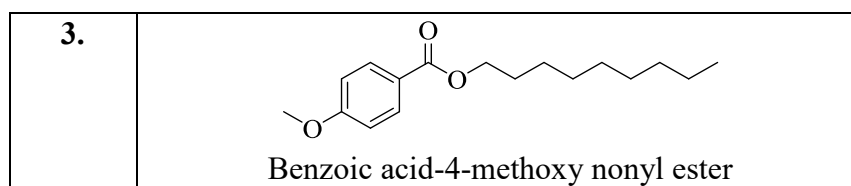
The second structure was ruled out because the acid shows the characteristic peak at *m/z* 45 by the alpha cleavage which was not observed in the mass spectrum of RDH-10. The fourth compound did not align with the mass spectral data of RDH-10 as the molecule lacked the peak at *m/z* 149. The fragmentation pattern and base peak at *m/z* 149 supported the structure number one to be the right structure for RDH-10. The dibutyl phthalate showed the molecular ion peak at *m/z* 278 in electron ionization mode. The peak at *m/z* 205 was observed by the loss of butoxy radical by α-cleavage from molecular ion peak. The base peak at *m/z* 149 was observed by the loss of butyl radical from the fragment ion peak at *m/z* 205 in such a way that the formation of five membered ring occurred. The peak at *m/z* 104 was observed by the loss of carboxyl group from base peak by bond rearrangement. The loss of carbon monoxide from fragment at *m/z* 104 resulted in the phenyl cation at *m/z* 77. Butyl radical cation appeared at *m/z* 56 by the loss of neutral fragment of 222 *a.m.u.* from molecular ion peak. The loss of methyl radical resulted in vinyl cation at *m/z* 41. The peak at *m/z* 29 corresponded to the ethyl cation which was observed due to the loss of 249 *a.m.u.* from molecular ion peak. The fragmentation scheme for RDH-10 is given in the **scheme 1.28**.
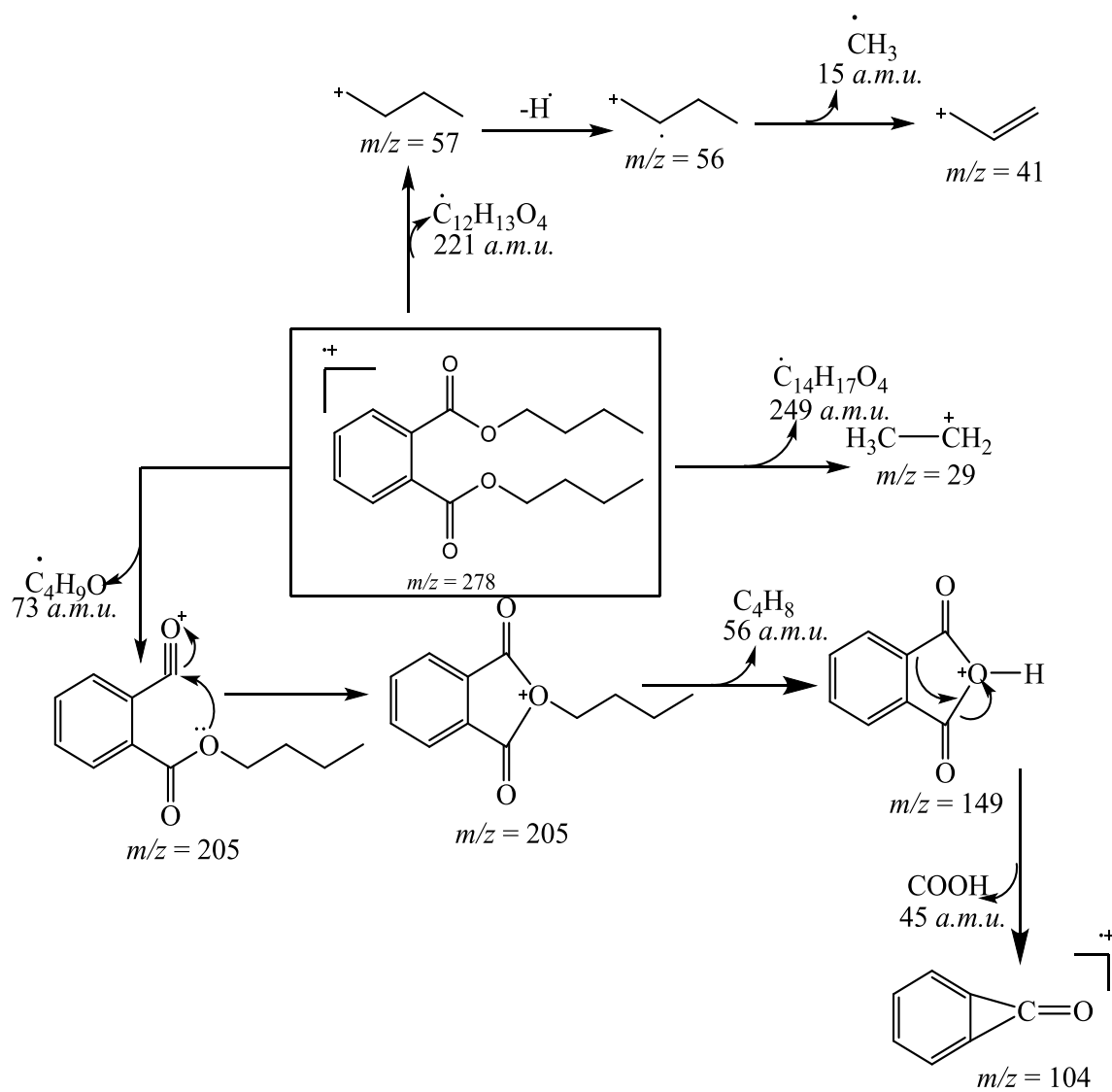
**Scheme 1.28** Fragmentation scheme for RDH-10

The list of volatile compounds identified by GC-MS analysis is given below in the table **1.25**.

**Table 1.25** Compounds identified by GC-MS analysis

| Code of the compound | Retention time (minutes) | Molecular ion peak (*m/z*) | Name of the identified compound |
|---|---|---|---|
| RDH-1 | 2.68 | 140 | Dec-1-ene |
| RDH-2 | 4.50 | 190 | Octyl benzene |
| RDH-3 | 4.86 | 214 | 2-Phenoxy benzoic acid |
| RDH-4 | 5.40 | 168 | Undec-8-ene-2-one |
| RDH-5 | 5.83 | 206 | 2,4-Di-tert-butyl phenol |
| RDH-6 | 6.50 | 266 | Nonadec-1-ene |
| RDH-7 | 7.68 | 128 | 2,4-Dimethyl heptane |
| RDH-8 | 8.78 | 198 | 6,10-Dimethyl undecan-2-one |
| RDH-9 | 10.09 | 270 | Hexadecanoic acid, methyl ester |
| RDH-10 | 10.54 | 278 | Dibutyl phthalate |

# CONCLUSION

The present research work is the first substantial mass spectrometric analysis of phytochemicals from the leaves of *Rhaphidophora decursiva.* A total of fourteen compounds were identified for the first time from genus *Rhaphidophora* by using HPLC-DAD-ESI-MS technique. The identified compounds include phenolic acids, apigenin *C*-glycosides, acacetin and a steroid type of compound. The identified compounds exhibit a wide range of medicinal properties. They could be used for antibacterial, anti-inflammatory, antifungal, anticancer, and antioxidant activities. Therefore, these compounds can serve as potential candidates for drug development.

This study also provided the GC-MS report of *Rhaphidophora decursiva* from which the ten hydrocarbons were identified for the first time. The chemical pool included dec-1-ene, octyl benzene, 2-phenoxy benzoic acid, undec-8-ene-2-one, 2,4-di-tert-butyl phenol, Nonadec-1-ene, 2,4-dimethyl heptane, 6,10-dimethyl undecan-2-one, hexadecnoic acid, methyl ester and dibutyl phthalate.

This work explored phytoconstituents that are helpful against various ailments. This study also vindicates the significance of phytochemical analyses of relatively less explored ornamental plants in comparison to herbaceous plants for the investigation of new classes of biologically active constituents. The current study bridged the gap present in the existing literature regarding the phytochemical analysis of the said plant using hyphenated techniques like GC-MS and LC-MS. The identified compounds have various biological properties that render this plant a suitable and easy to access alternative for various drugs. This very study paves the way for the further exploration of the plant that will be a healthy addition in the field of medicinal chemistry.

# REFERENCES

Anttonen, M. J. and Karjalainen, R.O. (2006). High-Performance Liquid Chromatography Analysis of Black Currant (*Ribes nigrum L.)* Fruit Phenolics Grown either Conventionally or Organically. *Journal of Agricultural and Food Chemistry*, *54*(20), 7530-7538.

Arsad, S. S., Esa, N. M., Hamzah, H. and Othman, F. (2013). Evaluation of Acute, Subacute and Subchronic Oral Toxicity of *Rhaphidophora decursiva* (Roxb.) Schott extract in Male Sprague Dawley Rats. *Journal of Medicinal Plants Research*, *7*(41), 3030-3040.

Arulpriya, P. and Lalitha, P. (2011). The Potential Use of *Rhaphidophora aurea* at Various Aspects. A Review (1958-2011). *Journal of Pharmacy Research*, *4*(11), 4006-4010.

Asfaram, A., Ghaedi, M. and Dashtian, K. (2017). Rapid Ultrasound-Assisted Magnetic Microextraction of Gallic Acid from Urine, Plasma and Water Samples by HKUST-1-MOF-$Fe_3O_4$-GA-MIP-NPs: UV–Vis Detection and Optimization Study. *Ultrasonics Sonochemistry*, *34*, 561-570.

Ballantine, J. A. and Pillinger, C. T. (1968). A Study of Rearrangement Processes in the Mass Spectra of Substituted diphenyl-ethers. *Organic Mass Spectrometry*, *1*(3), 447-458.

Boyce, P. C. (1999). The Genus *Rhaphidophora* Hassk. (Araceae-Monsteroideae-Monstereae) in Peninsular Malaysia and Singapore. *Gardens' Bulletin Singapore*, *51*, 183-256.

Cao, J., Yin, C., Qin, Y., Cheng, Z. and Chen, D. (2014). Approach to the Study of Flavone di-*C*-glycosides by High Performance Liquid Chromatography-Tandem Ion Trap Mass Spectrometry and its Application to Characterization of Flavonoid Composition in *Viola yedoensis*. *Journal of Mass Spectrometry*, *49*(10), 1010-1024.

Carbone, V., Montoro, P., de Tommasi, N. and Pizza, C. (2004). Analysis of Flavonoids from *Cyclanthera pedata* Fruits by Liquid Chromatography/Electrospray Mass Spectrometry. *Journal of Pharmaceutical and Biomedical Analysis*, *34*(2), 295-304.

Castro-Perez, J., Roddy, T. P., Nibbering, N. M., Shah, V., McLaren, D. G., Previs, S. and Hankemeier, T. (2011). Localization of fatty acyl and double bond positions in phosphatidylcholines using a dual stage CID fragmentation coupled with ion mobility mass spectrometry. *Journal of the American Society for Mass Spectrometry*, *22*(9), 1552-1567.

Chapagain, B. P. and Wiesman, Z. (2007). Determination of Saponins in the Kernel Cake of *Balanites aegyptiaca* by HPLC-ESI/MS. *Phytochemical Analysis*, *18*(4), 354-362.

Chen, J., Henny, R. J. and Liao, F. (2007). Aroids are Important Medicinal Plants. *Acta Hortica*, *756*,347-354.

Cuyckens, F. and Claeys, M. (2004). Mass Spectrometry in the Structural Analysis of Flavonoids. *Journal of Mass Spectrometry*, *39*(1), 1-15.

Deivanathan, S. K. and Prakash, J. T. J. (2023). Bio-synthesis of Silver Nanoparticles using Leaf Extract of *Rhaphidophora pertusa* and its Characterization, Antimicrobial, Antioxidant and Cytotoxicity Activities. *Research on Chemical Intermediates*, *49*(2), 423-439.

Esa, N. M. and Phuah, S. C. (2009). *Rhaphidophora decursiva* Leave*s*: Phenolic Content and Antioxidant Activity. *Journal of Tropical Agriculture and Food Science*, *37*(1), 61-66.

Es-Safi, N. E., Kerhoas, L. and Ducrot, P. H. (2007). Fragmentation Study of Globularin Through Positive and Negative ESI/MS, CID/MS, and Tandem MS/MS. *Spectroscopy Letters*, *40*, 695-714.

Firdaus, M. R., Ifora. and Oktavia, S. (2023). Phytochemical and Pharmacological Studies of *Rhaphidophora pinnata* (Lf) Schott.: A Review. *EAS Journal of Pharmacy and Pharmacology*. *5*(4).

Firdhouse, M. J. and Lalitha, P. (2017). Cytotoxicity of Spherical Gold Nanoparticles Synthesised Using Aqueous Extracts of Aerial Roots of *Rhaphidophora aurea* (Linden ex Andre) Intertwined Over *Lawsonia Inermis* and *Areca catechu* On MCF-7 Cell Line. IET Nanobiotechnology, *11*(1), 2-11.

Guerra, M., Cabral, M. H. and Paiva, A. C. S. (2015). Fragmentation Pathways of Diphenyl Ether Radical Cations. *International Journal of Mass Spectrometry*, *393*, 9-16.

Hertian, R., Muhaimin. and Sani, F. (2021). Efectiveness Test of (*Rapidophora pinnata* L. Schott) Leaf Extract for Wound Healing in Male Mice. *Indonesian Journal of Pharma Science*, 1(1), 11-20.

Kabir, M. S. H., Chakrabarty, N., Hasanat, A., Al Noman, M. A., Zaheed, F., Hasan, M., Kader, S. M. A., Hussain M. M., Chowdhury, T. A. and Ahmad, S. (2016). *In vivo* Hypoglycemic Effect of Ethanol Extract and its Fractions of *Rhaphidophora glauca* (Wall.) Schott Leaves with Area Under Curve (AUC) during Oral Glucose Tolerance Test (OGTT). *African Journal of Pharmacy and Pharmacology*, *10*(13), 250-256.

Kabir, M. S. H., Hossain, M. M., Hasanat, A., Rahman, M. M., Masum, M. A. A., Hasan, M. and Kamal, A. T. M. M. (2015). Anthelmintic and α-amylase inhibition effects of ethanol extract and its different fractions of *Rhaphidophora glauca* (Wall.) Schott leaves. IOSR J. Pharm. Biol. Sci, 10(3), 99-104.

Kharat, B. A., Said, M. S. and Dastager, S. G. (2022). Antifungal compound from marine *Serratia marcescens* BKACT and its potential activity against *Fusarium* sp. *International Microbiology*, *25*(4), 851-862.

Krenek, K. A., Barnes, R. C. and Talcott, S. T. (2014). Phytochemical Composition and Effects of Commercial Enzymes on the Hydrolysis of Gallic Acid Glycosides in Mango (*Mangifera indica L.* cv.„Keitt") Pulp. *Journal of Agricultural and Food Chemistry*, *62*(39), 9515-9521.

Lestari,D., Intan, L. and Fathnur, K. S. (2021). Testing the Effectiveness of Dragon Tail Leaf Ethanol Extract (*Rhaphidophora pinnata* (Lf) Schott) as Antihyperglycemia on Male White Mice Which Induced by Sucrose. *Manuntung Scientific Journal*, *7*(1), 100–110.

Li, S., Long, C., Liu, F., Lee, S., Guo, Q., Li, R., and Liu, Y. (2006). Herbs for Medicinal Baths Among the Traditional Yao Communities of China. *Journal of Ethnopharmacology*, *108*(1), 59-67.

Linnet, A., Latha, P. G., Gincy, M. M., Anuja, G. I., Suja, S. R., Shyamal, S., Shine, V. J., Sini, S., Shikha, P., Dan, M. and Rajasekharn, S. (2010). Anti-inflammatory, Analgesic and Anti-lipid Peroxidative Effects of *Rhaphidophora pertusa* (Roxb.) Schott. and *Epipremnum pinnatum* (Linn.) Engl. aerial Parts. *Indian Journal Of Natural and Resources.1*(1), 5-10.

Mabry, T., Markham, K. R. and Thomas, M. B. (1970). *The Systematic Identification of Flavonoids*. *pp.23-25*, New York: Springer-Verlag.

Markham, K. R. (1982). *Techniques of Flavonoid Identification*. pp.39, London: Academic press.

Markovic, S. and Tosovic, J. (2015). Application of Time-dependent Density Functional and Natural Bond Orbital Theories to the UV–vis Absorption Spectra of Some Phenolic Compounds. *The Journal of Physical Chemistry A*, *119*(35), 9352-9362.

Masfria, Harahap, U., Nasution, M. P. and Ilyas, S.(2014). Cytotoxic Activity, Proliferation Inhibition and Apoptosis Induction of *Rhaphidophora pinnata* (LF) schott Chloroform Fraction to MCF-7 Cell Line. *International Journal of PharmTech Research, 6*(4), 1327-1333.

Masfria, M., Marianne, M. and Permata, Y. M. (2019). Organic and Inorganic Analysis of *Rhaphidophora pinnata* (lf) Schott Water Extract. *Open Access Macedonian Journal of Medical Sciences*, *7*(22), 3790-3793.

Masfria, M., Marianne, M., Permata, Y. M., Octavio, S. and Mulyani, S. (2021). Antimutagenic Activity of Nanoparticles of *Rhaphidophora pinnata* Leaves in Mice using Micronucleus Assay. *Journal of Advanced Pharmaceutical Technology and Research*, *12*(3), 232-235.

Masfria, Sumaiyah. and Dalimunthe, A. (2017). Antimutagenic Activity of Ethanol Extract of *Rhaphidophora pinnata* (Lf) schott Leaves on Mice. *Scientia Pharmaceutica*,*85*(1), 7.

Masfria. (2015). Antibacterial Activity of Ethyl Acetate and Ethanol Extract of *Rhaphidophora pinnata* (L.f) Schott Leaf Against Four Types of Bacteria. *International Journal of ChemTech Research,.8*(6), 905-914.

Masfria., Harahap, U., Nasution, M. P. and Ilyas, S. (2013). The Activity of *Rhaphidophora pinnta* Lf. Schott leaf on MCF-7 Cell Line. *Advances in Biological Chemistry*, *3*(4), 2013.

Mashima, K., Hatano, M., Suzuki, H., Shimosaka M. and Taguchi, G. (2019). Identification and Characterization of Apigenin 6-*C*-glucosyltransferase Involved in Biosynthesis of Isosaponarin in Wasabi (*Eutrema japonicum*). *Plant and Cell Physiology*, *60*(12), 2733-2743.

Pascila, B., Sani K, F., Asra, R. and Samudra, A. G. (2020). Testing the Activity of Dragon Tail Leaf Ethanol Extract (*Rhaphidophora Pinnata* (Lf) Schott.) as Antihyperuricemia On Male White Mice. *Journal Manuntung Scientific*, *6*(02), 299-305.

Phukan, A., Chetia, B., Handique, J. G. and Kardong, D. (2016). Antimicrobial, Antioxidant Activities and RP-HPLC Analysis of Three Edible Medicinal Plants *Olax acuminata*, *Gnetum gnemon* and *Rhaphidophora hongkongensis*. *National Academy Science Letters*, *39*(2), 99-102.

Ponnusamy, A., Pottail, L. and Chithambharan, A. (2022). Isolation and Identification of Few Fatty Acid Esters from the Aerial Roots of *Rhaphidophora aurea* Twined Over Different Host Trees. *Indian Journal of Natural Products and Resources, 13*(2), 234-243.

Prodhan, Z. H., Faruq, G., Rashid, K. A. and Taha, R. M. (2017). Effects of Temperature on Volatile Profile and Aroma Quality in Rice. *International Journal of Agriculture and Biology*, *19*(5), 1065-1072.

Roowi, S. and Crozier, A. (2011). Flavonoids in Tropical *Citrus* Species. *Journal of Agricultural and Food Chemistry*, *59*(22), 12217-12225.

Sakushima, A., Coşkun, M. and Maoka, T. (1995). Hydroxybenzoic Acids from *Boreava Orientalis*. *Phytochemistry*, *40*(1), 257-261.

Salpin, J. Y. and Tortajada, J. (2002). Structural Characterization of Hexoses and Pentoses using Lead Cationization. An Electrospray Ionization and Tandem mass Spectrometric Study. *Journal of Mass Spectrometry*, *37*(4), 379-388.

Sani K, F., Magfirah, D., Yuliawati, Y., Elisma, E. and Lestari, U. (2023). Acute Toxicity Test of Ekor Naga (*Rhaphidophora pinnata* (Lf) Schott) Leaf Extract in Mice and Kidney Histological Examination. *Indonesian Journal of Cancer Chemoprevention*, *13*(3), 152-158.

Sasikumar, J. M. and Doss, P. A. (2006). *In Vitro* Antioxidant and Antibacterial Activity of *Rhaphidophora pertusa* stem. *Fitoterapia*, *77*(7-8), 605-607.

Sasikumar, J. M., Asha, S. K., Shamna, R., Maheshu, V. an Darsini, D. T. P. Effects of *Rhaphidophora pertusa* (Roxb.) Schott. Methanolic Extract on Acetaminophen-Induced Hepatic Injury in Albino Rats. *Medicinal and Aromatic Plant Science and Biotechnology*,*4*(1), 49-51.

Shui, G. and Peng, L. L. (2004). An Improved Method for the Analysis of Major Antioxidants of *Hibiscus esculentus* Linn. *Journal of Chromatography A*, *1048*(1), 17-24.

Sumaiyah, Masfria Dalimunthe, A. (2018). Determination of Total Phenolic Content, Total Flavonoid Content, and Antimutagenic Activity of Ethanol Extract Nanoparticles of *Rhaphidophora pinnata* (Lf) schott leaves *Rasayan Journal of Chemistry, 11*(2). 505-510.

Sumaiyah, S., Masfria, M. and Dalimunthe, A. (2020). Anti-Inflammatory Activity of *Rhaphidophora pinnata* (LF) Schott Leaf Extract. *Open Access Macedonian Journal of Medical Sciences*, *8*(A), 487-490.

Sumaiyah., Masfria. and Dalimunthe, A. (2018). Analgesic Activity of Ethanol Extract of *Rhaphidophora pinnata* Lf Schott Leaves in Mice Induced by Acetic Acid. *Science and Technology Publications,* 224-226.

Summaiyah, Masfria Dalimunthe, A. (2018). Analgesic Activity of Ethanol Extract of *Rhaphidophora pinnata* Lf Schott Leaves in Mice Induced by Acetic Acid. *Science and Technology Publications,* 224-226.

Summaiyah, Masfria Rusdi, I. Y. and Dalimunthe, A. (2018). The Preparation and Characterization of Ethanol Extract Nanoparticle from *Rhaphidophora pinnata* (Lf) Schott Leaves by using Arabic Gum and Dextrin. *Journal of Young Pharmacists*, *10*(2), 84-86.

Tao, J. H., Wang, D. G., Yang, C., Huang, J. H., Qiu, W. Q. and Zhao, X. (2015). Biotransformation of Luteoloside by a Newly Isolated Human Intestinal Bacterium using UHPLC-Q-TOF/MS. *Journal of Chromatography B*, *991*, 1-8.

Taylor, W. H., Sinha, A., Khan, I. A., McDaniel, S. T. and Esko, J. D. (1998). Primers of Glycosaminoglycan Biosynthesis from Peruvian Rain Forest Plants. *Journal of Biological Chemistry*, *273*(35), 22260-22266.

Terheijden, J., Van Koten, G., Vinke, I. C. and Spek, A. L. (1985). 1, 2-Methyl Shift Between Platinum and the Coordinated Aryl Group in the Reaction of Methyl Iodide with 2, 6-bis [(dimethyl amino) methyl] phenyl-N, N', C Complexes of Platinum (II). X-ray Crystal Structure of the Arenonium-Platinum Compound I. *Journal of the American Chemical Society*, *107*(10), 2891-2898.

Tsimogiannis, D., Samiotaki, M., Panayotou, G. and Oreopoulou, V. (2007). Characterization of Flavonoid Subgroups and Hydroxy Substitution by HPLC-MS/MS. *Molecules*, *12*(3), 593-606.

Uddin, M. M. N., Dash, R., Kabir, M. S. H., Rahman, M. M., Islam, M. N. and Paul, A. (2016). Cytotoxic, Antibacterial and Analgesic Activities of *Rhaphidophora glauca* (Wall.) Schott leaves. *Journal of Coastal Life Medicine, 4*(9), 750-756.

Walidah, H. M., Anayanti, A. and Yuandani, Y. (2020). Anti-Inflammatory Activity Test of *n*-Hexane Fraction Cream (*Rhaphidophora Pinnata* (LF) Schott.) on Carrageenan Induced Back Edema in Mice. *Asian Journal of Pharmaceutical Research and Development*, *8*(6), 33-38.

Wang, J., Davis, M., Li, F., Azam, F., Scatina, J. and Talaat, R. (2004). A Novel Approach for Predicting Acyl Glucuronide Reactivity via Schiff Base Formation: Development of Rapidly Formed Peptide Adducts for LC/MS/MS Measurements. *Chemical Research in Toxicology*, *17*(9), 1206-1216.

Wong, K. T. and Tan, B. K. H. (1996). *In Vitro* Cytotoxicity and Immunomodulating Property of *Rhaphidophora korthalsii*. *Journal of Ethnopharmacology*, *52*(1), 53-57.

Wong, K. T., Tan, B. K. H., Sim, K. Y. and Goh, S. H. (1996). A Cytotoxic Melanin Precursor, 5, 6-Dihydroxyindole, from the Folkloric Anti-cancer plant *Rhaphidophora korthalsii*. *Natural Product Letters*, *9*(2), 137-140.

Yang, Z., Yi, Y., Gao, C., Hou, D., Hu, J. and Zhao, M. (2010). Isolation of Inulin-Type Oligosaccharides from Chinese Traditional Medicine*: Morinda officinalis* How and their Characterization using ESI-MS/MS. *Journal of Separation Science*, *33*(1), 120-125.

Yeap, S. K., Alitheen, N. B., Ali, A. M., Omar, A. R., Raha, A. R., Suraini, A. A., and Muhajir, A. H. (2007). Effect of *Rhaphidophora korthalsii* Methanol Extract on Human Peripheral Blood Mononuclear Cell (PBMC) Proliferation and Cytolytic Activity toward HepG2. *Journal of Ethnopharmacology*, *114*(3), 406-411.

Yeap, S. K., Omar, A. R., Ho, W. Y., Beh, B. K., Ali, A. M. and Alitheen, N. B. (2011). Immunomodulatory Effect of *Rhaphidophora korthalsii* On Mice Splenocyte, Thymocyte and Bone Marrow Cell Proliferation and Cytokine Expression. *African journal of biotechnology*, *10*(52), 10744-10751.

Yin, P., Chen, H., Liu, X., Wang, Q., Jiang, Y. and Pan, R. (2014). Mass Spectral Fragmentation Pathways of Phthalate Esters by Gas Chromatography–Tandem Mass Spectrometry. *Analytical Letters*, *47*(9), 1579-1588.

Zhang, H. J., Tamez, P. A., Aydogmus, Z., Tan, G. T., Saikawa, Y., Hashimoto, K., Nakata, M., Hung, N. V., Xuan, L. T., Coung, N. M., Soejarto, D. D., Pezzuto, J. M., and Fong, H. H. S. (2002 a). Antimalarial Agents from Plants. III. Trichothecenes from *Ficus fistulosa* and *Rhaphidophora decursiva*. *Planta Medica*, *68*(12), 1088-1091.

Zhang, H. J., Tamez, P. A., Hoang, V. D., Tan, G. T., Hung, N. V., Xuan, L. T., Houng, L. M., Coung, N. M., Thao, D. T., Soejarto, D. D., Fong, H. H. S. and Pezzuto, J. .M. (2001). Antimalarial Compounds from *Rhaphidophora decursiva*. *Journal of Natural Products*, *64*(6), 772-777.

Zhang, H., Qiu, S., Tamez, P., Tan, G. T., Aydogmus, Z., Hung, N. V., Coung, N. M., Angerhofer, C., Soejarto, D. D., Pezzuto, J. M. and Fong, H. H. S. (2002 b). Antimalarial Agents from Plants II. Decursivine, A New Antimalarial Indole Alkaloid from *Rhaphidophora decursiva*. *Pharmaceutical Biology*, *40*(3), 221-224.